ISTANBUL TECHNICAL UNIVERSITY ★ EURASIA INSTITUTE OF EARTH SCIENCES

INVESTIGATIONS OF THE HYDRODYNAMICS OF LAKE VAN USING POM (PRINCETON OCEAN MODEL)

Master Thesis by

Ufuk Utku Turunçoğlu
(602001005)

Date of submission : **9 May 2003**

Date of defence examination : **27 May 2003**

Supervisor (Chairman) : **Prof. Dr. Nüzhet DALFES**

Members of the Examining Committee : **Prof. Dr. Mehmet KARACA**

Prof.Dr. Orhan YENİGÜN (BÜ.)

MAY 2003

İSTANBUL TEKNİK ÜNİVERSİTESİ ★ AVRASYA YERBİLİMLERİ ENSTİTÜSÜ

VAN GÖLÜ' NÜN HİDRODİNAMİĞİNİN POM (PRINCETON OCEAN MODEL) YARDIMI İLE ARAŞTIRILMASI

YÜKSEK LİSANS TEZİ

Ufuk Utku Turunçoğlu
(602001005)

Tezin Enstitüye Verildiği Tarih : 9 Mayıs 2003

Tezin Savunulduğu Tarih : 27 Mayıs 2003

Tez Danışmanı : Prof. Dr. Nüzhet DALFES

Diğer Jüri Üyeleri : Prof.Dr. Mehmet KARACA

Prof.Dr. Orhan YENİGÜN (B.Ü.)

MAYIS 2003

PREFACE

The development of computer technologies made possible investigations and realistic simulations physical proceses and phenomena which can be observed in the natural world. Because of the easy usage models and the complexity of the subject, numerical models are widely used in environmental sciences such as oceanography and meteorology, so scientists can create your own idealized environment and examine how the studied processes evolve in time and space.

Oceans and large water masses are one of the most important components of the climate system and understanding of their behavior can be helpful in understanding the dynamics of the environment. From this point of view, large lakes have a special place in oceanography and limnology because they are easier to study than the ocean.

Princeton Ocean Model was used for studying hydrodynamic properties of Lake Van under climatic forcing. One hopes that this first study will be help to provide a framework for future studies of Lake Van.

This research was supported by The Center of Excellence for Advanced Engineering Technologies grant 5007200302. The authors express thanks to supervisor Prof. Dr. Nüzhet Dalfes, Dr. Gökhan Danabaşoğlu, Research Assistants Barış Onol and Elçin Tan and also creator of the POM2k, Dr. John Hunter and POM users for helpful comments.

To my parents, Nilgün and Ayten Demirag, my brother Umut Turunçoglu and all of my family and friends who make life worth living.

May, 2003 Ufuk Utku TURUNÇOGLU

TABLE OF CONTENTS

LIST OF TABLES

LIST OF FIGURES

LIST OF SYMBOLS

A_H : Horizontal heat diffusivity

A_M : Horizontal kinematic viscosity (m^2/s)

C_{DE} : Aerodynamic transfer coefficient

C_{DH} : Aerodynamic transfer coefficient

c_p : Specific heat of air at constant pressure

C_T : The maximum internal gravity wave speed

f : Coriolis force

H : Bottom topography (m)

g : Gravity constant (m/s^2)

K_M : Vertical kinematic viscosity (m^2/s)

K_H : Vertical heat diffusivity

L : Latent heat of vaporization

L_{v0} : Value of L_v at 0 degrees

ρ^1 : Mean density

ρ : Air density

q : Turbulence kinetic energy (m^2/s^2)

$q^2\ell$. : Twice the turbulence length scale (m^3/s^2)

q_A : Specific humidity of the atmosphere (at reference height, z_r)

q_S : Specific humidity of the surface

T : Temperature (K)

T_a : Atmospheric temperature at z_r height

T_s : Water surface temperature

S : Salinity (psu)

U : x component of the horizontal velocities (m/s)

U_{MAX} : The expected maximum velocity

U_r : Mean wind speed at the standard height (z_r)

V : y component of the horizontal velocities (m/s)

ω : Velocity component normal to sigma layer (m/s)

η : Surface elevation

σ : Sigma coordinate

τ_{XX} : Friction in xx surface

τ_{XY} : Friction in xy surface

SUMMARY

INVESTIGATIONS OF THE HYDRODYNAMICS OF LAKE VAN USING POM (PRINCETON OCEAN MODEL)

Large lakes are interesting dynamically because they are under the similar forcing effect as the oceans, but it is not necessary to specify open boundary conditions in lake because of their geometry and therefore it is easier to formulate models of their hydrodynamics.

In this study, hydrodynamic behavior of Lake Van under a variety climatic forcings is investigated. POM (Princeton Ocean Model) was chosen for this study because of its wide range of usage and existence useful tools for setting up a specified problem. POM is a three dimensional, terrain-following sigma coordinate, free surface, primitive equation ocean model, which includes a turbulence sub-model. The model solves principal Navier-Stokes equations.

In order to study the behavior of the model for various basin shapes and different climatic forcings, various test cases have been examined, illustrating idealized lake geometries such as ellipsoid, flat bottom box and inclined bottom box. Through these test cases, it has been observed that the temperature distribution in the lake is closely related to wind forcing applied at the lake surface. Moreover, sensible, latent and upward longwave heat losses influence horizontal and vertical temperature distribution and currents in the lake.

After the all of these 'idealized geometry' simulations, POM was run for each season with 'real' lake bathymetry using long-time seasonal averages of forcing parameters. Seasonal simulations show that lake is controlled of the climatic forcing. In summer and winter, Lake Van is stratified and the mixing process is dominant in fall season. The seasonal climatic forcing induces gyres in the deepest region of the lake.

ÖZET

VAN GÖLÜ' NÜN HİDRODİNAMİĞİNİN POM (PRINCETON OCEAN MODEL) YARDIMI İLE ARAŞTIRILMASI

Büyük göllerin dinamik açıdan oldukça ilginçtirler çünkü okyanuslara etki eden aynı türden kuvvetlerin etkisi altındarırlar fakat oktanuslarda olduğu gibi göllerde açık sınır şartlar belirlemek gerekmez ve kapalı bir ortam içinde oldukları için göller üzerinde hidrodinamik çalışma yapmak daha kolaydır.

Bu çalışmada Van Gölü' nün iklimsel etkiler altındaki hidrodinamik davranışı incelenmiştir. Bu inceleme için geniş bir kullanım alanına ve çeşitli yardımcı programlara sahip, POM (Princeton Ocean Model) seçilmiştir. POM üç boyutlu, düşeyde topografyayı izleyen sigma kordinatı kullanan ve temel Navier-Stokes denklemlerini çözen bir modeldir.

Öncelikle modelin farklı iklimsel etkiler altındaki davranışını incelemek için çeşitli test simulasyonları yapıldı. Bu testlerde elipsoid ve kutu gibi idealize edilmiş geometriler kullanıldı. Sonuçta göldeki sirkülasyonun ve buna bağlı olarak sıcaklık dağılımının rüzgar ile büyük oranda ilişkili olduğu bulundu. Ayrıca gizli ısı, hissedilir ısı ve göl yüzeyinden atmosfere olan uzun dalga boylu ısı kayıplarının, göldeki ısı dağılımını, düşey ve yatayda meydana gelen hareketleri büyük ölçüde etkilediği anlaşılmıştır.

Tüm bu test simulasyonlarından sonra model herbir mevsim için ayrı ayrı mevsimsel ortalama değerler ile çalıştırılmış ve her bir mevsim kendi içinde değerlendirilmiştir. Mevsimsel simulasyonlar Van Gölü' nün büyük ölçüde iklimsel etkiler altında olduğunu göstermektedir. Yaz ve Kış aylarında göl düşey olarak termal tabakalaşmış bir yapıdadır. Sonbahar' da ise karışım tüm gölde baskın olan durumdur. Ayrıca mevsimsel etkiler ve rüzgar nedeniyle gölün derin olan bölgelerinde döngüsel akıntılar oluşmaktadır.

1. INTRODUCTION

1.1. Purpose

In the proposed project, main patterns of the surface currents, vertical circulation and temperature profile will be considered in a seasonal context for Lake Van. On the other hand, the main aims of this study are to understand the sensitivity hydrodynamic properties of Lake Van as related to atmospheric 'climate' forcing Moreover, in order to realize the behavior of the model to various basin shapes and different amount of atmospheric forcing, different test cases have been considered.

1.2. Literature Review

The main subject of the hydrodynamics of lakes is the investigation of the motion of water body (in different scales and forms) which is generated by external forces and with their interaction (K. Hutter, 1983). Because of the complexity of the subject, numerical models, which use fundamental physical principles, try to simulate these motions, which can be observed in the real world.

Numerical ocean models use different assumptions and physics such as hydrostatic equilibrium, incompressibility, free or rigid surface. It can be applied for a large water mass as a lake and the results of the simulations are used for forecasting of the physical structure of the large lakes (Killey et al., 1998).

Large lakes are particularly interesting dynamically because of their behavior similar to coastal ocean and it is easier to study than the coastal ocean because they are smaller in size, but most importantly because it is not necessary to specify open boundary conditions (Beletsky et al. 1997). Most of the studies about hydrodynamic modeling of lakes, examine vertical and horizontal circulations (upwelling and downwelling) which are generated by wind stress (V. Botte, A. Kay, 2002; B. V Chubarenko et al., 2001).

Dynamic and thermal structures of lake can be used for generating initial and boundary conditions in biological models (C. Chen et al., 2002) because thermal stratification and currents affect and organize the physical and biological process (Ahsan et al., 1999). In addition, atmospheric heating and cooling, along with the wind stress, determine the formation, maintenance and eventual destruction of the surface mixing layer and control other large and small scale processes such as circulations and internal wave generations (Ahsan et al., 1999).

Inland water or lake has a complex hydrodynamic structure and all process in different levels (epilimnion, metalimnion and hypolimnion etc.) should be studied separately and studying lake behaviors under thermal stratification condition (Bonnet et al., 2000; B. R. Hodges et al., 2000; J. Heinrich et al., 1981; E. A. Tsvetova, 1999).

The application of these studies have been made for the studying, forecast of the three-dimensional physical structure of inland water body (Kelley et al., 1998), obtaining initial and boundary conditions for analyzing of water quality using biochemical model (K. Taguchi, K. Nakata, 1998), understanding basin's ecosystem and studying three-dimensional spatial distribution of phytoplankton, dissolved organic matter, nutrients, mineral and dissolved oxygen in lake (V. V. Manshutkin et al., 1998).

Although, Lake Van is the largest soda lake on earth and fourth largest closed lake, hydrological studies and available measurements about it are insufficient. In late of 70's, hydrographical and geological properties of lake were studied by M.T.A., Ankara (Kempe et al., 1978). It consists of main vertical profile of temperature in summer, chemistry analysis of lake water. and all of the studied which is related with geology of Lake Van are collected in a book (Degens, E. T. and F. Kurtman, 1978).

Other studies are related with water level fluctuations (Şen, Z. et al., 2000) and effects of the climatic changes above it (M. Kadıoğlu et al., 1997).

1.3. Why is POM (Princeton Ocean Model)?

POM is a three-dimensional, sigma coordinate, free surface, primitive equation ocean model, which includes a turbulence sub-model. The model has been used for modeling of estuaries, coastal regions, lakes and open oceans.

POM was used in determining hydrodynamic properties of Lake Van because it has a wide range usage. There are over 1500 POM users of record and it easy to reach and share any knowledge using user-list. Moreover, there are more useful tools and simple subroutines for setting up a problem and studied version of it (Pom2k) creates NetCDF output data file and it is easy to visualization of it.

2. PRINCETON OCEAN MODEL (POM)

2.1. Introduction

In this chapter, it will be given some useful information about Princeton Ocean Model (POM). The main physical principles of the model, assumptions and structure of the code will be examined.

2.2. Description of Princeton Ocean Model (POM)

First version of The Princeton Ocean Model (POM) was developed in the late 1970's by Blumberg and Mellor for modeling of estuaries, coastal regions and open oceans hydrodynamic properties. Since then, it has been improved and used by most of people all over the world so that it has several different version and type such as MPI and HPF parallel versions of POM contributed by S. Piacsek (NRL), a non-Boussinesq version of POM, two-dimensional version of POM etc. In this study NetCDF output version that is called Pom2k was used for analysis. The original version of this code named "OZPOM" which is created by John Hunter from University of Tasmania in Australia.

POM is a three-dimensional sigma-coordinate primitive equation model with a free surface, using a time splitting technique to solve the equation of continuity, momentum and diffusion, using finite difference method. The external mode (barotropic mode) of the model is two-dimensional (2D) and it uses short time step because of computing surface elevation (high resolution). Unlike external mode, internal mode (baroclinic mode) of the model is three-dimensional (3D) and it uses long time step. Both of the modes (internal and external) are based on The Courant-Frederic's-Levy (CFL) condition.

The Level 2.5 Mellor-Yamada turbulence closure scheme is used for providing realistic parameterization of vertical mixing and governing surface and bottom boundary layers. Free surface elevation is also computed for simulating tides and storm waves. It uses second order horizontal differencing on Arakawa C grid in curvilinear orthogonal or rectilinear coordinates and sigma coordinate level that is a necessary attribute in dealing with significant topographical variability, in vertical. In sigma coordinate model vertical coordinate scaled with water column depth.

In this version, it has some case studies that should run with no additional data requirements such as seamount and conservation box problem. Users have to write their own code to set up specific problem or test cases which consist of initial condition and lateral and surface boundary conditions.

2.2.1. The Basic Equations

POM is a primitive equation model and it solves main equations of fluid motion in three-dimensional space using time splitting method. It is a terrain following sigma coordinate model which is used in many ocean applications. In the following section, consist of some of the principal equation and approximations which are used in POM.

The transformation (Blumberg and Mellor, 1980) between the Cartesian coordinate system and the sigma coordinate system can be written as,

$$x^* = x,\; y^* = y,\; \sigma = \frac{z-\eta}{H+\eta},\; t^* = t \qquad \text{(2.1a), (2.1b), (2.1c), (2.1d)}$$

x, y, z are the conventional Cartesian coordinates; $D \equiv H + \eta$ where *H(x, y)* is the bottom topography and $\eta(x, y, t)$ is the surface elevation. Sigma coordinate ranges from $\sigma = 0$ at $z = \eta$ to $\sigma = -1$ at $z = -H$.

The resulting sigma coordinate system that follows the bottom is depicted in the following figure (Mellor, 1998),

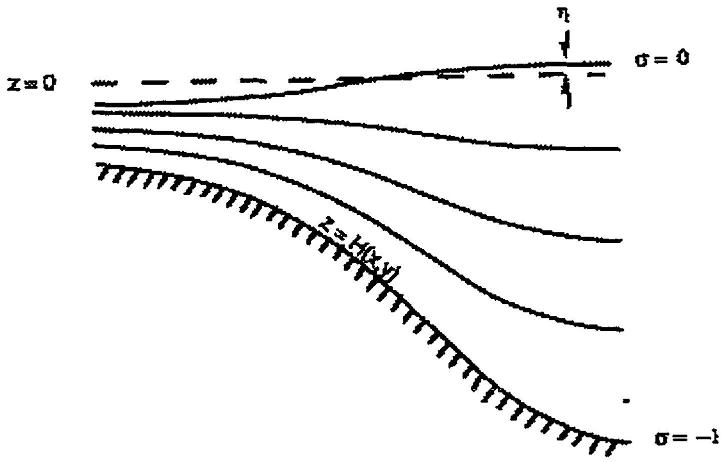

Figure 2.1 the sigma coordinate system

The basic equations can be written in horizontal Cartesian coordinates,

$$\frac{\partial DU}{\partial x}+\frac{\partial DV}{\partial y}+\frac{\partial \omega}{\partial \sigma}+\frac{\partial \eta}{\partial t}=0 \tag{2.2}$$

$$\frac{\partial UD}{\partial t}+\frac{\partial U^2 D}{\partial x}+\frac{\partial UVD}{\partial y}+\frac{\partial U\omega}{\partial \sigma}-fVD+gD\frac{\partial \eta}{\partial x}$$

$$+\frac{gD^2}{\rho_0}+\int_\sigma^0\left[\frac{\partial \rho'}{\partial x}-\frac{\sigma'}{D}\frac{\partial D}{\partial x}\frac{\partial \rho'}{\partial \sigma'}\right]d\sigma'=\frac{\partial}{\partial \sigma}\left[\frac{K_M}{D}\frac{\partial U}{\partial \sigma}\right]+F_x \tag{2.3}$$

$$\frac{\partial VD}{\partial t}+\frac{\partial UVD}{\partial x}+\frac{\partial V^2 D}{\partial y}+\frac{\partial V\omega}{\partial \sigma}+fUD+gD\frac{\partial \eta}{\partial y}$$

$$+\frac{gD^2}{\rho_0}+\int_\sigma^0\left[\frac{\partial \rho'}{\partial y}-\frac{\sigma'}{D}\frac{\partial D}{\partial y}\frac{\partial \rho'}{\partial \sigma'}\right]d\sigma'=\frac{\partial}{\partial \sigma}\left[\frac{K_M}{D}\frac{\partial V}{\partial \sigma}\right]+F_y \tag{2.4}$$

$$\frac{\partial TD}{\partial t}+\frac{\partial TUD}{\partial x}+\frac{\partial TVD}{\partial y}+\frac{\partial T\omega}{\partial \sigma}=\frac{\partial}{\partial \sigma}\left[\frac{K_H}{D}\frac{\partial T}{\partial \sigma}\right]+F_T-\frac{\partial R}{\partial z} \tag{2.5}$$

$$\frac{\partial SD}{\partial t}+\frac{\partial SUD}{\partial x}+\frac{\partial SVD}{\partial y}+\frac{\partial S\omega}{\partial \sigma}=\frac{\partial}{\partial \sigma}\left[\frac{K_H}{D}\frac{\partial S}{\partial \sigma}\right]+F_S \tag{2.6}$$

$$\frac{\partial q^2 D}{\partial t}+\frac{\partial U q^2 D}{\partial x}+\frac{\partial V q^2 D}{\partial y}+\frac{\partial \omega q^2}{\partial \sigma}=\frac{\partial}{\partial \sigma}\left[\frac{K_q}{D}\frac{\partial q^2}{\partial \sigma}\right]$$

$$+\frac{2K_M}{D}\left[\left(\frac{\partial U}{\partial \sigma}\right)^2+\left(\frac{\partial V}{\partial \sigma}\right)^2\right]+\frac{2g}{\rho_0}K_H\frac{\partial \tilde{\rho}}{\partial \sigma}-\frac{2Dq^3}{B_1 \ell}+F_q \qquad (2.7)$$

$$\frac{\partial q^2 \ell D}{\partial t}+\frac{\partial U q^2 \ell D}{\partial x}+\frac{\partial V q^2 \ell D}{\partial y}+\frac{\partial \omega q^2 \ell}{\partial \sigma}=\frac{\partial}{\partial \sigma}\left[\frac{K_q}{D}\frac{\partial q^2 \ell}{\partial \sigma}\right]$$

$$+E_1\ell\left(\frac{K_M}{D}\left[\left(\frac{\partial U}{\partial \sigma}\right)^2+\left(\frac{\partial V}{\partial \sigma}\right)^2\right]+E_3\frac{g}{\rho_0}K_H\frac{\partial \tilde{\rho}}{\partial \sigma}\right)\tilde{W}-\frac{Dq^3}{B_1}+F_\ell \qquad (2.8)$$

The transformation to the Cartesian vertical velocity is

$$W=\omega+U\left(\sigma\frac{\partial D}{\partial x}+\frac{\partial \eta}{\partial x}\right)+V\left(\sigma\frac{\partial D}{\partial y}+\frac{\partial \eta}{\partial y}\right)+\sigma\frac{\partial D}{\partial t}+\frac{\partial \eta}{\partial t} \qquad (2.9)$$

ω is the velocity component normal to sigma surfaces.

The horizontal viscosity and diffusion terms are defined according to,

$$F_x \equiv \frac{\partial \sigma}{\partial x}(H\tau_{xx})+\frac{\partial}{\partial y}(H\tau_{xy}) \qquad (2.10)$$

$$F_y \equiv \frac{\partial \sigma}{\partial x}(H\tau_{xy})+\frac{\partial}{\partial y}(H\tau_{yy}) \qquad (2.11)$$

where

$$\tau_{xx}=2A_M\frac{\partial U}{\partial x},\ \tau_{xy}=A_M\left(\frac{\partial U}{\partial y}+\frac{\partial V}{\partial x}\right),\ \tau_{yy}=2A_M\frac{\partial V}{\partial y} \qquad (2.12a),\ (2.12b),\ (2.12c)$$

Also,

$$F_\phi \equiv \frac{\partial}{\partial x}(Hq_x)+\frac{\partial}{\partial y}(Hq_y) \qquad (2.13)$$

$$q_x=A_H\frac{\partial \phi}{\partial x},\ q_y=A_H\frac{\partial \phi}{\partial y} \qquad (2.14a),\ (2.14b)$$

and Φ represents T, S, q^2, $q^2\ell$. The vertical mixing coefficients for momentum K_M and heat K_H, turbulent kinetic energy $q^2/2$ and turbulent length scale ℓ, horizontal diffusion for momentum A_M and heat A_H and these are controlled with inverse, horizontal turbulence Prandtl number.

2.2.2. Approximations

The Navier-Stokes equations for an incompressible fluid under the hypothesis of hydrostatic equilibrium and the Boussinesq approximation are used in POM.

In the Boussinesq approximation, one suppose that density differences are small in the sense that density variations are important in the Archimedean buoyancy force, but not, when density arises as a factor of a rate term (K. Hutter, 1983). On the other hand, the buoyancy drives the motion because of density varies little in which the temperature varies little. Thus the variation in density is neglected everywhere except in the buoyancy term.

2.2.3. Set up problem and defining constants

POM can be run for three different cases such as seamount, conservation box and specific problem but *"my_problem"* subroutine can be written for it. The seamount and conservation box subroutines are test cases for understanding how the model works. For defining a specific problem first of all *"my_problem"* subroutine must be customize. Structure of this part of the code depends on user and there are no strict rules about that but users must define some constants and construct their physical environment, boundary and initial conditions of the problem by code.

First of all it is necessary to define grid type and grid points coordinates. POM can be run both curvilinear orthogonal and rectilinear coordinates with "Arakawa C" differencing scheme. After choosing horizontal grid type, grid points coordinates can be calculate.

Fig. 2.2 and 2.3 represent internal and external grid structures of the model. Potential temperature, salinity, density and horizontal velocities are calculated in the middle of the sigma layers and vertical velocity and turbulence energy are estimated in each sigma layer in three dimensional internal mode.

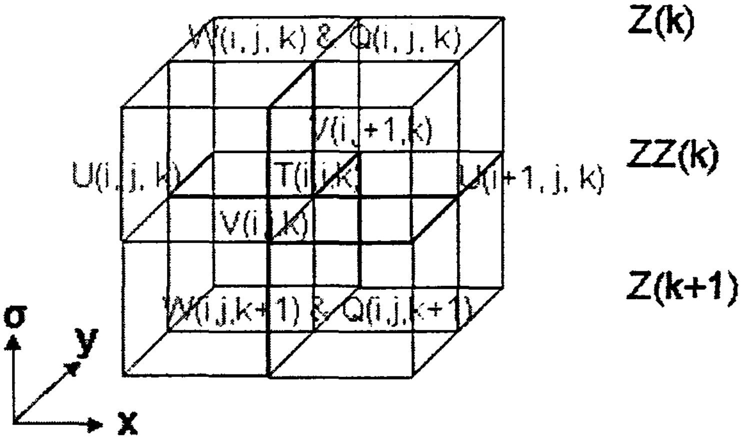

Figure 2.2 The three-dimensional internal mode grid structure (Q represents KM, KH, Q2, Q2L and T represents T, S and RHO)

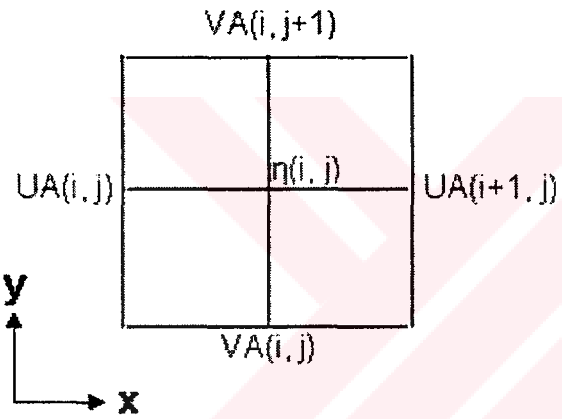

Figure 2.3 The two-dimensional external mode grid

There are some useful subroutine and program for pre-processing such as generating grid points and objective analysis but users have to be able to create your own pre-processing code for implementing their special problem into model.

After calculating coordinates of grid points and interpolating of the bathymetry data into cell center of the grid, land and sea masking must be apply. It must be more attention to masking process because land is set in POM as H=1 instead of 0 to allow division by H. There are three different masking variables (FSM, DUM and DVM); DUM is masking for u component of velocity, DVM, masking for v component of velocity and FSM masking for scalar variables. All of them must be set to 0 over land and 1 over water.

Initial and boundary conditions must be set in next step. If it is necessary to create setting time dependent, surface and lateral boundary conditions (such as wind stress, temperature and salinity flux etc.), this designation must be in beginning of the internal three-dimensional mode. This part of the code begins with a loop which is labeled with 9000.

It is necessary to notice during applying forcing component of the model;

Wind stress; stress and wind direction are opposite and eastward and northward winds stress have negative signs, eastward and northward currents have positive signs. On the other hand, if the wind is blowing from east to west or north to south, wind stress must be negative sign.

Flux components; sensible, latent heat (which involves only the evaporative component) and long wave radiation are defined as one value. The heat flux is positive when the water is cooling and negative when the water is warming. Latent heat and sensible heat can be calculated in Wm^{-2} unit using following formula for defining time dependent boundary condition.

$$SH = c_p \rho C_{DH} U_r (T_s - T_a(z_r)) \tag{2.15}$$

$$LH = L\rho C_{DE} U_r (q_s - q_a(z_r)) \tag{2.16}$$

$$L = L_{vo} - 2369T \tag{2.17}$$

where, c_p is the specific heat of air at constant pressure, ρ is air density, L is the latent heat of vaporization (can be calculated using Eq.2.17, where L_{v0} is the value of L_v at 0 degrees C, taken as 2500297.8 Jkg^{-1}, and T is the temperature in Celsius), U_r is mean wind speed at the standard height (z_r), T_s is water surface temperature, T_a is atmospheric temperature at z_r height, q_a and q_s are specific humidity of the surface and atmosphere (at reference height, z_r), C_{DE} and C_{DH} are aerodynamic transfer coefficients. If the wind speed at 10 m is 5 ms^{-1}, C_D=3.10^{-3}.

Constants, coefficients, parameters, mode and scheme are defined in beginning of the model. It is possible to select three different calculation types and it affects calculation of the bottom stress and 3D calculation can be made as prognostic and diagnostic.

It can be used two different advection scheme (centered and Smolarkiewicz iterative upstream scheme) but changing iteration step for Smolarkiewicz scheme is caused to more CPU time.

Jerlov water type controls how the ocean volume scatters light. Type I waters were represented by extremely clear oceanic waters. However, many water bodies were found to lie between Types I and II and the former was subsequently split into Types IA and IB. Type III waters are fairly turbid and some regions of coastal upwelling are so turbid that they are unclassified. To specify the penetration of short wave radiation, this classification is used.

External and internal time steps are related with grid size and maximum magnitude of velocity,

$$\Delta t_E \le \frac{1}{C_t}\left|\frac{1}{\delta x^2}+\frac{1}{\delta y^2}\right|^{-1/2} \qquad (2.18)$$

$$C_t = 2(gH)^{1/2} + U_{\max} \qquad (2.19)$$

$$\Delta t_I \le \frac{1}{C_T}\left|\frac{1}{\delta x^2}+\frac{1}{\delta y^2}\right|^{-1/2} \qquad (2.20)$$

$$C_T = 2C + U_{\max} \qquad (2.21)$$

where H is the depth of the location, U_{MAX} is the expected maximum velocity in Eq.2.18 and 2.19. According to this relationship between external time step and depth, as the depth increases the internal time step also decreases. In Eq.2.20, C_T is the maximum internal gravity wave speed and U_{MAX} is the maximum advective wave speed (Eq.2.21). The internal and external time steps are connected with a ratio of time step (*"ISPLIT"* variable in program) and typical value of the ratio is 30 for coastal ocean conditions.

Using value of grid size and velocity, CFL (The Courant-Fredrics-Levy) condition are calculated each loop (internal three-dimensional mode, labeled as 9000). If velocity is higher than defined constant value of maximum velocity, code stops because of the CFL condition and it gives "*abnormal job and user terminated*" error. For avoiding this error, time steps must be decrease or grid size must be increase.

Internal value of horizontal kinematic viscosity and heat diffusivity (*"AAM"* parameter in POM) coefficients can also cause *"abnormal job and user terminated"* error. Horizontal kinematic viscosity and heat diffusivity are connected each other with inverse horizontal turbulent Prandtl number (*"TPRNI"* parameter) and heat diffusivity affect the flux of heat from the surface to the bottom of lake. If the value of *"AAM"* is greater than a critical value, error occurs. *"AAM"* depends on grid size and velocity gradients. The diffusion component dominates the advection component in great kinematic viscosity value and error which is created by advective terms could be reduced. The grid cell Peclet number or cell Reynolds number can be used for calculating initial kinematic viscosity value. Small cell Reynolds number means it is diffusion dominated environment. Otherwise, large cell Reynolds number means it is advection dominated space.

Inverse horizontal turbulent Prandtl number is defined as dimensionless ratio between horizontal thermal diffusivities and horizontal momentum eddy viscosities and the typical value of it 0.2 but there are some test case application which it is assumed to be 1.0 (Beletsky et al., 1997).

It can be given specific data file for a seamless restart. This data had been crated by a previous run of the POM.

2.2.4. Structure of main program

After defining the problem and its initial, boundary conditions, the program begins to forecast variables. To compute baroclinic pressure gradient, density must be calculated by equation of state UNESCO (Mellor, G. L., 1991).

POM uses a mode-splitting technique to solving internal and external variables; external mode solves surface elevation and vertically time average wave speed to using in the internal mode and it uses density and vertically means velocity that is created by internal mode for calculating surface elevation. Subroutine ADVAVE also calculates the bottom stress in external mode and boundary conditions and velocity is defined by using subroutine BCOND.

Internal step compute three-dimensional variables that are separated into a vertical diffusion time step and an advection plus horizontal diffusion time step. It solves fully three-dimensional temperature, turbulence and current structure.

Advection part of the internal mode is solved by subroutine ADVT and vertical diffusion part is solved by subroutine PROFT. Both of them are calculated for temperature and salinity.

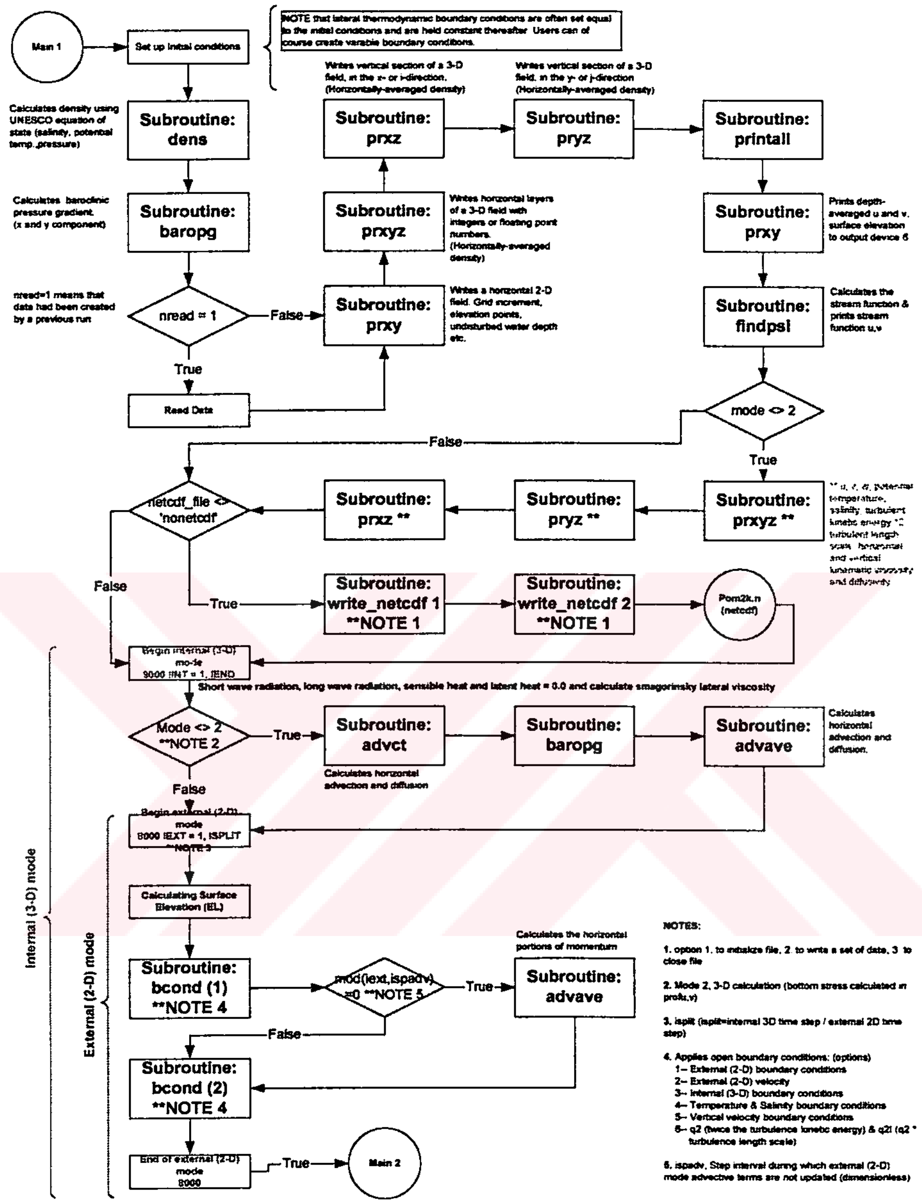

Figure 2.4 Structure of the main program (Part 1)

Beginning of the internal mode, POM calculates Smagorinsky lateral viscosity and the vertical averages of three-dimensional variables for using in two-dimensional external mode and two-dimensional external mode and all time dependent surface and lateral boundary conditions are set up in this section of model. Wind stress, heat and salinity fluxes are defined in this part of the code. External mode calculations results in updates for surface elevation and vertically averaged velocities. The internal mode calculation results in updates for velocity components (U and V), temperature and salinity.

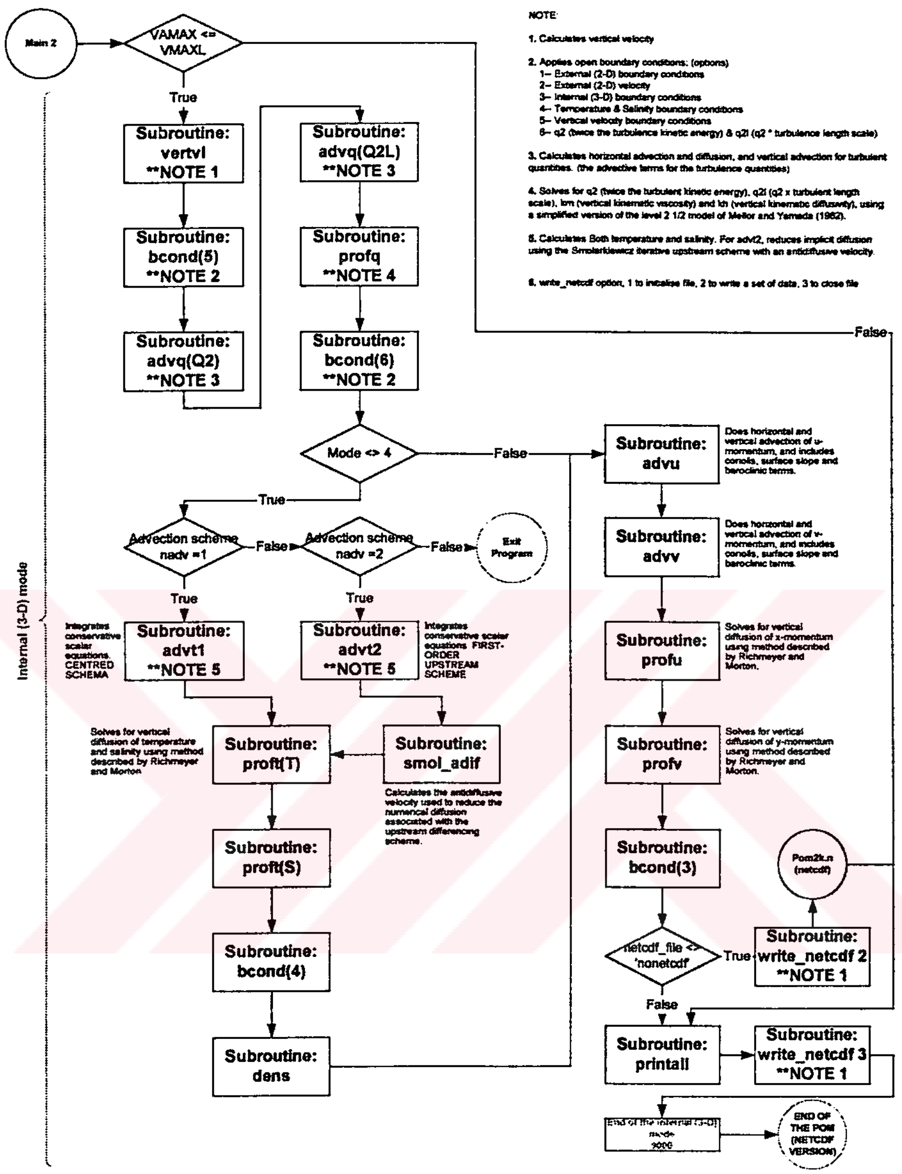

Figure 2.5 Structure of the main program (Part 2)

After finishing two-dimensional external loop (labeled with 8000), using external mode calculations, sigma coordinate vertical velocity, vertical temperature and salinity, turbulence kinetic energy and scale is calculated (see Eq.2.5, 2.6, 2.7, 2.8 and 2.9). Figure 2.4 and 2.5 is the flow chart which is represents both internal and external mode and process in the program.

2.2.5. Input and Output of Model

Used version of POM creates a NetCDF file to analysis of data. NetCDF (network Common Data Form) is an interface for array-oriented data access and it is a collection of software libraries for C, FORTRAN, C++, Java, and PERL. The NetCDF libraries define a machine independent format for representing scientific data.

NetCDF data is self-describing because it consists of information about the data it contains, Architecture-independent because it can be accessed by computers with different ways of storing integers, characters and floating-point numbers, Direct-access because of accessing efficiently small subset of large dataset, without first reading through all preceding data and Sharable so one writer and multiple readers may simultaneously access the same NetCDF file.

2.3. Possible Error Sources in POM

POM uses sigma coordinate in vertical which is used in both atmospheric and oceanic numerical models because of the following bottom or surface topography. The main advantage of the sigma coordinate is that a smooth representation of the bottom topography in ocean models. Nevertheless sigma coordinate has some disadvantage such as pressure gradient error.

Models which use terrain following coordinates, have suffered from errors in the horizontal component of the pressure gradient over step topography. It takes large, comparable in magnitude and opposite in sign value near step topography. In fact that it causes only computational error in velocity and can be detected in the case of an initially horizontally homogeneous density filed that, in theory, should produces zero velocity (Mellor et al., 1998).

It is defined as a problem of "hydrostatic consistency" associated with the sigma coordinate system. If a finite difference scheme to be hydrostatically consistent, it would supply following condition,

$$\left|\frac{\sigma}{D}\frac{\partial D}{\partial x}\right|\delta x < \delta\sigma \qquad (2.22)$$

It is known that this error is reduced by subtracting the area averaged density before evaluating density gradients (Mellor et al., 2000). The results show that if the finite difference schema satisfies the condition for hydrostatic consistency (Eq.2.22), the error can be reduced to tolerable levels with sufficiently high resolution (Haney R. L., 1991) and also greater kinematic viscosity values can be reduced error terms.

Step topography has an important role in ocean modeling. The reducing error studies are separate into four main categories (detailed information see, Song Y. T., 1998),

Vertical Interpolation Method; in this method, sigma coordinates are converted into z coordinate before calculating pressure gradient force terms but special care is necessary for reducing error. Extrapolation often required and if the interpolation is required each time step; it would be very costly in computational meaning.

Subtract reference state; this technique is formulating pressure gradient force as derivation of a chosen reference state. It is easy to implant to the model but it is insufficient for large modeling studies and long-term integration of it may not be small.

Higher order method; Using high order scheme can be reduce numerical error in computation of pressure gradient force but this approach fails to achieve significant improvement in some cases and it may need more computational time.

Retaining integral properties; it is based on the following formula,

$$\left.\frac{\partial p}{\partial x}\right)_z = \frac{\partial p}{\partial x} - \frac{\sigma}{h}\frac{\partial p}{\partial \sigma}\frac{\partial h}{\partial x} \qquad (2.23)$$

3. STUDY AREA AND DATA

3.1. Introduction

Lake Van is situated on eastern Anatolia in Turkey at about 43°E longitude and 38.5 °N latitude and its elevation is 1648 m (Figure 3.1).

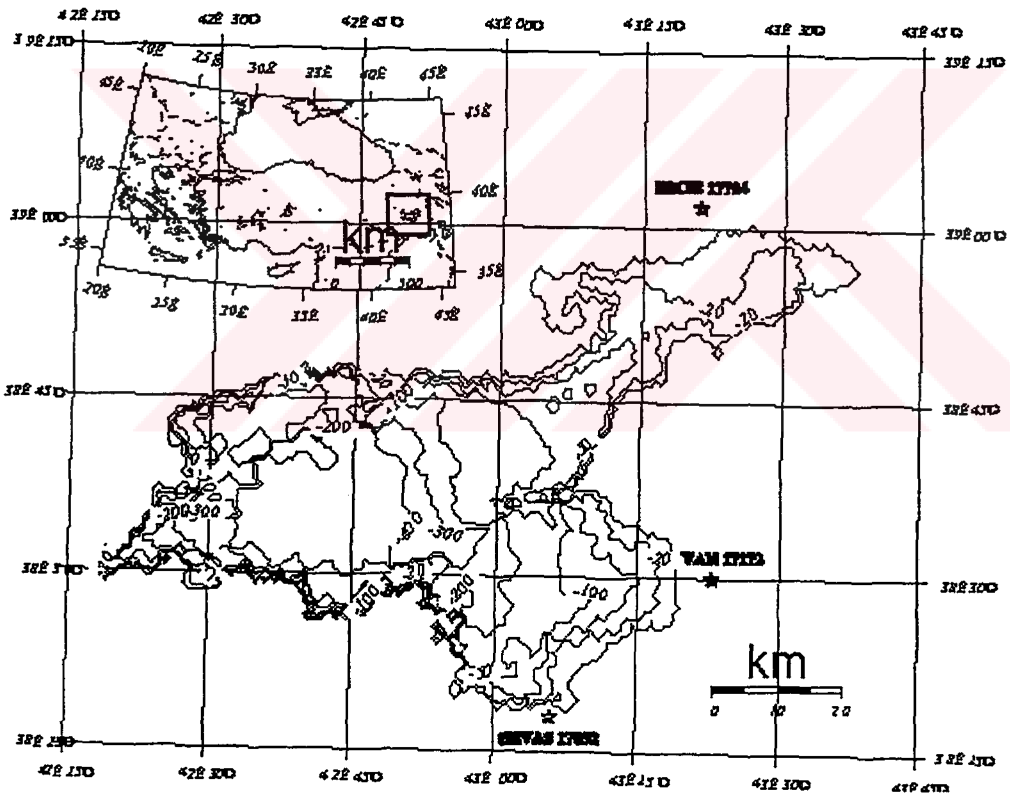

Figure 3.1 Location Map of Lake Van in Mercator projection

It has a surface area of 3574 km^2, volume of 607 km^3 and maximum recorded depth in the lake is 451m (Wong et al., 1978). The lake basin is separated into two parts by the Erek and Eastern Fans. Deveboynu Basin (surface area 11 km^2) which is elongated north-south direction and its average depth is 430 m. Tatvan Basin is much larger than Deveboynu Basin (surface area 440 km^2) and its average depth is 445 m (Wong et al., 1978).

It is a closed lake which loses their water by evaporation only. Closed lakes with morphology of rift lakes are comparatively seldom (Kempe et al. 1978).

The hydrological features have similarities with the open oceans, in winter arctic downwelling occurs, in summer an equatorial warm surface layer is formed, and in autumn or early winter upwelling encountered in the lake (Kempe et al. 1978).

3.2. Origin of Lake Van

Lake Van is the product of an extensive volcanic eruption of the Nemrut volcanic mountain during the Late Pleistocene (Blumenthal et al. 1964). Lake is surrounded by mountains and hills such as in the southwest Nemrut and Süphan, is located in the north of the lake and its level rose rapidly with northeast-southwest fluvial system was dammed (Kadıoğlu et al., 1987).

3.3. Climate of Region

Lake Van is located in about 43°E longitude and 38.5 °N latitude and its elevation is 1648 m. In this latitude winter is very severe and during this time mean temperature is generally under 0 °C. The coldest month of the region is January at -6.2 °C and all stations average of temperature is -4.79 °C in winter. Temperature reaches its maximum value between July and September (around 20 °C) and late of the September it starts to decrease but annual average of the temperature is above the 8 °C.

It is clear that precipitation is the highest value in April and May. In winter normally falls as snow and in late spring there is a rainy season. Summer time is the warmest and driest months but precipitation begin to increase with autumn as temperature decrease. The annual average of the precipitation is 492.64 mm. Runoff is the maximum value in May because of snow melt and heavy rain (Kadioğlu et al., 1997).

As a result of the seasonal variation of the atmospheric conditions (precipitation, temperature etc.) and river discharge, lake level rises from January to June and falls during the rest of the year. Maximum rise in lake level is from April to May and the strongest decrease occurs between September and October (Kempe et al., 1978).

3.4. Data

3.4.1. Climate Data

Climate data of the Lake Van region were provided by National Meteorological Center, NMC MRF (T40 L18) 1992 Model.

It used for the AMIP experiment is a research version of the 1992 operational NMC Medium-Range Forecast (MRF) model, which is a modified form of the model documented by the NMC Development Division (1988).

The model has spectral triangular 40 (T40), roughly equivalent to a 3 x 3 degrees latitude-longitude horizontal resolution and there are 18 unevenly spaced sigma levels.

The solar constant is the AMIP-prescribed value of 1365 W/m^2. Both seasonal and diurnal cycles in solar forcing are simulated and the surface solar absorption is determined from the surface albedo, and longwave emission from the Planck equation with emissivity of 1.0.

Table 3.1 Diagnostic Long-time and ensemble average of temperature and heat fluxes from NOAA NCEP EMC CMB: Climate Modeling Branch (L, Longwave, S, Shortwave)

42.18750 E 37.67308 N	Temperature (°C)		Downward Flux (W/m2)		Surface Heat Flux (W/m2)		Upward Flux (W/m2)		Momentum Flux (dyn/cm^2)	
	Air	Skin	L	S	Latent	Sensible	L	S	U flux	V flux
JAN	1,09	2,18	256,72	121,06	-21,79	-8,79	319,86	32,59	0,04606	0,04931
FEB	2,2	3,6	255,79	162,73	-36,47	-15,24	326,36	39,76	0,05528	0,04337
MAR	5,17	6,88	261,12	226,32	-67,38	-23,59	342,66	49,06	0,07092	0,03924
APR	9,4	11,06	276,05	294,08	-110,68	-25,46	364,91	60,84	0,07905	0,03068
MAY	15,44	16,75	299,98	351,69	-146,84	-21,77	396,05	74,44	0,04222	0,00822
JUN	22,6	24,65	334,11	379,46	-138,54	-35,93	440,65	80,81	0,01364	-0,00374
JUL	30,59	34,44	368,64	379,44	-85,19	-66,3	498,84	75,37	-0,02749	-0,00105
AUG	33,94	38,52	368,55	347,97	-28,89	-78,92	522,45	70,3	-0,02366	0,01869
SEP	28,56	32,66	337,98	293,93	-22,05	-66,92	482,29	59,47	-0,01302	0,00021
OCT	19,36	22,39	299,3	220,72	-21,36	-42,43	420,12	46,44	-0,00714	0,00736
NOV	9,68	11,38	272,49	150,93	-25,62	-17,82	362,65	33,81	0,01027	0,02596
DEC	2,97	4,08	258,73	114,72	-22,01	-8,45	328,24	28,05	0,03022	0,04286
WINTER	2,09	3,29	257,08	132,84	-26,76	-10,83	324,82	33,47	0,04385	0,04518
SPRING	10	11,56	279,05	290,7	-108,3	-23,61	367,87	61,45	0,06407	0,02605
SUMMER	29,04	32,54	357,1	368,96	-84,21	-60,38	487,31	75,49	-0,01251	0,00463
AUTUMN	19,2	22,14	303,26	221,86	-23,01	-42,39	421,69	46,57	-0,00330	0,01118
ANNUAL	15,08	17,38	299,12	253,59	-60,57	-34,3	400,42	54,24	0,02303	0,02176

The date range of the available data is between February 1950 and February 1995. It is calculated averages of ensemble runs of the model (M=13) and then the long-time average was calculated all of the variables in 42.18750 E, 37.67308 N location. Monthly, seasonal and annual long-time average of the variables can be seen in Table 3.1 and Fig.3.2 shows that yearly cycle of the used variables. ULW, Upward Longwave Flux, USW, Upward Shortwave Flux, DLW, Downward Longwave Flux and DSW, Downward Shortwave Flux. Net longwave flux is the difference between downward and upward longwave flux.

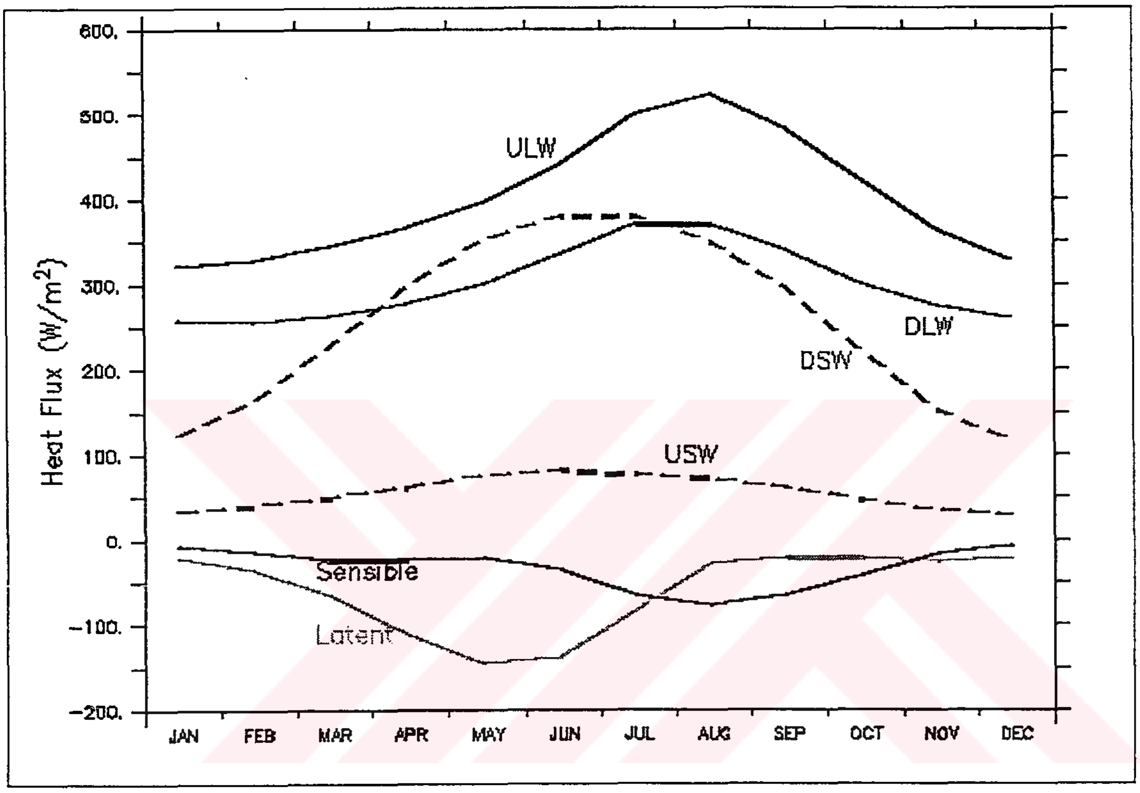

Figure 3.2 T40 Diagnostic Long-time averages of monthly heat fluxes in Longitude, 42.1875 E and Latitude, 37.67308 N from NOAA NCEP EMC CMB: Climate Modeling Branch

3.4.2. Bathymetry Data

Bathymetry data of the Lake Van were digitized using various GIS program (ArcView and ER Mapper) from Lake Van map which is published by Turkish Navy Department of Navigation, Hydrography and Oceanography in 1983 (No: 9008).

The bathymetries were modified in order not to exceed hydrostatic consistency criterion for sigma coordinates. In Chapter 5, it is given detailed information about hydrostatic consistency.

4. GRID GENERATION PROGRAMS

4.1. Introduction

There is various kind of grid generation program for POM. In the oceanic modeling applications are preferred to use boundary fitted curvilinear orthogonal grid because of reducing computational error and increasing stability. In this section, it is given some useful information about grid generation programs which can be used in modeling with POM and then *"LAKEGRID"* grid generation program which is written for lake studies, will be introduced.

4.2. Curvilinear Orthogonal Grid Generation Programs

"CURVIGRID.F" generates grid using four edges of the girded domain in latitude and longitude values and it can be altered to rectilinear coordinates by setting CS parameter to 1. It uses orthogonality conditions in Eq.4.1 and 4.2.

$$\left(\frac{\partial x}{\partial s}\right)_j = -\left(\frac{\partial y}{\partial s}\right)_i, \left(\frac{\partial y}{\partial s}\right)_j = -\left(\frac{\partial x}{\partial s}\right)_i \qquad (4.1), (4.2)$$

"GRID.F" uses similar technique with *"CURVIGRID.F"* but it can be plotted interpolated data using NCAR Graphics routines or MATLAB m file.

Lastly, there is another grid generation program which is working under MATLAB. It is a MATLAB toolbox which is called as *"SEAGRID"*. It is written by Dr. Charles R. Denham.

4.3. LAKEGRID Grid Generation Program

4.3.1. Introduction

POM has an ability to use both curvilinear orthogonal coordinates and simple rectangular Cartesian grid but if the boundary of the study area very indented (it has a lot of convex and concave part), available curvilinear orthogonal grid generation programs are insufficient for generating grid.

"LAKEGRID" was written in FORTRAN 95 and it is ability to produce rectangular Cartesian grid for some simple test case such as quadrangle, circular and ellipsoid but in this study it is used for creating grid and masking in flat bottom box, inclined bottom box, ellipsoid test cases and real lake. Also, it uses sigma coordinates in vertical.

It is taken advantage of some other grid generation programs such as *"GRID.F"* in POM ftp site. It was written by John Wilkin of Woods Hole Oceanographic Institution and has been changed and extended by George Mellor and Tal Ezer from Princeton University. *"PNPOLY"* subroutine is written by Randolph Franklin, University of Ottawa.

4.3.2. Input and Output Files

For generating grid of real lake case, two ASCII file must be given to program as input file. One of them is *"CONTOUR.XYZ"* which is consist of two column in degree unit (Longitude, Latitude) and other is *"BATHYMETRY.XYZ"* file that has three column, first two data column are same as *"CONTOUR.XYZ"* and next column is bathymetry data in meter unit and depths must be positive values.

It is not necessary to give any file to generating grid for the test cases. Program creates boundary and bathymetry data itself.

The program creates two ASCII file which is used in POM *"my_problem"* subroutine. *"POMGRID.TXT"* is consist of following variables of the grid points; depth (*H*), masking variables (*FSM, DUM* and *DVM*), area of the cell *T*, *U* and *V* (*ART, ARU* and *ARV*), Coriolis value (*COR*), rotation, x and y coordinates of the grid cell (*C, E, U* and *V*) and grid spacing for each cell. Other file, *"POMSIGMA.TXT"* consists of sigma level data such as sigma level thickness, coordinates of the center of sigma levels etc.

4.3.3. Definition of the Subroutines

"DIST" function calculates distance between two points in meter unit. Point data must be geographic coordinates in degree unit. This function is adapted from SEAGRID MATLAB toolbox which is created by Dr. Charles R. Denham, U.S. Geological Survey. Also, *"DIST"* is used for calculating average distance between bathymetry observation points which is used in *"CRESSMAN"*.

"CELLCOOR" subroutine calculates coordinates of the grid points *U, V, E* and *C*. It is adapted from POM2K test cases.

"CRESSMAN" subroutine interpolates scattered data into grid points using Cressman method which is created by George P. Cressman in 1959. In this method, the residuals are weighted depending only upon the distance between the grid point and the observation. *"DIST"* is used for defining the radius of influence. If the depth is less than minimum depth which is specified in parameter section, value of real depth is changed to minimum depth.

"DEPTH" subroutine adapted from *GRID.F* program. It calculates sigma levels coordinates and thicknesses.

"MASK" subroutine apply sea and land masking to grid cell. It uses depth data, if depth equal to 1, it assumes land and if depth grater than 1, it is water. POM assumes that land is 1 meter depth to insure division by H. It is also calculates cell area and Coriolis value of each cell.

"PNPOLY" subroutine is the main part of the code. It determines whether a point is inside or outside a boundary area. The result is used for calculating bathymetry and applying masking. A vertical line is drawn through the point and if it crosses the polygon an odd number of times, the point is inside of the polygon. This is called the *Jordan Curve Theorem.*

"SLPMIN" subroutine is used for smoothing topography in order to insure hydrostatic inconsistency and pressure gradient force errors.

"ZTOSIG" subroutine converts z levels to sigma levels. Vertical sigma levels can be depth of the levels. This data preserve in *ZS* variable.

4.3.4. Program Structure

MOD, BMODE, CMODE and SMODE parameters control running styles of the program in the beginning. Different combinations of the mode variables supply various kind of test case and even real lake boundary with constant depth. After definitions of the parameters and coefficients, it creates boundary data for test cases and read boundary data of the real lake (if real lake case chosen).

It finds maximum and minimum value of grid quadrant which contains all of the boundary vertexes and it calculates grid count in x and y direction for defining dimensions of the arrays.

After finding dimension of the arrays, coordinates of the grid points are calculates using *"CELLCOOR"* subroutine. Next step is defining grid points whether a point is inside or outside a boundary area using *"PNPOLY"* subroutine.

The depth is designated as land in all points which is the outside of the boundary area and created (for test cases only) or read bathymetry data interpolated in to center of the grid pointes using *"DIST"* function and *"CRESSMAN"* subroutine.

The land and water masking are calculated using result of the *"PNPOLY"* subroutine and than using result of the *"PNPOLY"* both depth data and sigma levels are computed. After computing masking variables, bathymetry data are smoothed using *"SLPMIN"* subroutine.

Time step for each cell and hydrostatic inconsistency factor on bottom layer (should be less than 1 for stability) are calculated and controlled.

5. APPLICATIONS OF THE MODEL

5.1. Simple Test Cases

In order to how the model works and gives response to different amount of forcing, it is examined for various lake shape, bathymetries, wind and heat flux forcing. Three main basin types are used in test cases which are called ellipsoid (EL), flat bottom box (BC) and inclined bottom box (BI). EL and BI basin shape and bathymetries can be seen in Figure 5.1 and 5.2. All of the basins have same surface area of 3600 km^2 which is equal to Lake Van's.

Every one of the test case simulations has same initial temperature distribution in vertical and horizontal scale and it is assumed that the lake is isothermal and not stratified. Annual average temperature of Lake Van is used to setting up initial conditions of test cases, so both atmospheric temperature (*TATM*) and vertical temperature distributions of lake are constant in 9 °C.

At the beginning of the all test case simulations, there is no motion in the lake and free surface is initially flat. The lateral boundary conditions are no-slip namely tangential and normal components of the velocity set to zero at the lake boundary.

The Lake Van centered at latitude 38.5 N. so that the Coriolis parameter is assumed to be constant at $f = 10^{-4}\ s^{-1}$. A rectangular horizontal grid with a uniform spacing ($\Delta x = \Delta y$) of 1 km was used and 20 vertical sigma levels were used with closer spacing near the surface at z= 0, 1, 2, 3, 5, 8, 12, 18, 25, 35, 50, 70, 100, 125, 150, 175, 200, 225, 250 and 300 m.

Horizontal diffusion is calculated with Smagorinsky eddy parameterization (*HORCON* parameter is 0.1); horizontal momentum diffusion is assumed to be equal to horizontal thermal diffusion (Inverse horizontal turbulent Prandtl number is 1.0).

For test case reference density is set to a constant value 1020 kg/m^3 and salinity is constant in 20 psu which is same as Lake Van. To insure computational stability, POM uses an internal mode time step of 180 s and external mode time steps of 6 s for the 1 km grid.

The wind stress increases linearly from zero to its maximum value over 24 hours and it remains constant at this maximum value for the duration of the model simulation. It is used two different wind speed for simulating strong wind (5 m/s) and light wind cases (1 m/s) and Table 5.1 is represented wind speed and its stress equivalents.

Table 5.1 Applied Wind Stress in test cases

Wind Direction	m/s	N/m2	m2/s2
N-S and E-W	1.0	0.00125	0.00125×10^{-3}
	5.0	0.031	0.031×10^{-3}
NE-SW (5 m/s) x and y component	2.236	0.006	0.006×10^{-3}

The net solar radiation at the ground peaks near local solar noon (Hartmann D. L., 1994). It begins to increase with sun rise from zero to its maximum value and after solar noon it starts to decrease until sunset so short wave flux is applied using a sinusoidal function between sunrise and sunset time. It begins to increase at 10:00 AM and it reaches its maximum value in 14:00 PM. After solar noon it starts to go down until sunset time (18:00 PM). In fact that annual average of the sunshine time is about 7.5-8 hours in the region of Lake Van.

The downward long wave radiation has almost no diurnal variation because of the small diurnal variation of air temperature in the free atmosphere (Hartmann D. L., 1994), so it is assumed that there is no diurnal variation in downward longwave radiation in test cases and downward longwave radiation and air temperature remain constant during simulation. Unlike downward longwave radiation, the net longwave loss depends on daytime surface temperature and it varies with net radiation during day. It increases from sunrise to midday and then it decreases. Upward longwave radiation (black body emission from the surface) is calculated using Stefan-Boltzmann Law (Eq.5.1).

$$E = \varepsilon\sigma T_s^4 \tag{5.1}$$

where ε is the emissivity (0.9 for the water surface), σ Boltzmann's constant is 5.67 10^{-8} $Wm^{-2}K^{-4}$) and Ts is the lake surface temperature.

Latent and sensible heats are given constant during simulations. It is used three different amounts of flux 20, 40 and 80 W/m^{-2} for simulating strong and light heat loss cases.

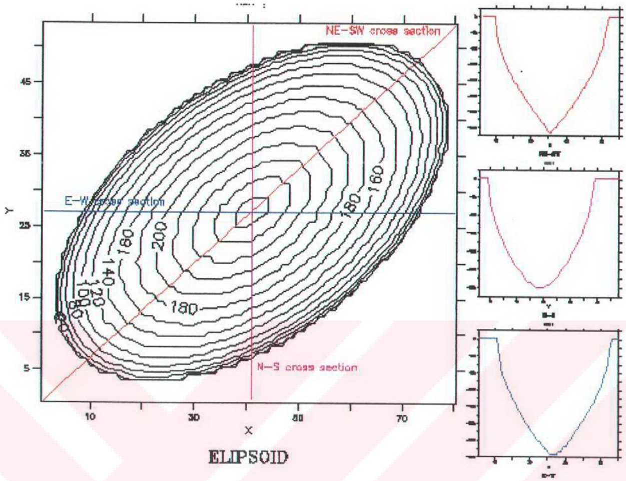

Figure 5.1 The ellipsoid Lake Bathymetry (EL)

Ellipsoid test case uses ellipsoid function to constructing bathymetry and boundary of lake. It has elliptical depth profile of maximum depth 300 m in which long axis is about 20.75 km and short axis is about 13.75 km (see Figure 5.1). It is rotated about the z-axis in 35 degree because of being same orientation angle in Lake Van.

Bottom topographies of the BI slopes in north-south direction form its minimum value of 10 m to maximum value of 300 m (Figure 5.2). Initial and boundary conditions are the same as EL.

Flat bottom box test case (BC) has a constant depth of 300 m and its shape of boundary is square.

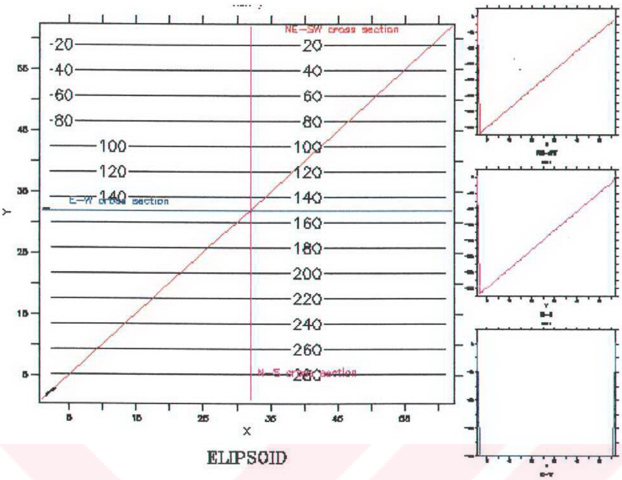

Figure 5.2 The inclined Bottom Box Lake Bathymetry (BI)

It is given a reference code for all of the model runs because of having systematic structure of figures (see Table 5.2).

Table 5.2 The reference codes and initial conditions of test cases

ELLIPSOID				FLAT BOTTOM BOX				INCLINED BOTTOM BOX			
Reference Code	Wind Speed (m/s)	Direction	Latent + Sensible (W/m^2)	Reference Code	Wind Speed (m/s)	Direction	Latent + Sensible (W/m^2)	Reference Code	Wind Speed (m/s)	Direction	Latent + Sensible (W/m^2)
EL1NN20	1.0	N	20	**BC1NN20**	1.0	N	20	**BI1NN20**	1.0	N	20
EL1NN40	1.0	N	40	**BC1NN40**	1.0	N	40	**BI1NN40**	1.0	N	40
EL1NN80	1.0	N	80	**BC1NN80**	1.0	N	80	**BI1NN80**	1.0	N	80
EL1NE20	1.0	NE	20	**BC1NE20**	1.0	NE	20	**BI1NE20**	1.0	NE	20
EL1NE40	1.0	NE	40	**BC1NE40**	1.0	NE	40	**BI1NE40**	1.0	NE	40
EL1NE80	1.0	NE	80	**BC1NE80**	1.0	NE	80	**BI1NE80**	1.0	NE	80
EL1EE20	1.0	E	20	**BC1EE20**	1.0	E	20	**BI1EE20**	1.0	E	20
EL1EE40	1.0	E	40	**BC1EE40**	1.0	E	40	**BI1EE40**	1.0	E	40
EL1EE80	1.0	E	80	**BC1EE80**	1.0	E	80	**BI1EE80**	1.0	E	80
EL5NN20	5.0	N	20	**BC5NN20**	5.0	N	20	**BI5NN20**	5.0	N	20
EL5NN40	5.0	N	40	**BC5NN40**	5.0	N	40	**BI5NN40**	5.0	N	40
EL5NN80	5.0	N	80	**BC5NN80**	5.0	N	80	**BI5NN80**	5.0	N	80
EL5NE20	5.0	NE	20	**BC5NE20**	5.0	NE	20	**BI5NE20**	5.0	NE	20
EL5NE40	5.0	NE	40	**BC5NE40**	5.0	NE	40	**BI5NE40**	5.0	NE	40
EL5NE80	5.0	NE	80	**BC5NE80**	5.0	NE	80	**BI5NE80**	5.0	NE	80
EL5EE20	5.0	E	20	**BC5EE20**	5.0	E	20	**BI5EE20**	5.0	E	20
EL5EE40	5.0	E	40	**BC5EE40**	5.0	E	40	**BI5EE40**	5.0	E	40
EL5EE80	5.0	E	80	**BC5EE80**	5.0	E	80	**BI5EE80**	5.0	E	80

** NN and EE represents N (Northerly) and E (Easterly) winds

All of reference codes of the model runs (test case and real lake case) are based on following logic; first two characters represent basin type and geometry of the test lake, next one character is wind velocity in m/s unit, following two character are wind direction (for east, EE and north is NN) and last two character are sum of latent and sensible heat forcing in W/m^2 unit. List of the test cases and initial values of the wind and heat flux can be seen in Table 5.2.

5.2. Results of the Test Cases

In the following sections the results from these test case experiments are examined. The main aim of the section is defining effect of the climatic and atmospheric forcing over different lake basin and lake shape.

All of the test case result can be seen in Appendix A, B and C.

5.2.1. Ellipsoid (EL)

Ellipsoid test case was created using ellipsoid function and it is rotated about the z axis in 35 degree. The Cartesian coordinate system located at left-bottom corner of the ellipsoid. The test case was run throughout 50 days with same wind, air temperature, latent heat and sensible heat forcing. Unlike these constant variables longwave radiation change during simulation depend on surface and air temperature differences.

The components of the heat loss term are sum of the latent heat, sensible heat and upward longwave heat. Longwave heat term is same for all test cases but sensible and latent heat changes. 20, 40 and 80W/m^2 are only represent sum of latent and sensible component of the upward heat flux.

Lake surface temperature has the highest value in 20W/m^2 cases in all wind direction and wind speed because of the heat loss is much smaller than the other cases (see Apx.B.1a-f) and the temperature is range of 10.5-12 °C in 10 m depth. The effect of the wind direction and speed in the lake surface temperature is much stronger in high wind speed and high heat loss cases. Because, shallow region of the lake gets cold much faster than deeper part of the lake and this colder water mass and energy are transferred to shore regions which is in wind direction.

At the beginning of the simulation atmosphere and lake have same temperature but it start to change during simulation and lake surface temperature becomes colder than the air temperature in 80W/m^2. As a result, density of the cold lake surface water getting denser and thermohaline circulation produces in the shore regions.

The observations show that the surface current speed is typically about 2 to 3 % of the wind speed. This can be seen in surface current figures (Apx.C.4, 5, 6 a-f). For example, maximum surface current velocity is 0.075 m/s in EL1EE20 (Apx.C.4a) and the EL5EE20 case is 0.168 m/s and average velocity are 0.009 and 0.02 m/s but when heat loss is too much (80W/m^2), velocity of the surface currents are little bit higher (maximum 0.21 for EL5EE80 and 0.4 for EL1EE80). This can be high surface friction or viscosity of the water in cold surface water because viscosity of water is related with kinetic energy.

Free surface elevation indicates similar behavior with temperature structure in horizontal. Temperature causes thermal expand and surface elevation increases in these regions (Apx.A.3a-f). Thermal expansion of the upper layer of the lake at a particular region is generally seasonal and it may not affect the long term lake level change. Otherwise, increasing surface elevation is related with wind speed closer. The surface elevations in strong wind case (5m/s) are higher than the light wind case. In 20 W/m^2 case, it is 0.4-0.5 cm in strong wind case (Apx.A.1a, c and e) and it is about 0.05-0.2 cm in the light (1m/s) wind case (see Apx.A.1b, d, and f). This value of the surface temperature is much less in 40 W/m^2.

According to Ekman Theory, the surface water velocity is at 45 to the right of the wind direction in the northern hemisphere. As a result of the theory surface elevation should be its highest value is about at 45 to the right of the wind direction and this can be observe in all test cases except 80 W/m^2 case (see Apx.A.1, A.2 and A.3a-f). In this case temperature differences is much more effectual and the highest surface elevation occurs in the deepest part of the lake namely, center of the lake because it is much more warm than shore.

5.2.2. Flat Bottom Box (BC)

The horizontal temperature distribution is homogeny in light wind cases and strong wind cases produce warmer areas near shore in which wind is blowing onshore.

Temperatures are about 10.5-11 °C at 10 m depth in relatively less heat loss cases (20 W/m^2) and it decreases to 9-9.5 °C in high heat loss cases. The horizontal temperature distribution of the both strong and light wind cases are chaotic in highest heat loss case (80 W/m^2) and average temperature is 8.5-9 °C at 10 m depth (less than initial temperature of lake). In high heat loss case, it is not any effect of the wind direction and velocity above the temperature distribution (Apx.C.3 a-f).

The highest surface elevation seen in shore region and it is similar to temperature plots. Unlike ellipsoid case, surface elevation has been formed with wind in flat bottom and high heat loss case.

Gyre can be observed in less heat loss and strong wind case (Apx.C.5 a and f). Velocities of surface current are decreasing as soon as heat loss increasing. The average velocities are about 0.04 m/s and maximum value of it is 0.1-0.15 m/s in weak heat loss and strong wind case (Apx.C.5 b, d and f).

5.2.3. Inclined Bottom Box (BI)

Velocity of the surface currents is a function of square root of depth and gravity in shallow regions. From point of this view, it is decrease from south to north because the bottom topography of the BI slopes in north-south direction and direction of the currents turn on to the left of the basin in inclined bottom box case (Apx.C.7 and 8 a-f).

Temperature distribution is similar with flat bottom box case but north part of the box is shallow and it is warmer than deeper part of the lake in low heat loss case. On the contrary, shallow region is colder than longshore region in the high heat loss case. Also, maximum temperatures are in surface flow direction because of the transferring of the heat energy.

High surface elevation zones are become intense in direction of the currents and warmer regions because of the thermal expansion of the lake water. The change of volume of the water depends on temperature change and this effect the surface elevation in warm regions.

6. REAL LAKE CASE

6.1. Introduction

In this chapter, it is examined the basic hydrodynamic properties (main temperature and circulation pattern) which is controlled by seasonal variations of the climatic forcing in the Lake Van. The objective is to understand the seasonal cycle of the lake.

6.2. Setting Up Real Lake Case (Seasonal)

The lake is represented a rectangular Cartesian grid with equal spacing of 1 km (122 × 81 points) and the axis is aligned bottom left corner of the lake. In the vertical, 20 σ levels were used with closer spacing near the surface (Sigma levels; 0.0000, -0.0083, -0.0166, -0.0333, -0.0666, -0.1333, -0.2000, -0.2666, -0.3333, -0.4000, -.04666, -0.5333, -0.6000, -0.6666, -0.7333, -0.8000, -0.8666, -0.9333, -0.9666, -1.0000)

To insure computational stability, the POM uses internal mode time steps 180 s and external mode time step 6 s in real lake case. The minimum depth of the lake is corrected to 10 m and the bathymetry was modified so that the ratio of depths of any two adjacent grids did not exceed 0.1 (with *SLPMAX*, 20 times) in order get the hydrostatic consistency criterion for sigma coordinates.

NMC MRF Diagnostic data set was used in seasonal simulations of Lake Van. It is calculated monthly long-time and ensemble average of downward shortwave radiation, air temperature, meridional and zonal momentum flux from NMC MRF model data set and it is given to model as a time dependent boundary conditions.

All seasonal simulations are started from same initial temperature and salinity distribution. Horizontal and vertical structure of temperature was assumed to be constant in 12 °C and salinity is set to constant value (20 psu) in Lake Van. It is assumed to be a closed system and there is no water input and output (*VFLUX* parameter is zero) to the lake.

To calculate the net longwave radiation at the surface, the downward longwave radiation coming from atmosphere (from NMC MRF data), the temperature of the lake surface (from POM) and the longwave emissivity of the surface, ε are used. The upward longwave flux is calculated from Stefan-Boltzmann Law (Eq.5.1) and ε, is assumed to be 0.98.

Sensible and latent heat was calculated using differences between air and lake surface temperature and Bowen Ratio. The Bowen ratio is the ratio of the sensible cooling to the latent cooling of the surface (Hartmann, D. L., 1994) and it is given 0.1 as typical value of over water. Latent and sensible heat was calculated using Eq.2.15, 2.16 and 2.17 in Chapter 2.

The momentum flux and heat fluxes are continuously applied during simulations and diurnal cycle of the heat fluxes is neglected.

The simulation time of the each season was chosen to be 100 days in order to observe seasonal variation in Lake Van.

6.3. Analysis of Pressure Gradient and Hydrostatic Inconsistency Errors

The test case was simulated with real lake bathymetry in order to defining magnitude of hydrostatic inconsistency and pressure gradient error.

The "hydrostatic inconsistency" condition arises if the local depth change over a horizontal grid box exceeds the thickness between two consecutive σ levels at that location (Danabaşoğlu, 2000).

It is assumed not to be forcing (heat and momentum) to the lake and model span up 100 days like real lake simulations. The maximum slope parameter which is estimated using following formula,

$$r = \frac{\delta H}{2\overline{H}} \tag{6.1}$$

where $0 < r < 1$. Here δH, is the difference in adjacent cell depths and $\overline{H}$ is the mean of the depth and the calculated maximum value of the slope parameter are 0.486.

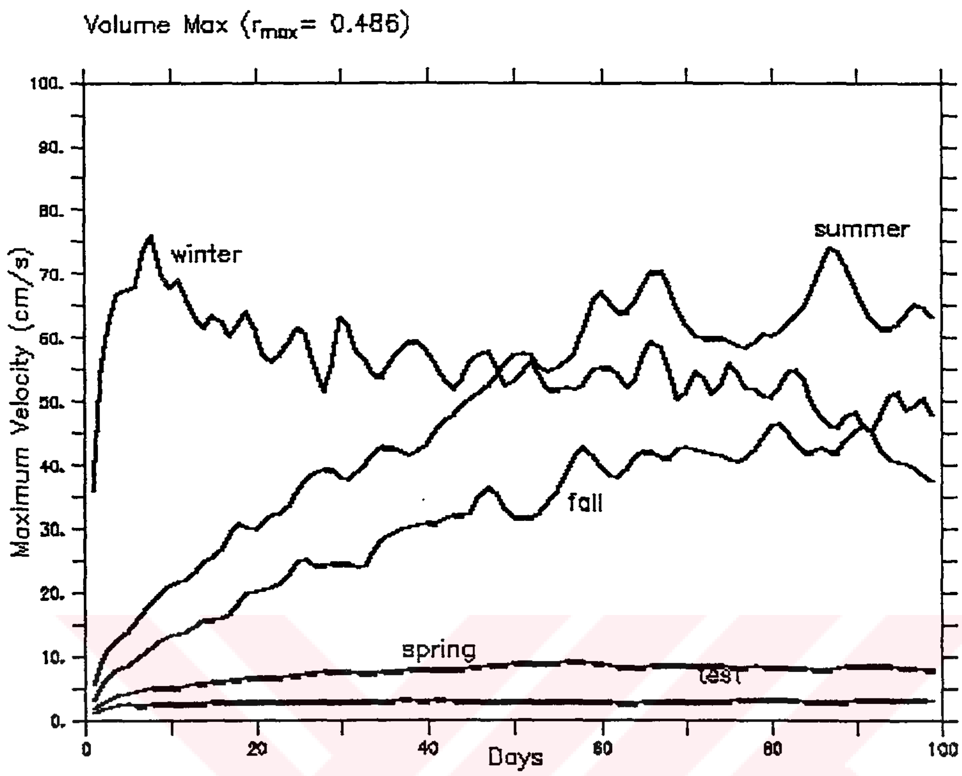

Figure 6.1 Time series of the maximum velocities (cm/s)

The last day of the test simulation is used to estimate pressure gradient error in the real lake simulation. Stream function of the test simulation compared with seasonal ones.

The time series of the maximum velocity and turbulence kinetic energy plots show that effect of the pressure gradient error is the highest amount in the spring simulation. The error ratio in the spring case is about %30 of the estimated value but error is much more less in other seasonal real lake simulation such as fall, summer and winter. In these cases, error is about %5 percent (see Fig. 6.1).

The error is relatively large from the beginning of the simulation. Figure 6.2 shows the time evolution of the maximum turbulence kinetic energy and the kinetic energy rapidly goes down after 10 days in winter simulation because of the net heat loss of the lake. On the other hand, the error becomes larger in the course of time in winter case. The vertical structure of the mixing is characterized by the production of turbulent kinetic energy which is related to the vertical shear profile.

The result of the spring simulation is much more sensitive to pressure gradient error and the results depend on the magnitude of the error but a small error in computing either term near step topography can result in a large error in the total pressure gradient force (Haney, 1991).

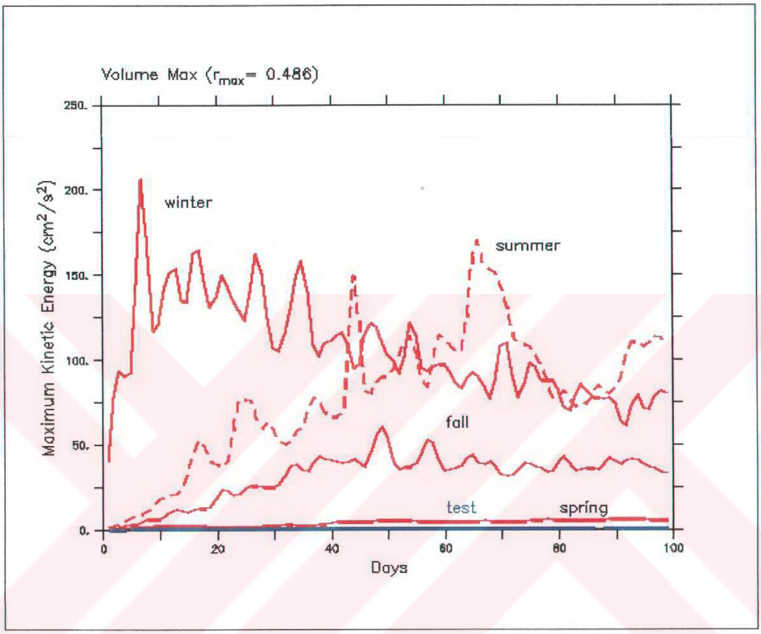

Figure 6.2 Time series of the maximum turbulence kinetic energy (cm^2/s^2)

It is clear that, near step topography error terms are larger. The deepest region of the Lake Van has also largest topographic slopes (Tatvan and Deveboynu basin) and the pressure gradient error becomes intense in these regions.

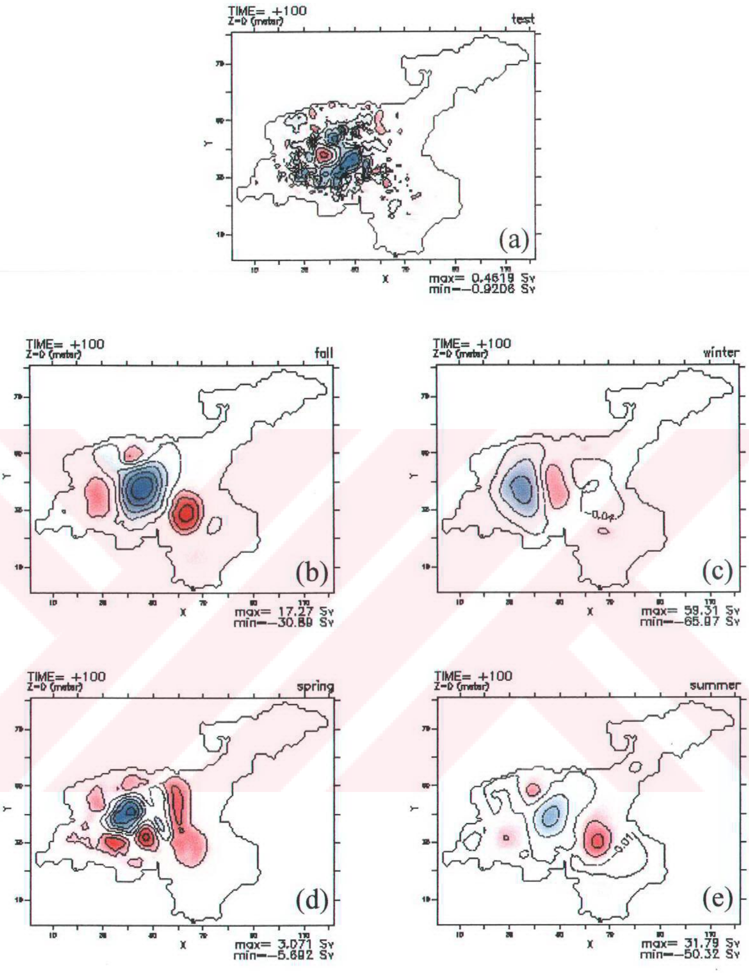

Figure 6.3 Stream function of the season and test cases after 100 days.

Stream function of the seasons and non-forcing test case show the maximum pressure gradient error regions (Fig. 6.3 a-e). Magnitude of the error can be neglect in seasonal simulations except spring (Fig. 6.3).

6.4. Result and Discussion

Each seasonal simulation was started from own initial conditions which is calculated from NMC MRF model dataset and operated for 100 days. The first 10 days was eliminated from analysis and following 90 days was used for calculating average of the variables in order to defining seasonal properties of Lake Van.

The two main cross-section and four points are considered in vertically and temperature profiles will be given this point and cross sections. The location of the points and the cross-sections can be seen in Fig.6.4.

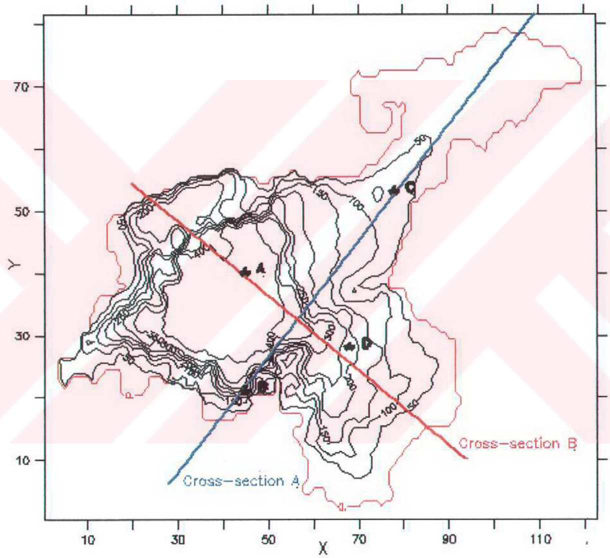

Figure 6.4 Locations of points and cross sections (A) and (B)

The coordinates of the points are A, 45-40, B, 45, 21, C, 78, 53 and D, 68, 28.

The currents are then a result of the combined effects of the thermohaline motions and of the wind driven ones (Pickard, G. L. and Emery, W. J., 1990) and the free surface elevation which is good indicative of upper thermocline circulation (Drakopoulos, P. G., 1999), and it can be used for describe general circulation of the basin.

The blue regions on the surface elevation figures are negative and red regions are positive surface elevation. The negative value represents that cyclonic circulation (anti-clock wise in the northern hemisphere and clockwise in the southern) and positive means that anti-cyclonic circulation.

6.4.1. Fall

The wind is blowing from NNW and its velocity is about 1 m/s in fall. The seasonal average of the air temperature is 19.2 °C and downward longwave heat flux is 303.26 W/m^2, shortwave heat flux, 221.86 W/m^2.

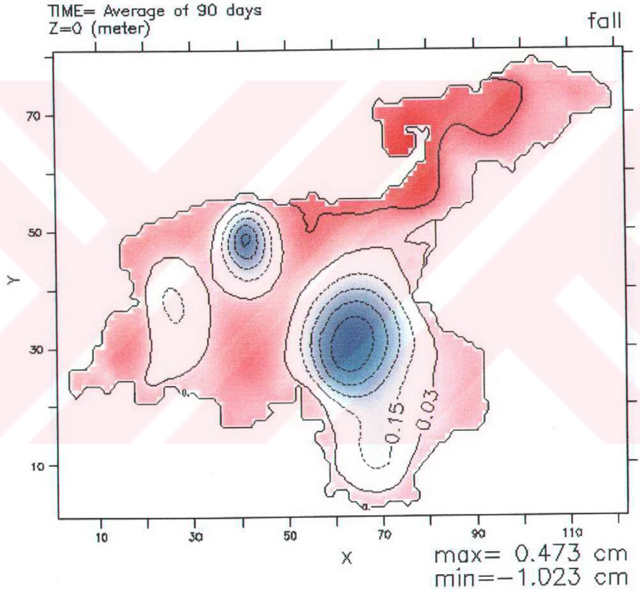

Figure 6.5 The time-averaged free surface elevation in cm (fall)

The free surface elevation for fall condition is shown in Fig.6.5. There is two main circulation region can be seen. One of them is in Deveboynu Basin and the other is Tatvan Basin region. The maximum value of the surface elevation is in the center of the cyclonic circulation and its value is about 1 cm.

The surface circulation pattern can be seen in Fig.6.6 during fall. It is clear that gyres are on the deepest part of the basin and the highest temperature regions because surface elevation depends on wind stress, depth and density. In seasonal simulations, density is only function of temperature (no salinity variations) and wind stress uniformly over the whole region.

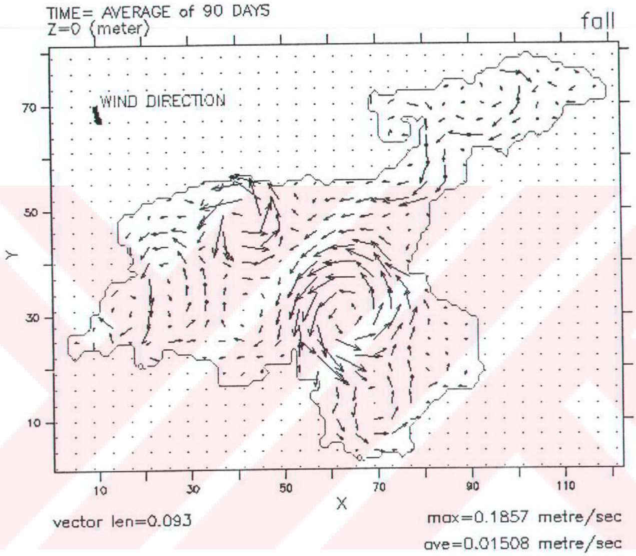

Figure 6.6 The time-averaged surface currents (fall)

There is a flow from Erciş Gulf (north-east region of the Lake Van) to Deveboynu Basin and the cyclonic circulations are observed as presented in Fig.6.6. The maximum velocity of the current is about 19 cm/s and the average value of flow field is 1.5 cm/s.

Figure 6.7 show that vertical structure of the currents in points A-D. It must be a deep flow at 25m in point C and it is the opposite direction of the surface current. In B point, u component of the current changes its direction in spite of the strong bathymetry gradient.

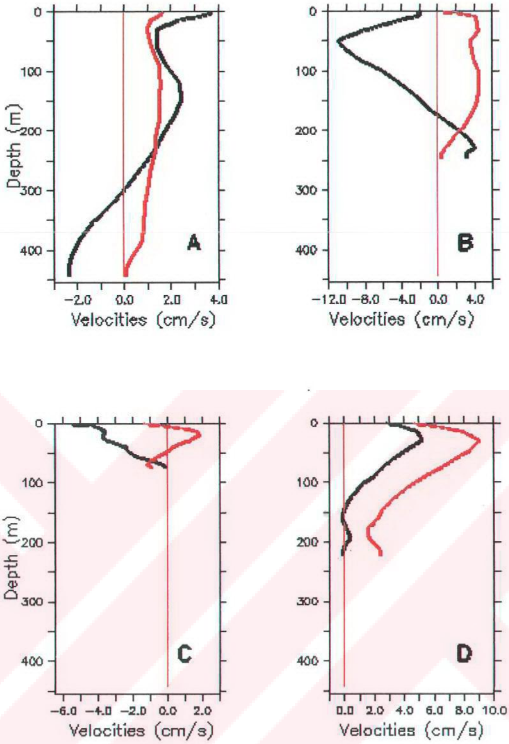

Figure 6.7 The vertical distribution of the current (bold black lines, u component of the current and bold red lines, v component) in fall

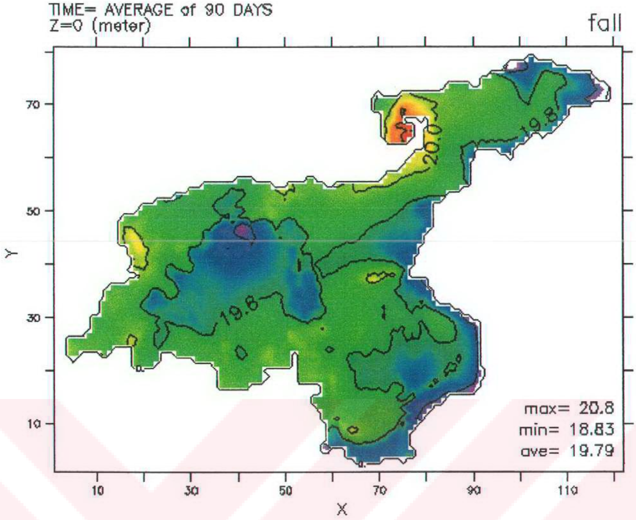

Figure 6.8 The time-averaged surface temperature in fall.

Temperature distribution is horizontally uniform in about 20 °C but in the deepest part of the lake is colder than shallow region (Fig 6.8) but horizontal temperature value is quite higher than the initial value of the lake (12 °C) because of the net heat gain (downward minus upward heat flux). Moreover, it is fairly near to the average atmospheric temperature (~19 °C) in this season.

The overall temperature distribution is controlled by circulation. The much more warmed up shallow regions loss their heat energy because of the circulations and it is transported to much colder region.

Following figures represent temperature distribution in cross-section ***A***. The bold line in Fig.6.9 represents that initial temperature (12 °C) value of the lake. Locations of the cross-section can be seen in Fig.6.4.

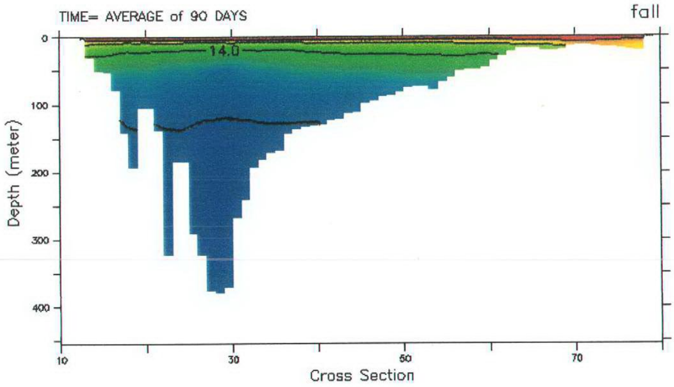

Figure 6.9.The time-averaged temperature distribution in cross section (A) (fall)

The detailed plot of the vertical temperature distribution show closest view of the surface region (Fig.6.10).

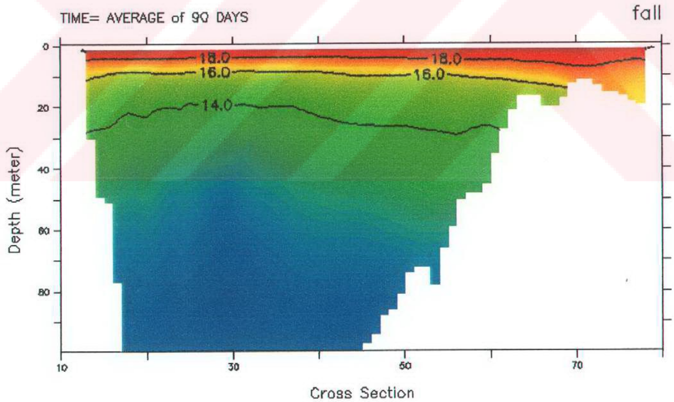

Figure 6.10 Detailed temperature distributions in cross-section A (first 100m)

As the cross-section ***A***, Figure 6.11 and 6.12 show temperature profile of the cross-section ***B***. Both of the cross-sections are similar and the dense cold water lies in less denser warm water.

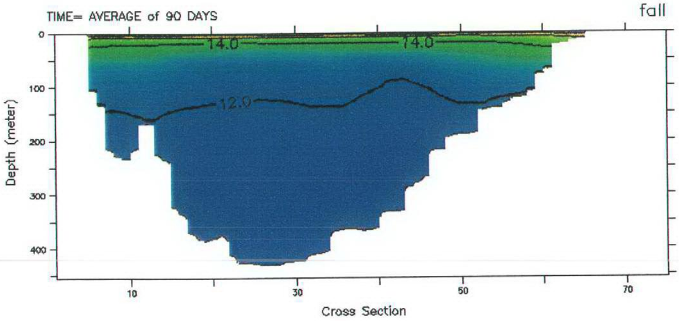

Figure 6.11 The time-averaged temperature distribution in cross section (B) (fall)

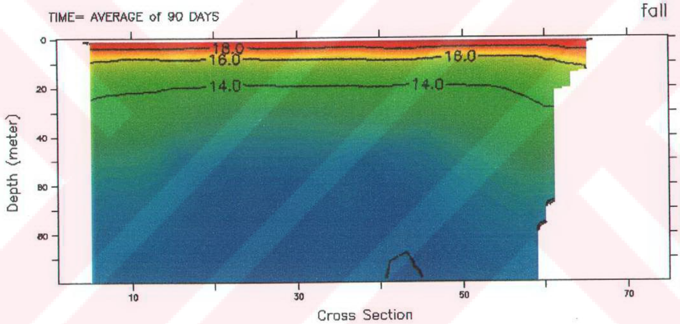

Figure 6.12 Detailed temperature distributions in cross-section B (first 100m)

The first few meters is assumed to be mixed layer (mixed layer or epilimnion; the upper, wind-mixed layer of a thermally stratified lake) and the thermohaline zone reach to 50 m depth (metalimnion; the middle or transitional zone between the well mixed epilimnion and the colder hypolimnion layers in a stratified lake; this layer contains the thermocline, but is loosely defined depending on the shape of the temperature profile) and above this layer hypolimnion (the bottom, and most dense layer of a stratified lake) is found. The mixed layer is the same temperature because of mixing due to wind waves. This can be seen clearly in temperature profiles of sample points (see Fig.6.9 and 6.11).

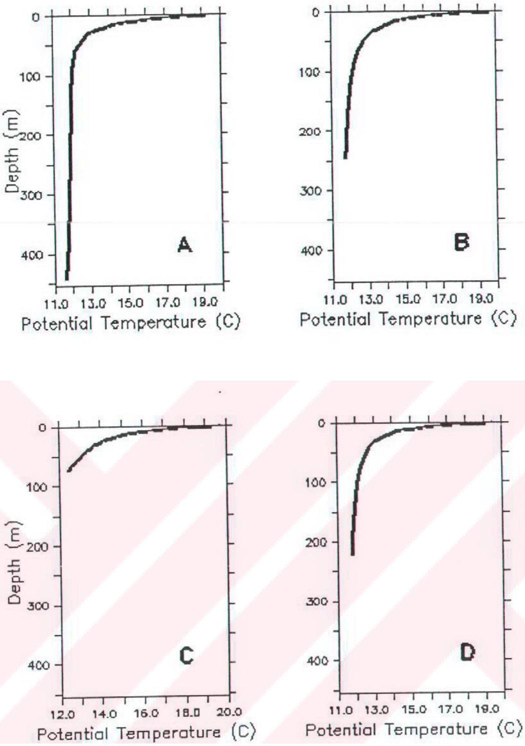

Figure 6.13The time-averaged vertical profiles of the potential temperature in points (fall)

The vertical profiles of the temperature are shown in Fig.6.13. In the fall, surface water becomes as dense as deeper water and sinks. The downward movement of surface water forces deeper water upward and the water begins to circulate, and this is called fall turnover and the circulation is also enhanced by winds. As a result, the vertical mixing increases and mixed layer and thermocline become deeper (Fig. 6.13).

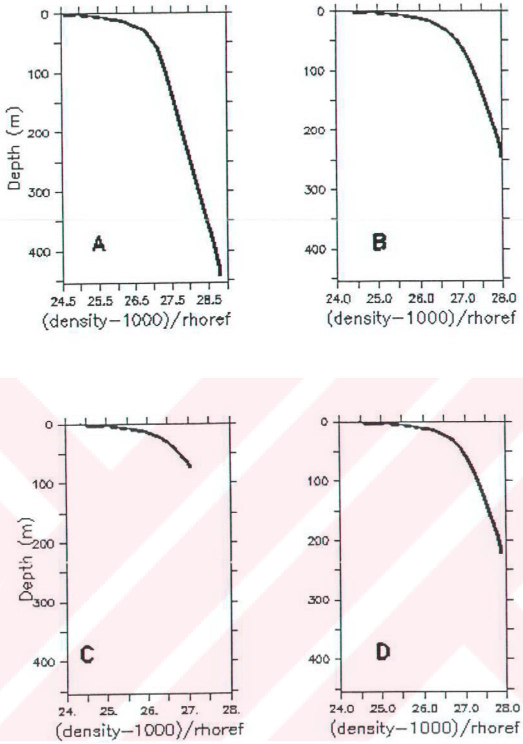

Figure 6.14 The time-averaged vertical profiles of the normalized density in points (fall). The values multiply with 1000.

The vertical profiles of the normalized actual density can be seen in Fig.6.14. The density normally increases as depth increases in Fig.6.14. If the density increases rapidly with depth, called the pycnocline and below this layer density increases more slowly. Pycnocline level is about 25 m for all sample points.

The distribution of the density in the vertical direction is important because it is indicator of the static stability. In fall simulation, the water mass is stable because relatively denser water mass lies under the less dense water mass. The pycnocline layer acts as a partial barrier to mixing of deep and surface water and also as a layer that slows down sinking particles.

6.4.2. Winter

In the winter, the direction of the wind turns to the NNW from NE and the wind speed is increases from 1 m/s to 3 m/s. The downward longwave radiation is increases to 257.08 W/m^2 as air temperature and downward shortwave radiation goes down to 132.84 W/m^2 because of the low sun angle. The seasonal average of the air temperature is about 2 °C.

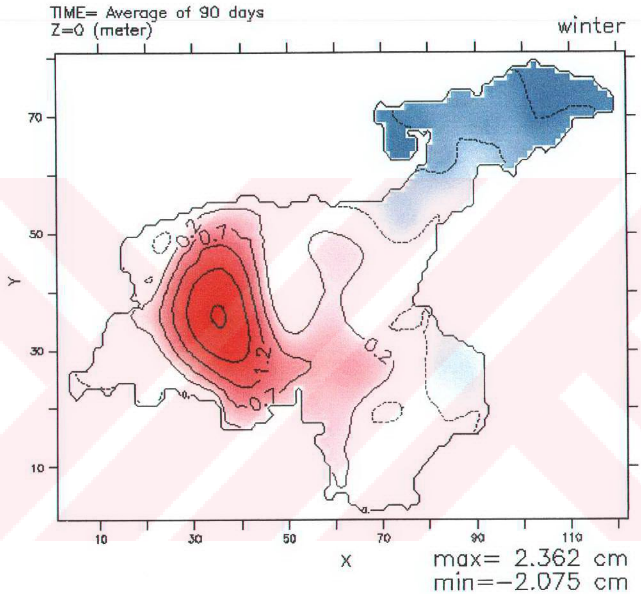

Figure 6.15 The time-averaged free surface elevation in cm (winter)

There is an anti-cyclonic circulation on the contrary of fall and it is located in Tatvan Basin region. Strong winds causes to positive surface elevation which is the highest rate in the middle of the gyre (see Fig.6.15). The maximum surface elevation is 2.3 cm and there is no thermal expansion effect over the surface elevation in winter.

The anti-cyclonic circulation can be seen more clearly in Fig.6.16 which shows the surface current vectors.

The flow to the Erciş Gulf was observed in winter. Unlike fall, direction of the flow is opposite way and much more strong because of the greater wind speed (from 1 m/s in fall to 3 m/s in winter), the greater the frictional force acting on the lake surface causes the stronger the surface current (see Fig.6.16) and there is a weak circulation in Erek Fan region. The average flow speed is about 4 cm/s in the lake but it is the maximum in the gyre region (~ 45 cm/s).

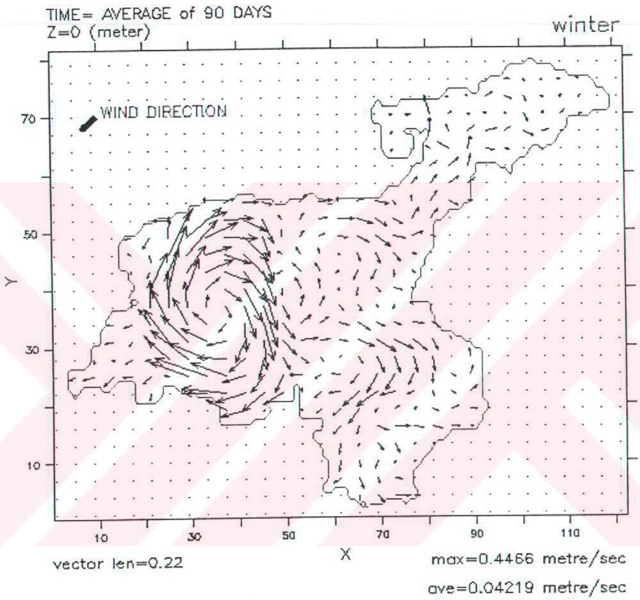

Figure 6.16 The time-averaged surface currents in winter.

Interesting features can be observed in Fig. 6.16 for winter. There is a surface current which is opposite side of the wind direction, throughout the Erek Fan. It is transfer the relatively warm water to the Ercis Gulf which is shallow and cold.

The vertical structure of the currents can be seen in Figure 6.17. The velocities are higher than fall season because of the strong winds and it affects deeper part of the lake. Unlike fall season, in C point direction of the u and v component of current does not change and it is almost homogeny structure.

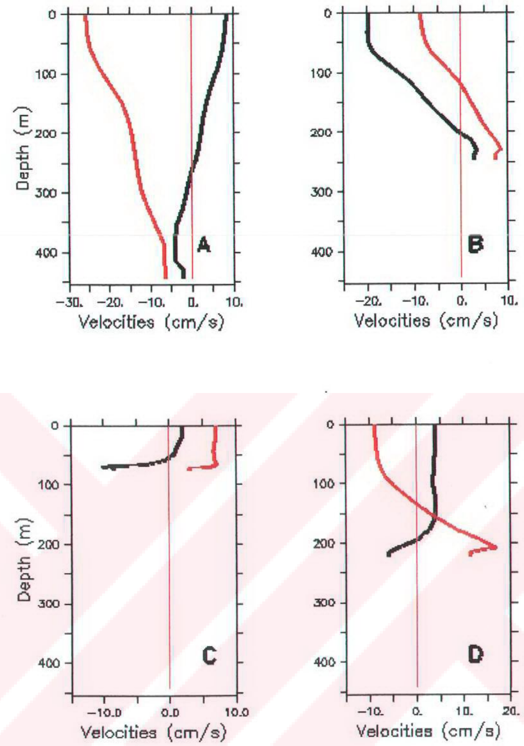

Figure 6.17 The vertical distribution of the current (bold black lines, u component of the current and bold red lines, v component) in winter

The depth of frictional influence (the depth at which the water velocity is opposite to the surface velocity) is taken as a measure of the depth to which the surface wind stress affects water motion and it is in the deeper than fall season (Fig.6.17).

For the real lake simulations, density only is a function of temperature because salinity is constant and there is no water inflow with precipitation and outflow with evaporation (*VFLUX*=0). The circulation can be divided into two parts, the thermohaline and wind driven components. To obtain information about the reason of the circulation this two components must be study. The gyre must be the superposition of these two components.

The horizontal temperature distribution of the lake is different from fall case. In winter, the net heat budget is negative value and lake is start to getting cold. The coldest parts of the lake are shallow regions such as Erciş Gulf and Eastern Fan.

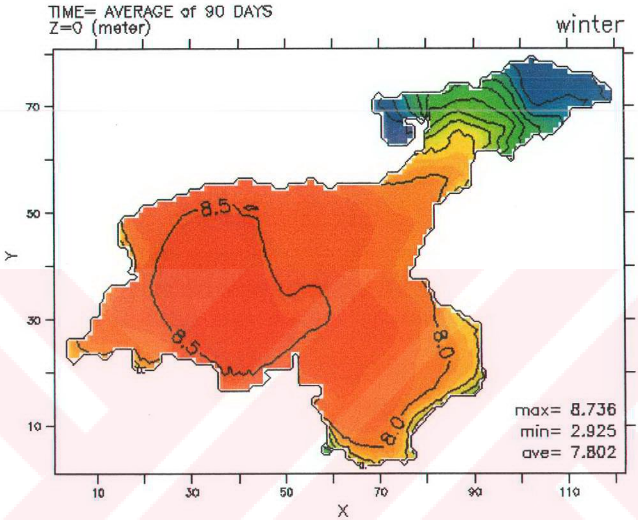

Figure 6.18 The time-averaged surface temperature in winter.

The average temperature of the lake surface is about 7.8 °C and the maximum value is ~ 9 °C which is the center of the gyre (Fig.6.15 and 6.16). The coldest part of the lake is Ercis Gulf region in which surface temperature is 3 °C (Fig.6.18).

The following figure show that the vertical cross-section of the temperature distribution in Lake Van (Fig.6.19). The vertical distribution of the heat is almost uniform.

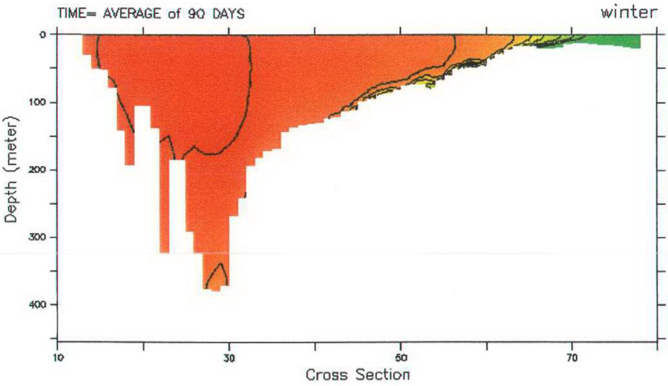

Figure 6.19 The time-average temperature distribution in cross section (A) (winter)

It is shown that detail of the cross-section ***A*** (Fig.6.20).

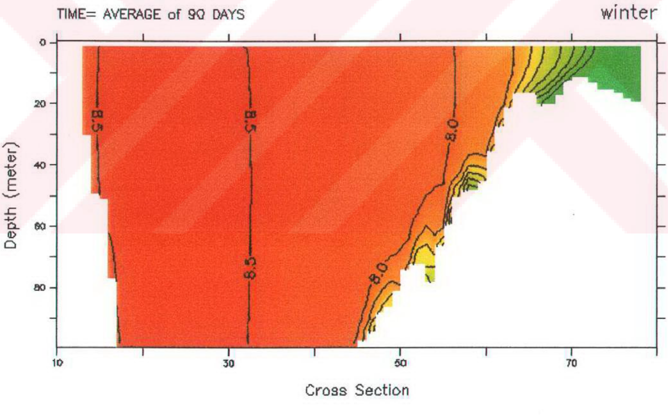

Figure 6.20 Detailed temperature distributions in cross-section A (first 100m)

The cold and denser water sink into the deepest part of the lake (Fig 6.20) because the shallow region becomes colder and the density difference occurs.

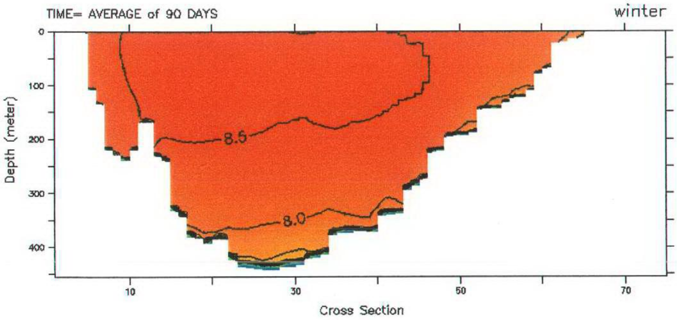

Figure 6.21 The time-average temperature distribution in cross section (B) (winter)

The vertical profiles of the temperature are shown in Fig.6.22. Otherwise the fall simulation, stratification does not appear in winter. The mixed layer can be seen more clearly than fall season. All lake is mixed and temperature differences between upper and lower levels are small.

In fact that surface temperature low and the mixed layer is deep in winter. It is typically the warmest layer in the winter lies in hypolimnion.

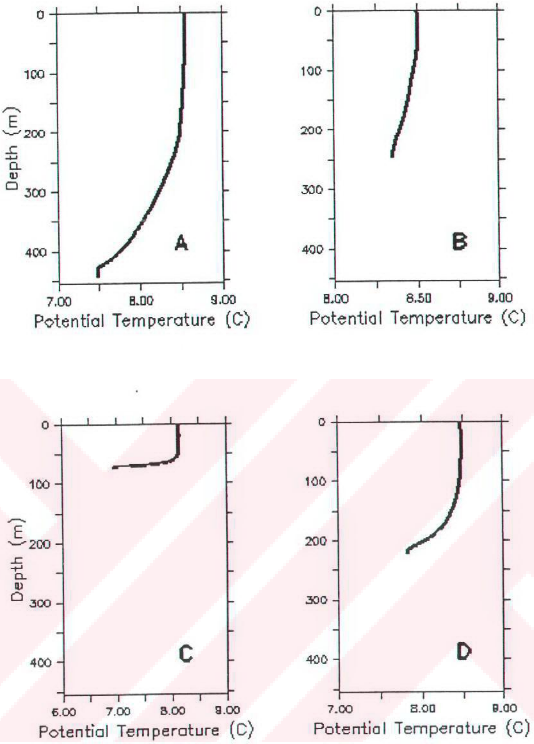

Figure 6.22 The time-averaged vertical profiles of the potential temperature in points (winter)

In the winter, cooling of surface waters increases their density and they sink. Continued cooling creates an isothermal water column. This water column is well mixed and there is no seasonal thermocline (isothermal). This mixing continues until surface freezes but there is no evidence to freezing in the Lake Van. This phenomenon can be seen in Fig.6.22.

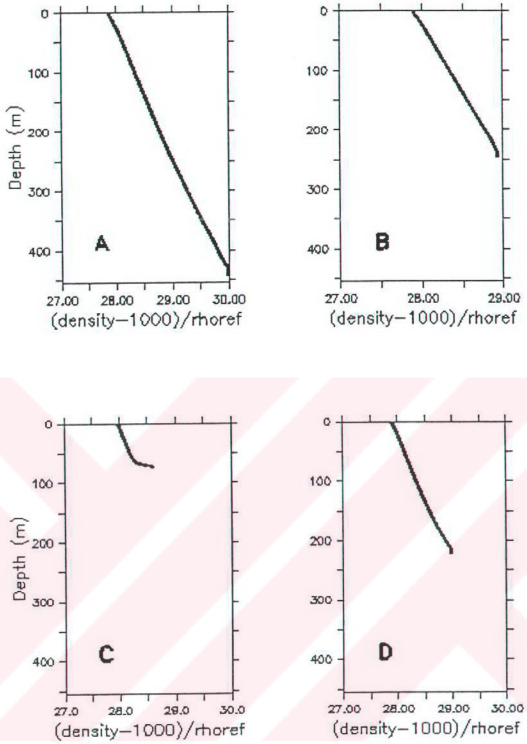

Figure 6.23 The time-averaged vertical profiles of the normalized density in points (winter). The values multiply with 1000.

There is a much smaller increase of density with depth than in fall and the seasonal pycnocline is less evident (Fig 6.23). The density of lake is increasing rapidly until bottom of the lake (no shear at the pycnocline).

6.4.3. Spring

The wind blowing from ENE direction and it is seasonal average is 3.2 m/s. The downward longwave heat flux is 279.05 W/m^2 and downward shortwave flux, 290.70 W/m^2. The seasonal average of the air temperature is 10 °C.

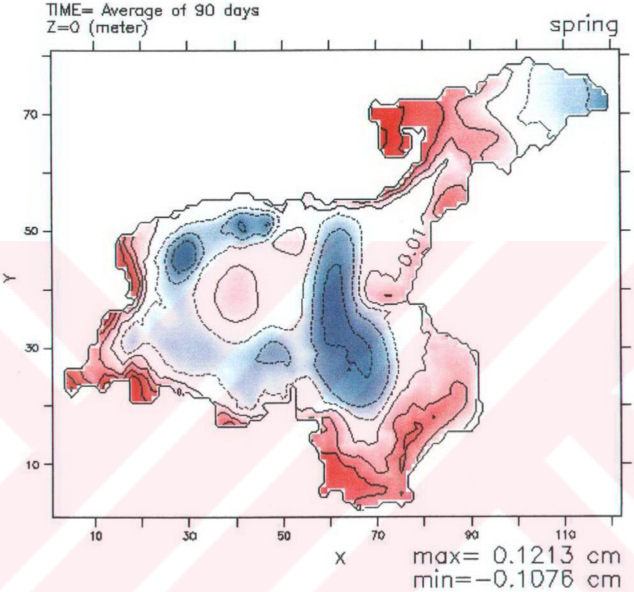

Figure 6.24 The time-averaged free surface elevation in cm (spring)

Surface elevation show that the gyres which can be observed in winter, have not appear in spring. The general flow field does not exist in this season (see Fig.6.24) but there is a weak cyclonic circulation in Erek Fan-Deveboynu Basin region. The maximum surface elevation is 0.12 cm.

Surface currents can be seen in Fig.6.25. The strong anti-cyclonic circulations in winter weaken and disappear in spring. The maximum current speed is 4.5 cm/s and the average value is 0.4 cm/s.

The highest wind speed is in spring and this must be cause more strong currents in the lake but the current velocities is less than previous season.

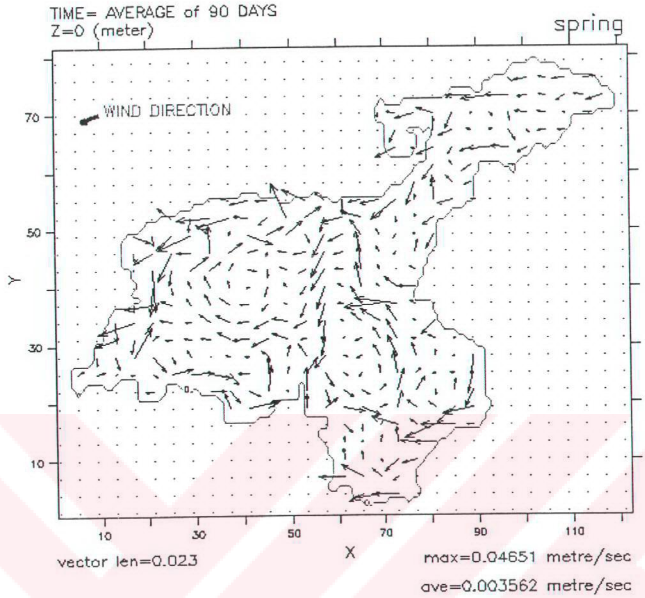

Figure 6.25 The time-averaged surface currents in spring.

It fact that the winds and currents are intimately related but the reason of the circulation is not only wind-driven, it also effected from horizontal temperature distribution of the lake. In spring simulation, the lake is vertically uniform (temperature and density distribution) and the temperature effect is not exist.

Fig.6.26 shows vertically profile of the u and v component of current. The velocities of the current components are 10 times lower than the winter case in spite of strong wind. In addition, it is behavior is chaotic.

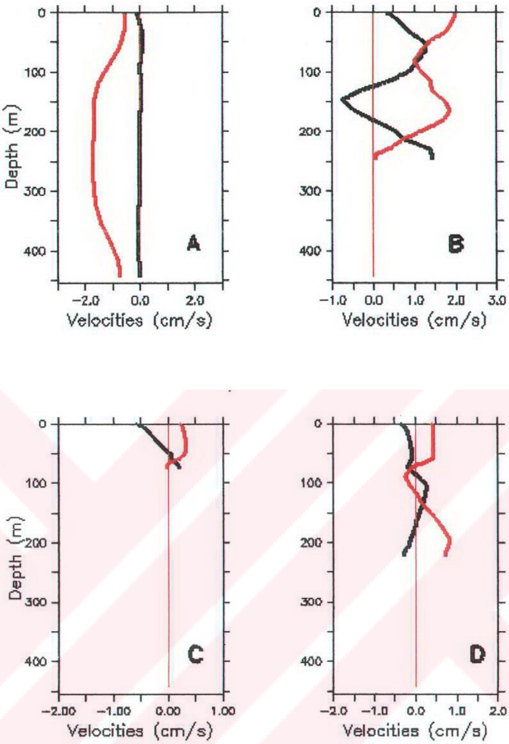

Figure 6.26 The vertical distribution of the current (bold black lines, u component of the current and bold red lines, v component) in spring

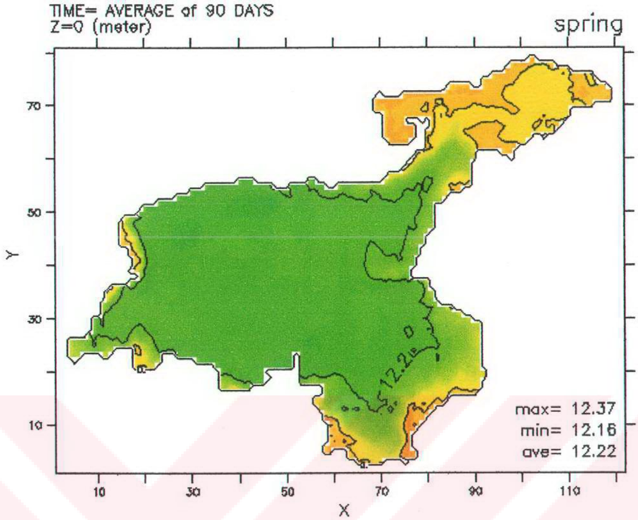

Figure 6.27 The time-averaged surface temperature in spring.

In spring, temperature distribution over lake is uniform structure and the average value is 12.3 °C (Fig 6.27). There is a little net heat gain but it is not sufficient to create a big temperature differences in the lake. The vertical structure of the temperature is same as horizontal, but the 12 °C isotherm is in the range from the 150-200 m.

After winter, the temperature and density of lake water becomes similar from top to bottom. The uniform water density allows the lake to mix completely, recharging the bottom water with oxygen and bringing nutrients up to the surface. This is called spring overturn

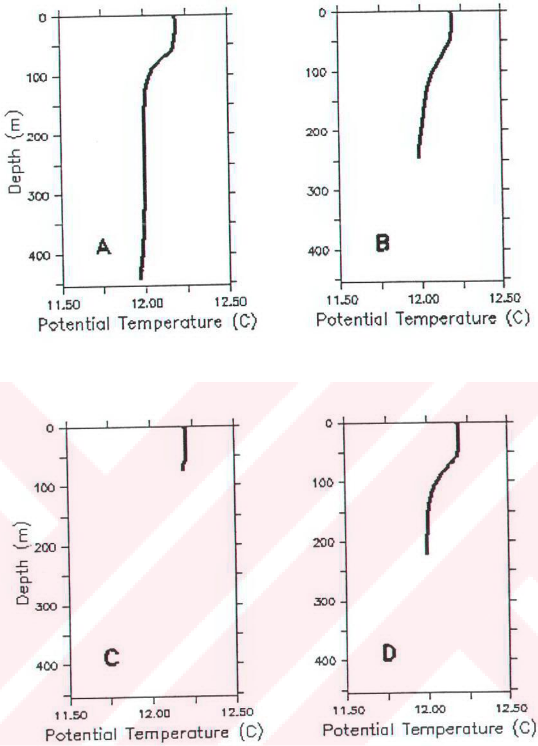

Figure 6.28 The time-averaged vertical profiles of the potential temperature in (A-D) (spring)

The time-averaged vertical temperature distribution in sample points can be seen in Fig.6.28. The vertical profile of potential temperature show that uniform distribution form surface to bottom of the lake in spring.

The vertical temperature distribution is an indicator of the mixing process. In the spring, stratification is weak and there is still mixing in the lake but at the end of the spring the thermal stratification becomes strong and mixing stops.

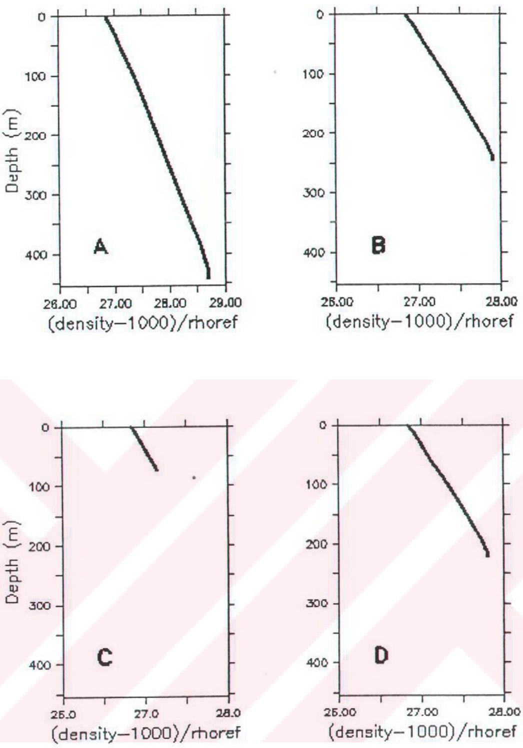

Figure 6.29 The time-averaged vertical profiles of the normalized density in points (spring). The values multiply with 1000.

The density decreases rapidly as depth increases all the point (Fig 6.29). The water is static stable in this season. There is no pycnocline layer. Temperature and density distribution are harmonious in vertically.

6.4.4. Summer

In summer, wind is blowing from WNW, 1.2 m/s. The direction is same with spring but it is much lighter. There is net heat gain in this season and downward longwave heat flux is 357.10 W/m^2 and shortwave heat flux is 368.96 W/m^2. Average air temperature is 29 °C during summer.

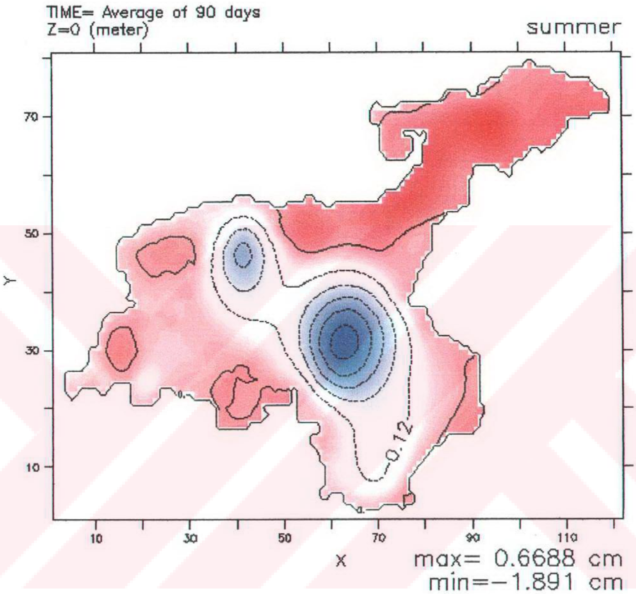

Figure 6.30 The time averaged surface elevation in summer.

The two gyres can be observed in the lake (Fig.6.30) and this two cyclonic circulation region become stronger at the end of the summer (in fall season). Deveboynu and Tatvan basin are the location of the gyres. The maximum surface elevation in the center of gyre and its value is about 2 cm.

The gyres can be seen more clearly in Fig.6.31. The maximum current speed is 27 cm/s and the average value of it is 2 cm/s. There is a flow from Erciş Gulf to Tatvan basin throughout Erek fan. The direction of the flow is same with fall season simulation but in winter this direction is opposite (See Fig.6.31, 6.16 and 6.6).

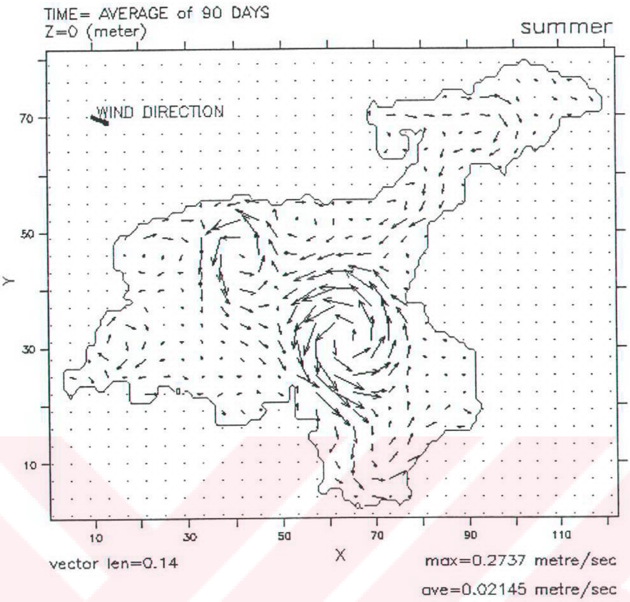

Figure 6.31 the time averaged surface currents in summer.

The reason of the changing flow direction must be related with wind direction. In winter, wind blowing from NE and the flow direction is to the Erciş Gulf but in summer the wind is almost opposite direction and the direction of the current to the Tatvan Basin.

In fall and spring, flow pattern is same as between winter and summer but the velocity of the currents much smaller.

The following figure represent that the vertical structure of the current in chosen sample points (Fig.6.32). The flow which is the throughout Erek Fan, can be seen in Fig.6.32 C. The surface current changes its direction as depth increases.

The velocity of the current is larger than simulation of the spring season. It must be increased wind speed and downward radiation because both of them apply forcing (heat and momentum) into the lake and it is transform into mechanical energy in order to conservation of the energy.

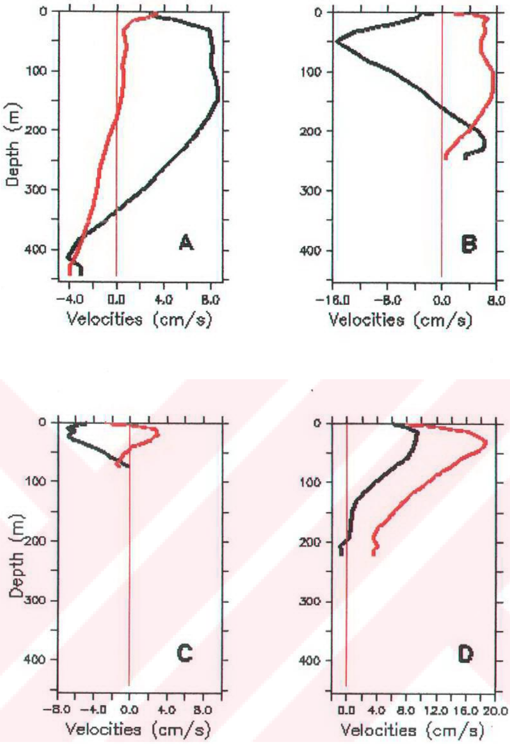

Figure 6.32 The vertical distribution of the current (bold black lines, u component of the current and bold red lines, v component) in summer

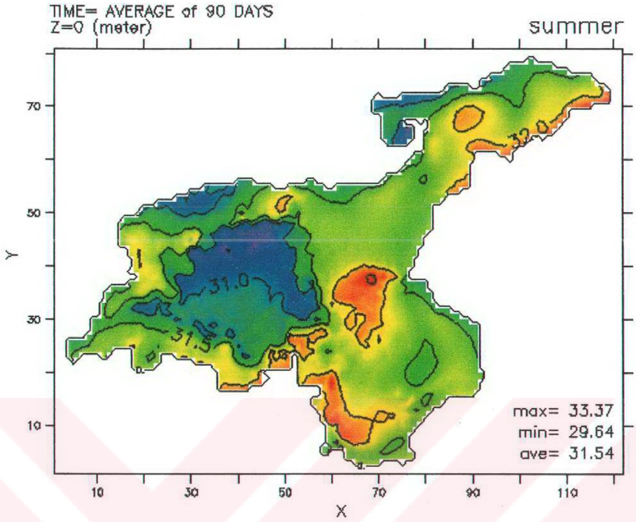

Figure 6.33 The time-averaged surface temperature in summer.

The lake surface temperature varies form 30 °C to 33 °C (Fig 6.33). The south-east shore of the lake is warmer because of the wind introduced currents. The deep part of the lake is a little colder than the shallow regions.

Following figures show the potential temperature profiles in cross-section A and B (Fig.6.34, 35, 36 and 37). The stratification can be seen more clearly form figures. The isotherm of initial temperature of the lake (12 °C) is in the 150m depth.

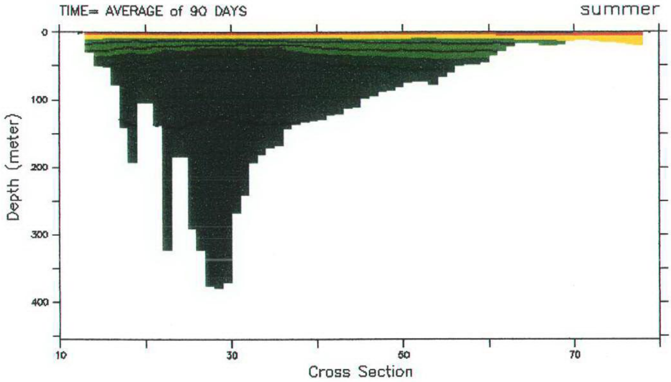

Figure 6.34 The time-average temperature distribution in cross section (A) (Summer)

Strong stratification can be seen in Fig.6.35 and 6.36.

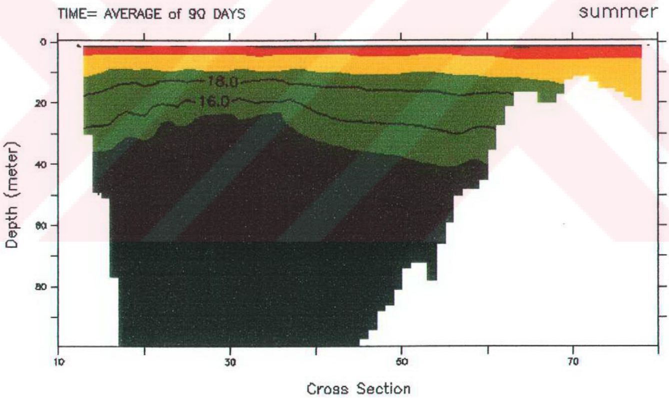

Figure 6.35 Detailed temperature distributions in cross-section A (first 100m)

The temperature distribution of cross-section B same as A and 12 °C isotherm lies in 150 m depth.

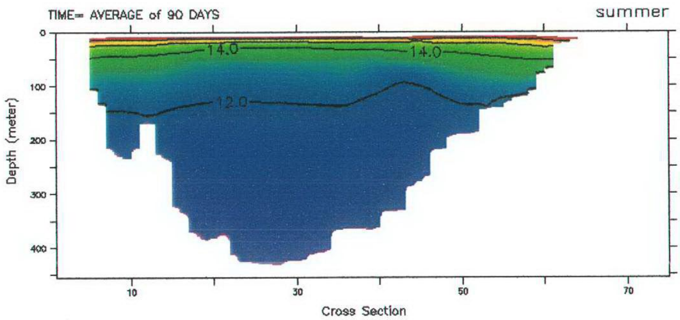

Figure 6.36 Average temperature distribution for cross-section B (Summer)

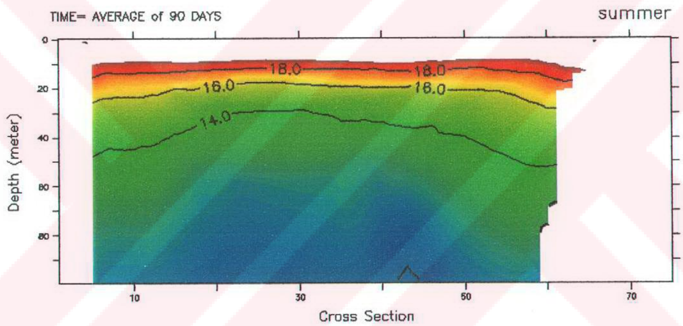

Figure 6.37 Detailed temperature distributions in cross-section B (first 100m)

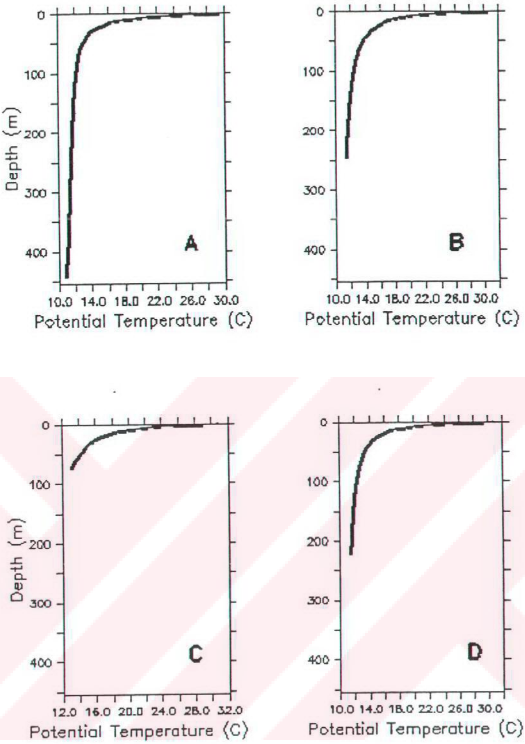

Figure 6.38 Vertical profiles of the potential temperature in A-D (Summer)

The lake becomes highly stratified and vertical mixing practically stops because of the warm surface layer (less dense). The mixed layer is very shallow and thermohaline layer is very thick.

The surface mixing layer is too thick and the thermohaline level is about 20 m depth in all of the sample points (Fig 6.38). Above the thermohaline, temperature continues to decreases slowly.

As a result, there is a thermal discontinuity between the epilimnion and hypolimnion and in this layer temperatures rapidly changes.

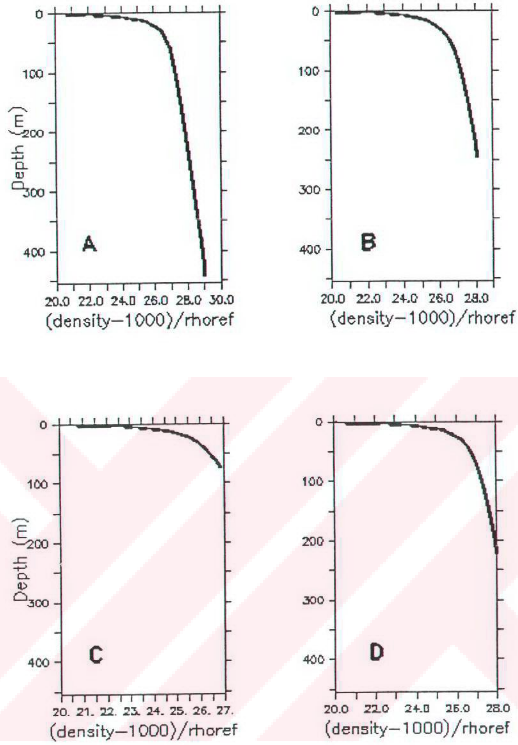

Figure 6.39 The time-averaged vertical profiles of the normalized density in points (summer). The values multiply with 1000.

As the surface waters warm, they also become less dense than the water below. This density difference soon becomes sufficient to prevent circulation within the water column and the lake is divided into three regions (Fig 6.39).

The pycnocline level is in the same level with thermohaline and the density grows with depth.

6.5. Comparison with the NOAA AVHRR data

In this section, SST data of the Lake Van which is estimated of monthly with NOAA AVHRR image from February 1988 to January 1999 (Sari, M et al., 2000) are compared with seasonal lake surface temperature data calculated with POM model.

Following table shows monthly minimum, maximum and average water surface temperature of the Lake Van (Table 6.1).

Table 6.1 NOAA AVHRR Data (Water Surface Temperature) from (Sari, M. et al., 2000)

		NOAA AVHRR Data			
Season	Month	Min	Max	Ave	Error ±
WINTER	Dec.	6,60	9,70	8,50	0,73
	Jan.	3,60	7,70	6,13	0,98
	Feb.	-1,00	2,90	2,46	0,38
SPRING	March	3,10	7,30	4,24	0,83
	April	6,80	13,50	9,51	0,96
	May	9,60	14,90	11,48	0,87
SUMMER	June	13,50	17,70	15,46	0,98
	July	19,10	22,40	20,64	1,13
	Aug.	18,40	22,40	21,34	0,54
AUTUMN	Sept.	19,30	22,40	20,86	0,71
	Oct.	12,00	16,10	14,82	0,86
	Nov.	7,90	12,20	10,87	1,25
AVERAGE	Winter	3,07	6,77	5,70	0,70
	Spring	6,50	11,90	8,41	0,89
	Summer	17,00	20,83	19,15	0,88
	Autumn	13,07	16,90	15,52	0,94

The seasonal averages of the AVHRR data are used for estimating differences with POM model results. The next table shows the seasonal average POM data and the difference (Table 6.2).

Table 6.2 Comparison of the AVHRR and POM Lake Surface Temperature (unit °C)

	NOAA AVHRR Data			POM Model Data			Differences (AVHRR-POM)		
	Min	Max	Ave	Min	Max	Ave	Min	Max	Ave
Winter	3,07	6,77	5,70	2,93	8,74	7,80	0,14	-1,97	-2,11
Spring	6,50	11,90	8,41	12,16	12,37	12,22	-5,66	-0,47	-3,81
Summer	17,00	20,83	19,15	29,64	33,37	31,54	-12,64	-12,54	-12,39
Autumn	13,07	16,90	15,52	18,83	20,80	19,79	-5,76	-3,90	-4,27

The lake surface temperatures are higher than the AVHRR data for all of the seasonal simulation results. This could be given initial temperature of Lake Van at the beginning of the seasonal simulations (12 °C).

If the previous season average of lake surface temperature used in the seasonal simulations of POM, the results would be much closer to AVHRR data but during seasonal simulations the AVHRR data are unavailable and an average value was used in simulations.

The highest differences are in the summer season and it is reach to 12 °C and the minimum ones are in winter simulation case. This must be seasonal thermal stratification of the lake. In summer, the lake is stratified and there is no mixing. As a result, the thermal energy is forced to be thin layer of the lake (only 10-20 m). However, there is no stratification in winter and the vertical mixing exists in the lake and the thermal energy becomes diffused to whole lake volume.

The current, depth and rivers have an effect over the surface temperature distribution in the Lake Van (Sari, M et al., 2000). This result is appropriate with seasonal model simulations (see seasonal result of the POM).

Unfortunately, the complete absence of appropriate measurements does not allow a more accurate evaluation of these simulations.

6.6. Future works

First of all the pressure gradient and hydrostatic inconsistency problem will be solved using techniques which is explained in Chapter 4. The subtracting reference density is used partially in POM but other techniques are tried for reduced error. It is studied for implementation of new high order scheme by designer of model.

To simulating seasonal behavior of the Lake Van much accurate the NOAA AVHRR data will be used as an initial condition.

The effects of rivers can be included into model because the fresh water flux and heat transfer with river are affected hydrodynamic structure of the Lake Van.

The atmospheric model can be used for creating initial and time dependent boundary condition of the POM. Coupled Atmosphere-Ocean model can be studied.

Inverse Ocean modeling techniques can be used for defining seasonal structure of the Lake Van and NOAA AVHRR data can be used for this aim.

REFERENCES

Ahsan, A. K. M. Q. and Blumberg, A. F., 1999.Three-dimensional hydrothermal model of Onondaga Lake. *Journal of Hydraulic Engineering*, **125**, 912-923.

Beletsky, D., O'Connor, W. P., Schwab, D. J., and Dietrich, D. E., 1997. Numerical Simulation of Internal Kelvin Waves and Coastal Upwelling Fronts. *Journal of Physical Oceanography*, **27**, 1197-1215.

Blumberg, A. F. and Mellor, G. L., 1978.A coastal ocean numerical model. *Mathematical Modeling of Estuarine Physics Proc. Int. Symp.*, 203-214.

Blumenthal, M. M., Kaaden, V. D., and Voldavetz, V. I., 1964.Catalogue of the active volcanoes of the world including sofatara fields. Part XVII Turkey and Caucasus. *International Association of Volcanology*, 23.

Bonnet, M. P., Poulin, M., and Devaux, J., 2000. Numerical modeling of thermal stratification in a lake reservoir. Methodology and case study. *Aquatic Sciences*, **62**, 105-124.

Botte, V. and Kay, A., 2002. A Model of the wind-driven circulation in Lake Baikal. *Dynamics of atmospheres and oceans*, **35**, 131-152

Chen, C., Ji, R., Schwab, D. J., Beletsky, D., Fahnenstiel, G. L., Jiang, M., Johengen, T. H., Vanderploeg, H., Eadie, B., Budd, J. W., Bundy, M. H., Gardner, W., Cotner, J., and Lavrentyev, P. J., 2002. A Model study of the coupled biological and physical dynamics in Lake Michigan. *Ecological Modeling*, **152**, 145-168.

Chubarenko, B. V., Wang, Y., Chubarenko, I. P., and Hutter, K., 2001. Wind-driven current simulations around the Island Mainau (Lake Constance). *Ecological Modeling*, **138**, 55-73.

Danabaşoglu, G. and McWilliams, J. C., 2000. An Upper Ocean Model for Short-Term Climate Variability. *Journal of Climate*, **13**, 3380-3411.

Degens, E. T. and Kurtman, F., 1978. The Geology of Lake Van. Vol. 169, The Geology of Lake Van, The Mineral Research and Exploration Institute of Turkey, 158 pp.

Haney, R. L., 1991. On the Pressure Gradient Force over Steep Topography in Sigma Coordinate Ocean Models. *Journal of Physical Oceanography,* **21**, 610-619

Hartmann, D. L., 1994. Global Physical Climatology. Vol. 56, International Geophysical Series, Academic Press, 411 pp.

Heinrich, J., Paul, J., and Lick, W., 1981. Temperatures and Currents in a stratified lake: A two dimensional analysis. *Journal of Great Lakes Research,* **7**, 264-275.

Hodges, B. R., Imberger, J., Laval, B., and Appt, J., 2000. Modelling the Hydrodynamics of Stratified Lakes. *HydroInformatics 2000 Conference*, 1-14.

Hutter, K., 1984. Hydrodynamics of lakes. Springer-Verlag, viii, 341 pp.

Pickard, G. L., and Emery, W. J., 1990. Descriptive Physical Oceanography, An Introduction, 5th edition.. Butterworth Heinemann, 320 pp.

Kadıoğlu, M., Şen, Z., and Batur, E. R., 1997. The greatest soda-water lake in the world and how it is influenced by climatic change. *Annales Geophysicae*, **15**, 1489-1497.

Kelley, J. G. W., Hobgood, J. S., Bedford, K. W., and Schwab D. J., 1998. Generation of Three-Dimensional Lake Model Forecasts for Lake Erie. *Weather and Forecasting*, **13**, 659-687.

Kempe, S., Khoo F., and Gürleyik Y., 1978. *Hydrography of Lake Van and Its Drainage Area*. Vol. 169, The Mineral Research and Exploration Institute of Turkey, 30-44 pp.

Mellor, G. L., 2003: User Guide to A Three-Dimensional, Primitive Equation, Numerical Model. June 1998 ed. 41 pp.

Mellor, G. L., 1991: An equation of state for numerical models of ocean and estuaries. *Journal of Atmospheric and Oceanic Technology*, **8**, 609-611

Mellor, G. L., Oey L. Y., and Ezer, T., 1998. Sigma Coordinate Pressure Gradient Errors and the Seamount Problem. *Journal of Atmospheric and Oceanic Technology*, **15**, 1122-1131

Mellor, G. L., Hakkinen S., Ezer T., and Patchen R., 2000. A generalization of a sigma coordinate ocean model and an intercomparison of model vertical grids, In: Ocean Forecasting: Theory and Practice, N. Pinardi (Ed.), Springer-Verlag, In Press, 2000.

Manshutkin, V. V., Astrakhantsev, G. P., Yegorava, N. B., Rukhovets, L. A., Simo, T. L., and Petrova, N. A., 1998. Mathematical modeling of the evolution and current conditions of the Ladoga Lake ecosystem. *Ecological Modeling*, **107**, 1-24.

Sarı, M., Polat, I., Saydam, A. C., 2000. The Observation of Annual Variation of Surface Temperature of The Lake Van by NOAA AVHRR Satellite Images. *Doğu Anadolu Bölgesi IV. Su Ürünleri Sempozyumu, 28-30 June 2000, Erzurum, Sempozyum Kitabı,* 825-842 pp

Song, T. Y., 1998. A General Pressure Gradient Formulation for Ocean Models, Part I: Scheme design and Diagnostic Analysis. *Monthly Weather Review*, **126**, 3213-3230

Şen, Z., Kadıoğlu, M., and Batur, E. R., 2000. Stochastic Modelling of the Van Lake Monthly Level Fluctuations in Turkey. *Theoretical and Applied Climatology*, **65**, 99-110.

Taguchi, K., Nakata, K., 1998. Analysis of water quality in Lake Hamana using a coupled physical and biochemical model. *Journal of Marine Systems*, **16**, 107-132.

Tsvetova, E. A., 1999 Mathematical modeling of Lake Baikal hydrodynamics. *Hydrobiologia*, **407**, 37-43

Wang, Y., and Hutter, K., 2002. Methods of substructuring in lake circulation dynamics. *Advances in Water Resources*, **23**, 399-425

Wong, H. K., and Degens, E. T., 1978. The Bayhymetry of Lake Van, Eastern Turkey. Vol. 169, The Mineral Research and Exploration Institute of Turkey, 6-10 pp.

APPENDIX A

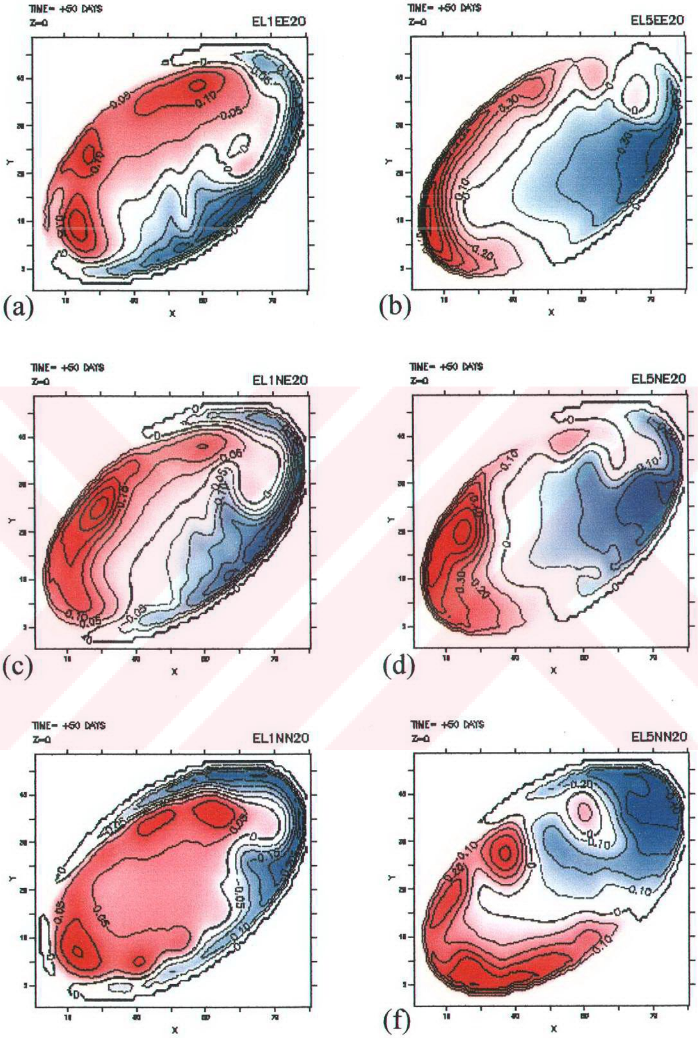

Appendix A.1 Free Surface Elevation after 50 days in ellipsoid, Latent + Sensible 20 W/m²

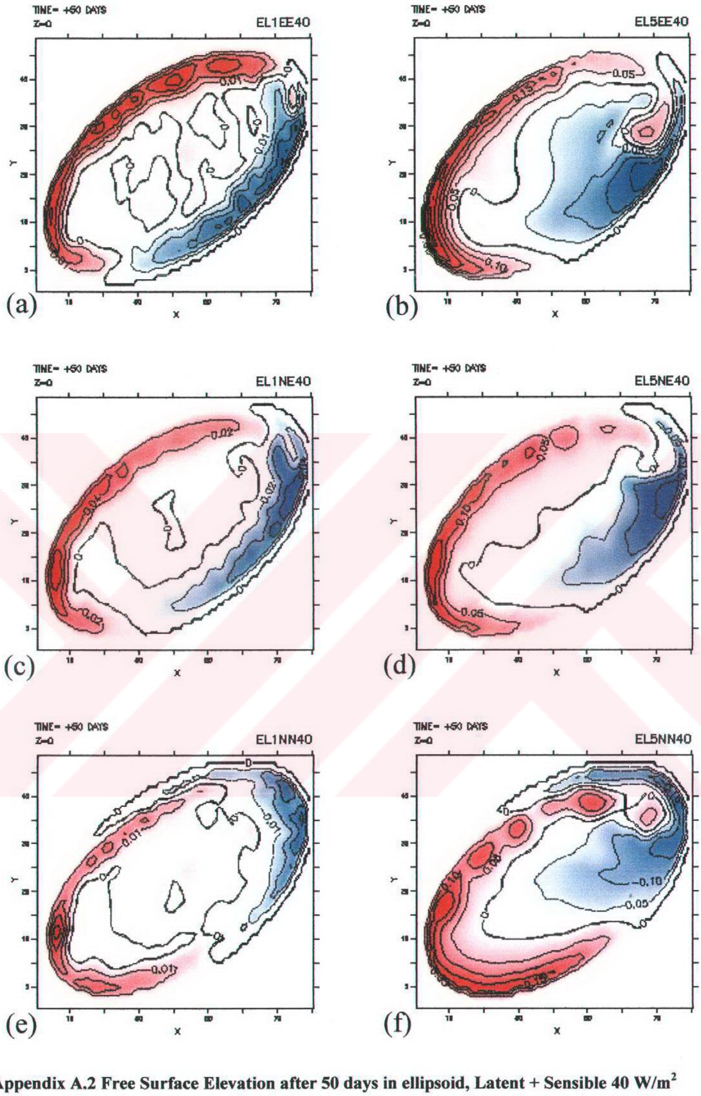

Appendix A.2 Free Surface Elevation after 50 days in ellipsoid, Latent + Sensible 40 W/m^2

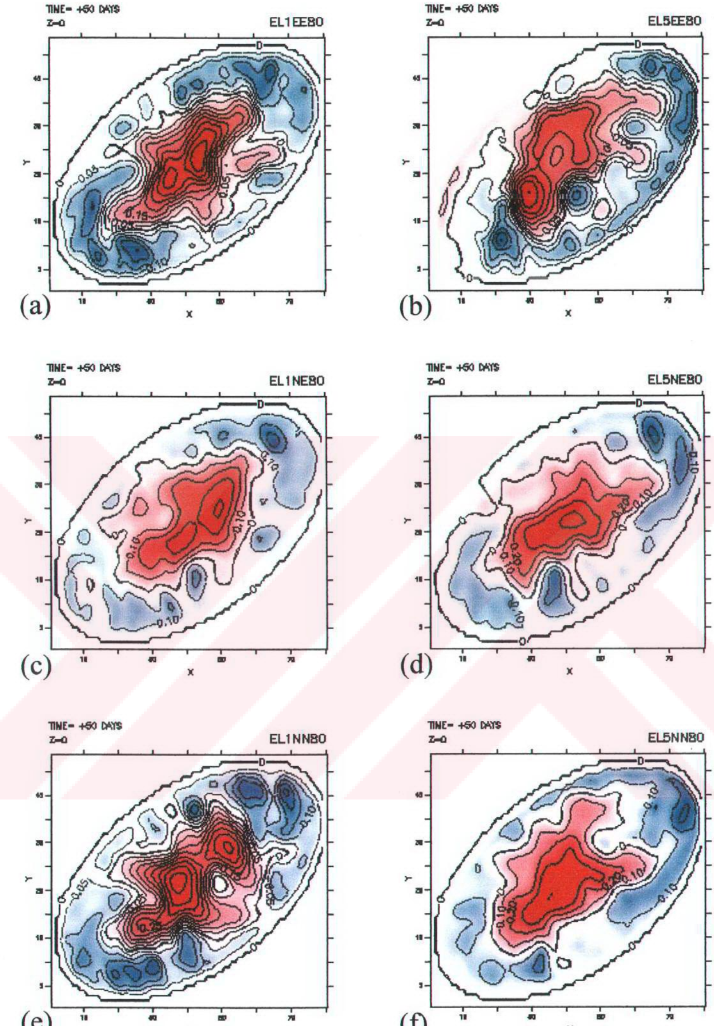

Appendix A.3 Free Surface Elevation after 50 days in ellipsoid (EL), Latent + Sensible 80 W/m^2

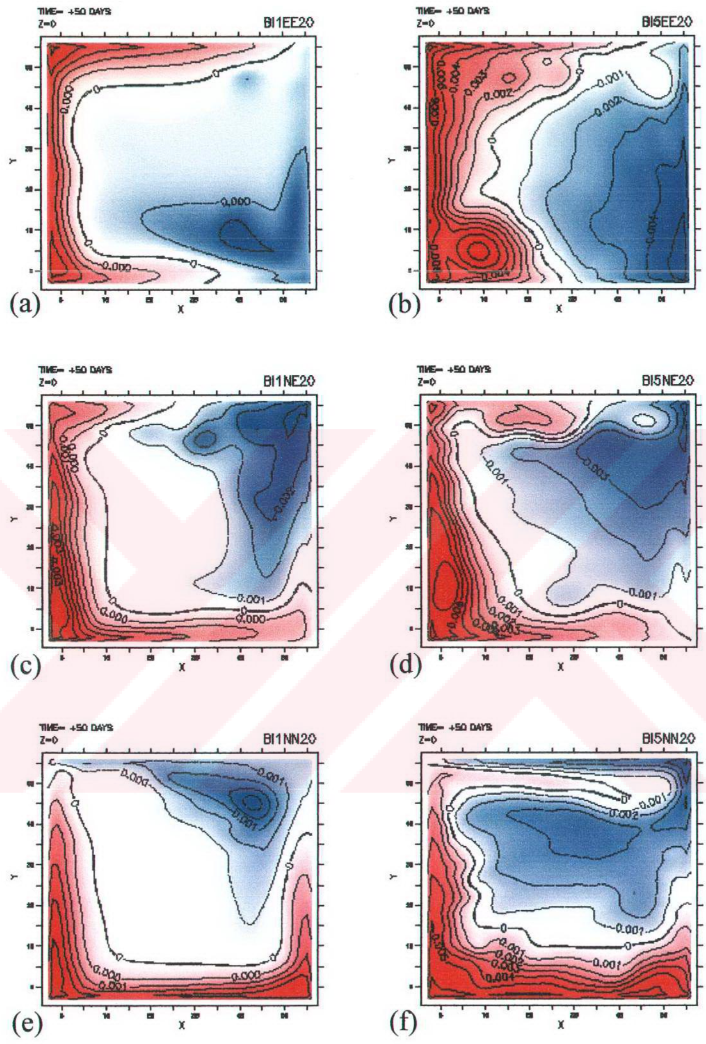

Appendix A.4 Free Surface Elevation after 50 days in inclined bottom box (BI), Latent + Sensible 20 W/m^2

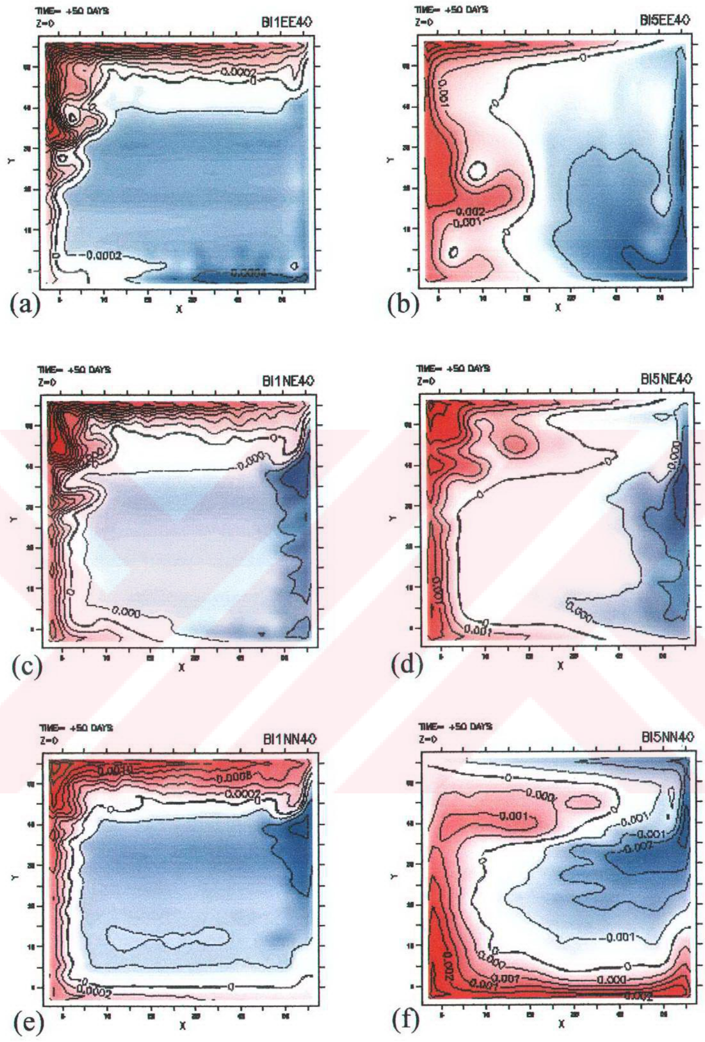

Appendix A.5 Free Surface Elevation after 50 days in inclined bottom box (BI), Latent + Sensible 40 W/m²

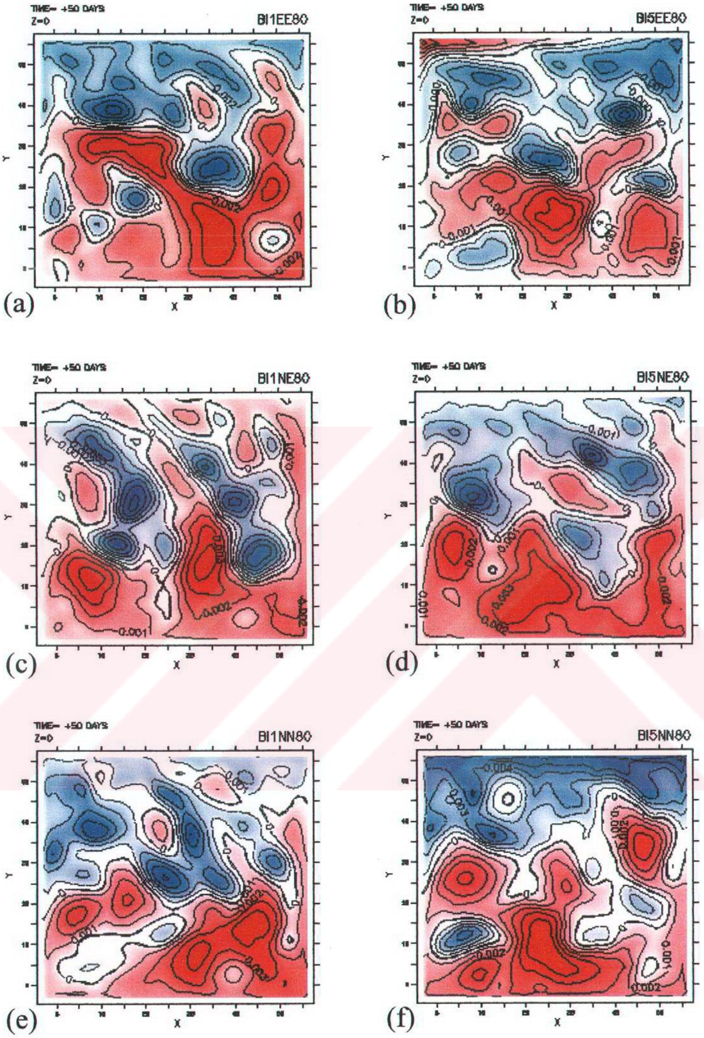

Appendix A.6 Free Surface Elevation after 50 days in inclined bottom box (BI), Latent + Sensible 80 W/m^2

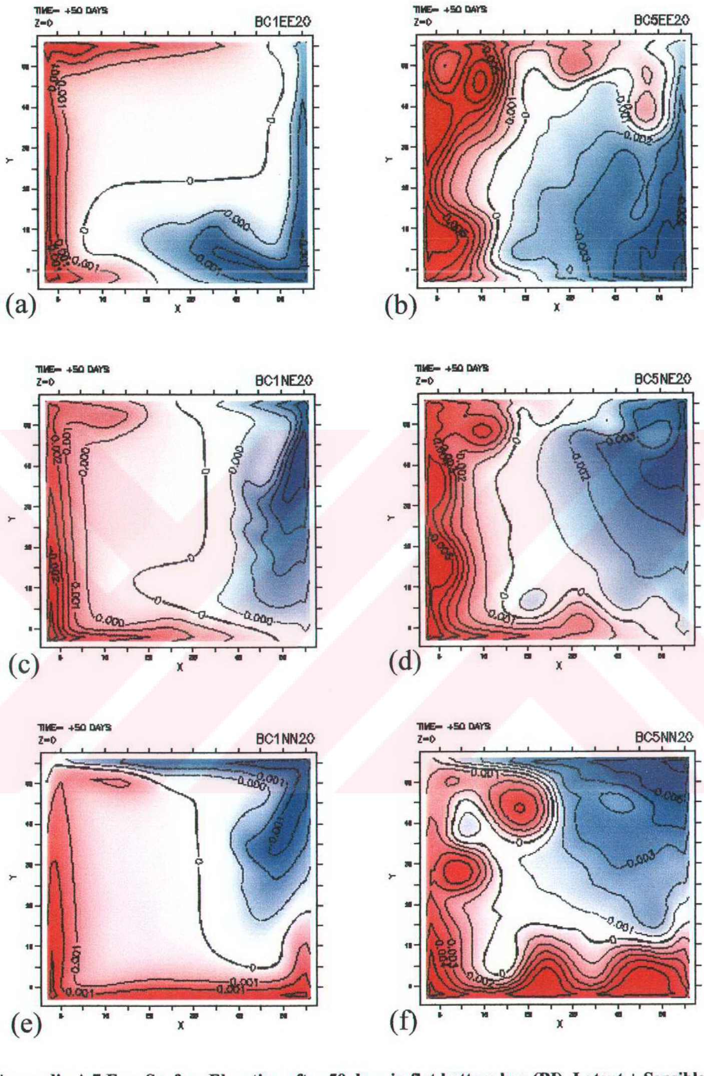

Appendix A.7 Free Surface Elevation after 50 days in flat bottom box (BI), Latent + Sensible 20 W/m^2

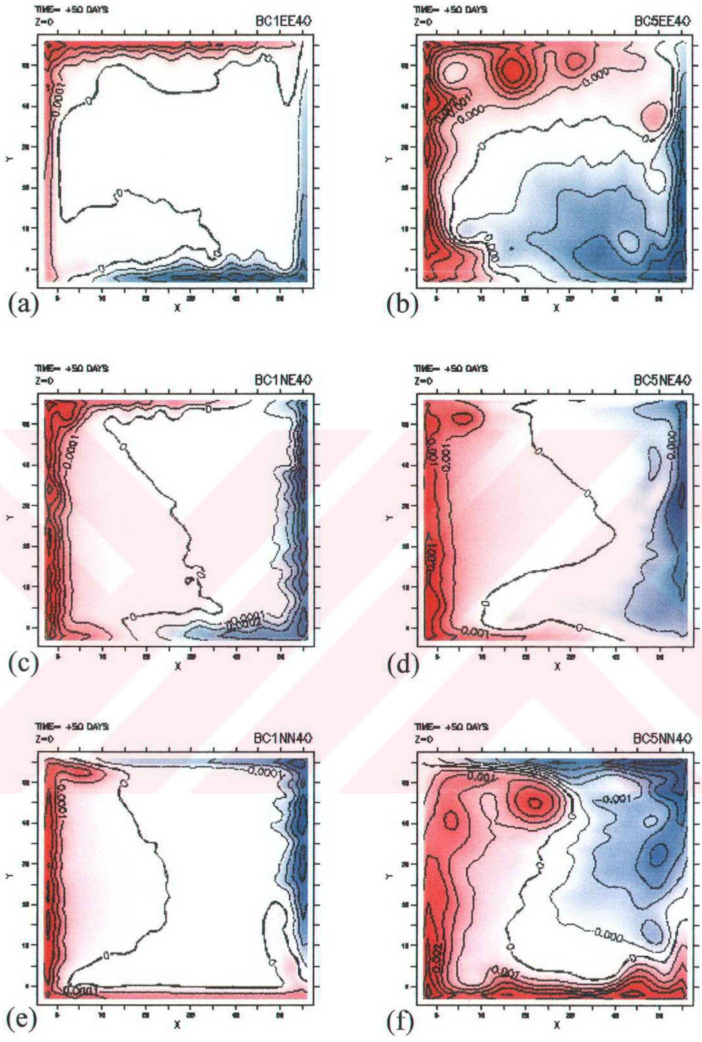

Appendix A.8 Free Surface Elevation after 50 days in flat bottom box (BC), Latent + Sensible 40 W/m^2

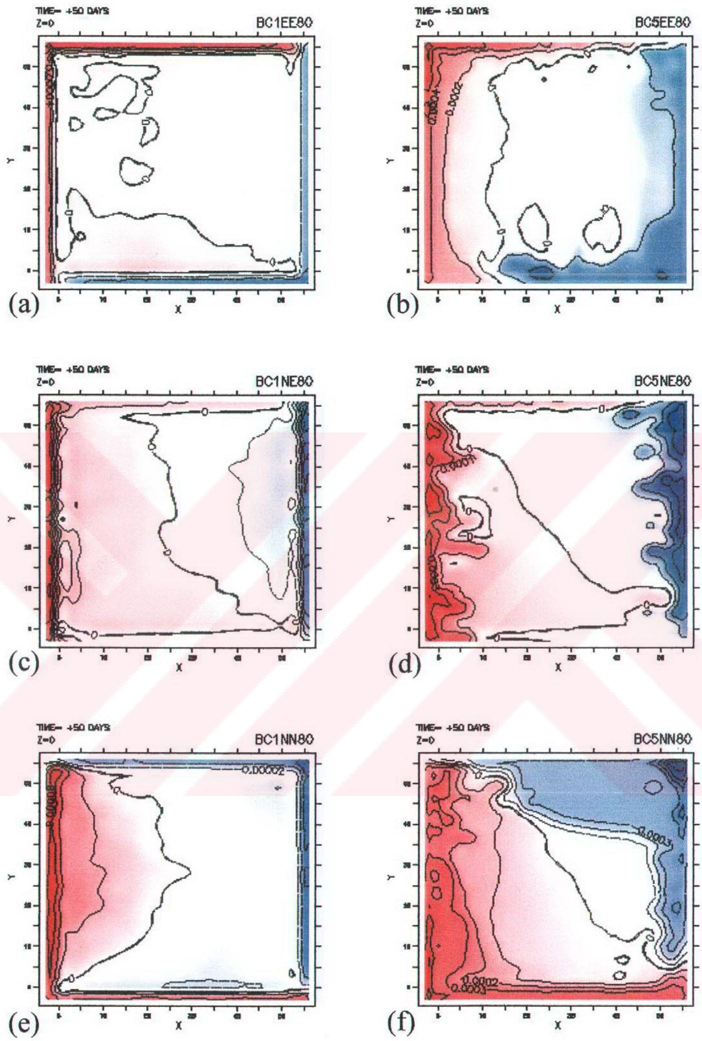

Appendix A.9 Free Surface Elevation after 50 days in flat bottom box (BC), Latent + Sensible 80 W/m^2

APPENDIX B

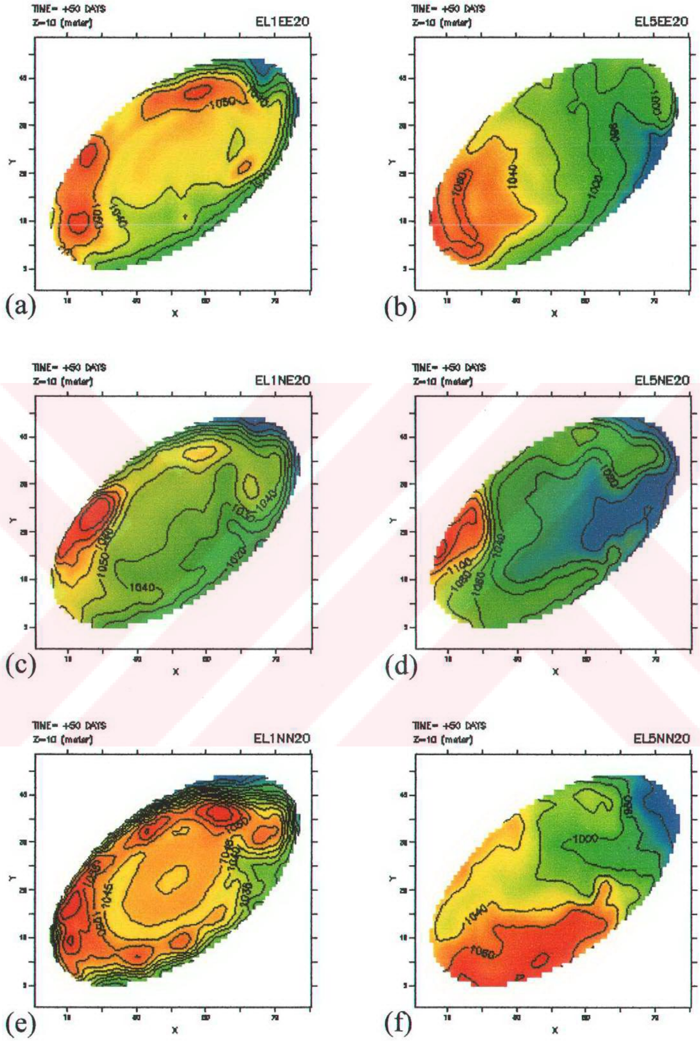

Appendix B.1 Potential temperature at 10 meter depth after 50 days in ellipsoid (EL), Latent + Sensible 20 W/m²

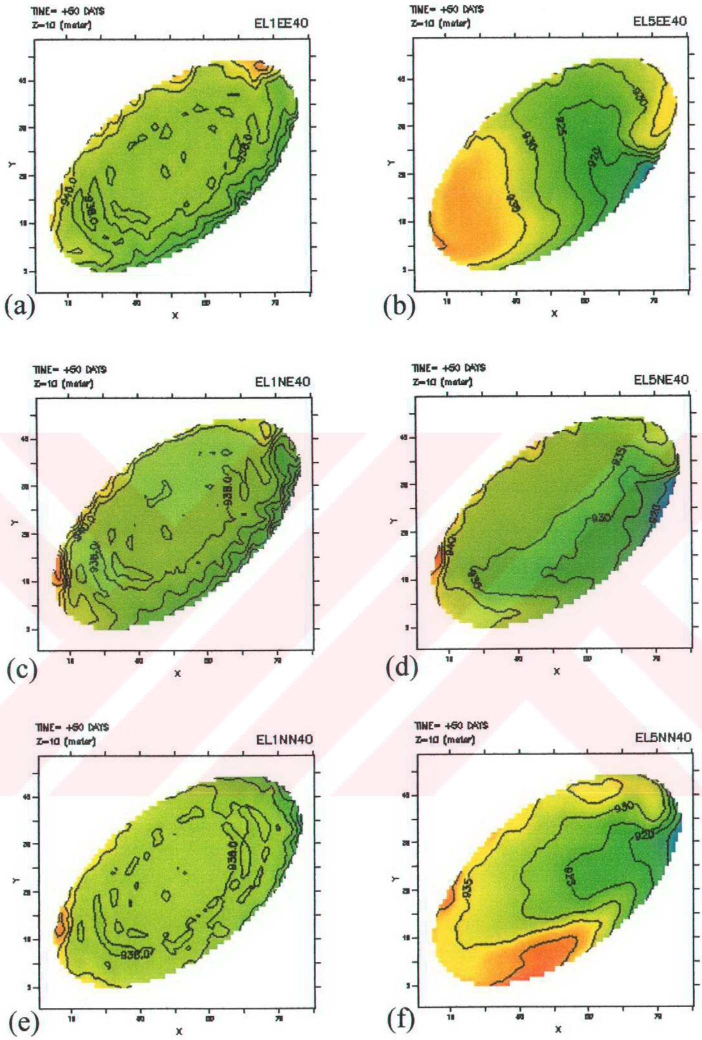

Appendix B.2 Potential temperature at 10 meter depth after 50 days in ellipsoid (EL), Latent + Sensible 40 W/m^2

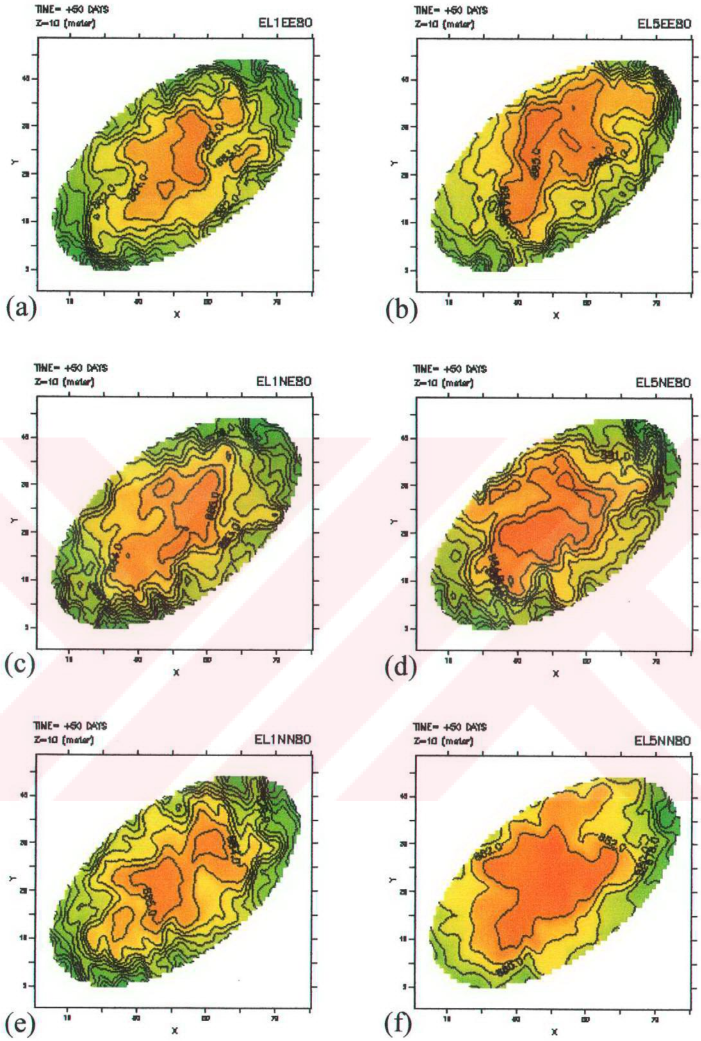

Appendix B.3 Potential temperature at 10 meter depth after 50 days in ellipsoid (EL), Latent + Sensible 80 W/m^2

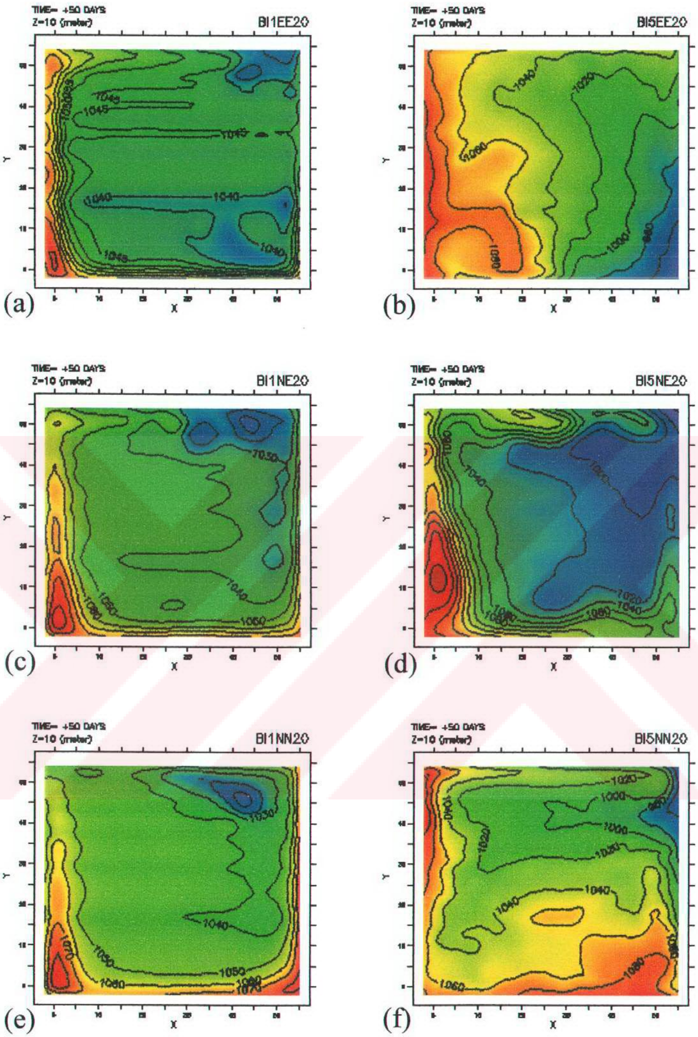

Appendix B.4 Potential temperature at 10 meter depth after 50 days in inclined bottom box (BI), Latent + Sensible 20 W/m^2

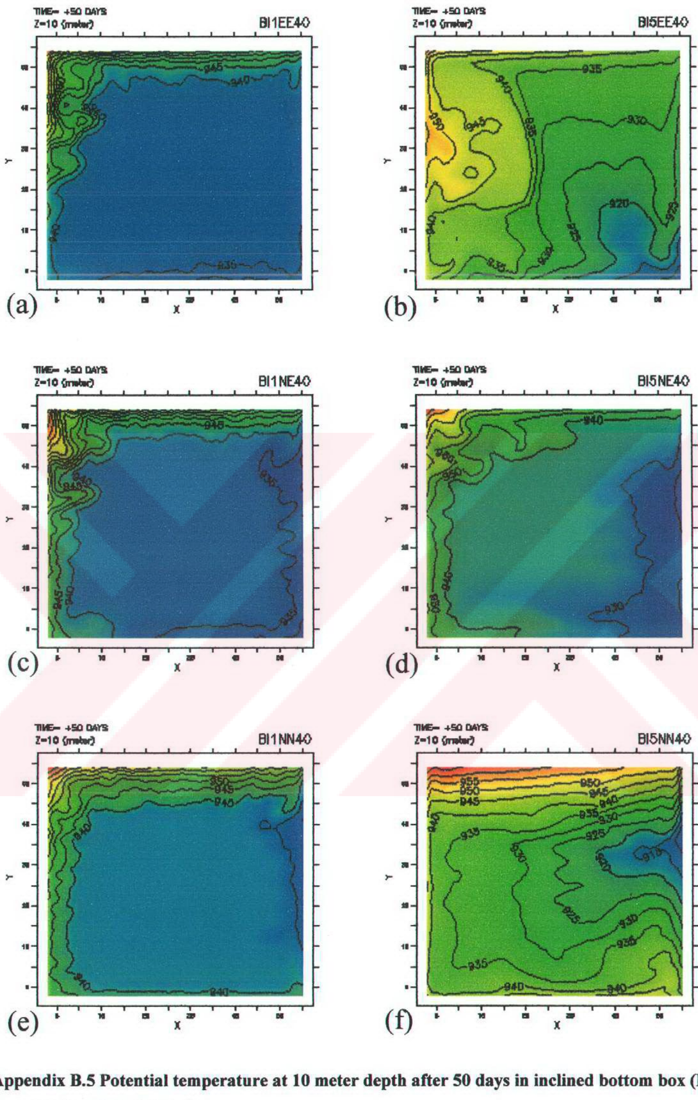

Appendix B.5 Potential temperature at 10 meter depth after 50 days in inclined bottom box (BI), Latent + Sensible 40 W/m^2

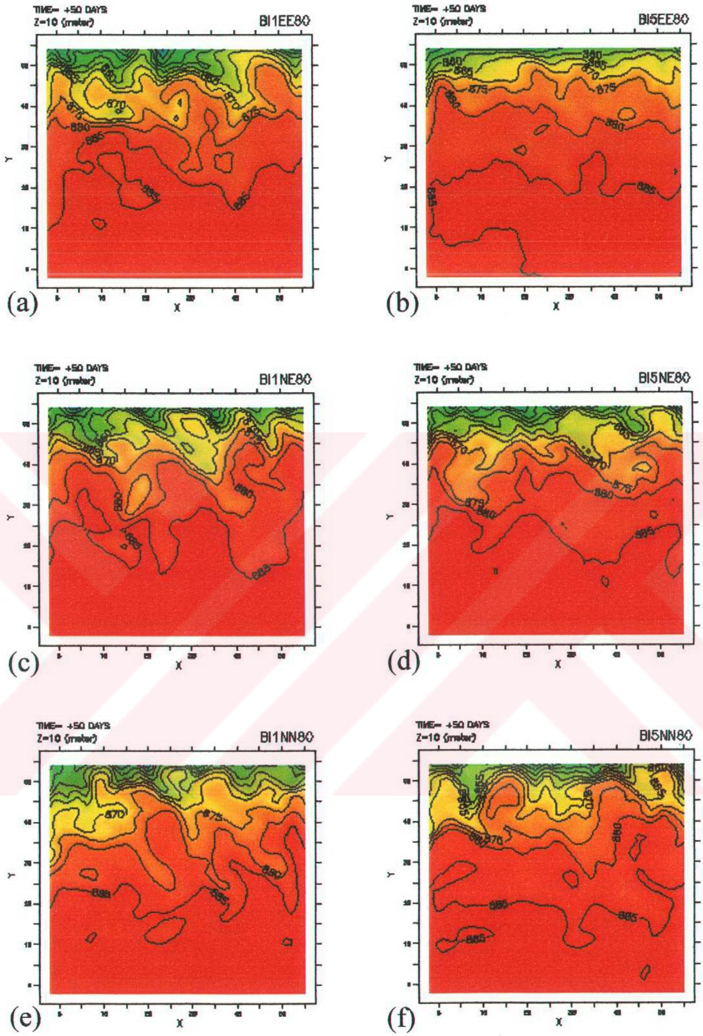

Appendix B.6 Potential temperature at 10 meter depth after 50 days in inclined bottom box (BI), Latent + Sensible 80 W/m^2

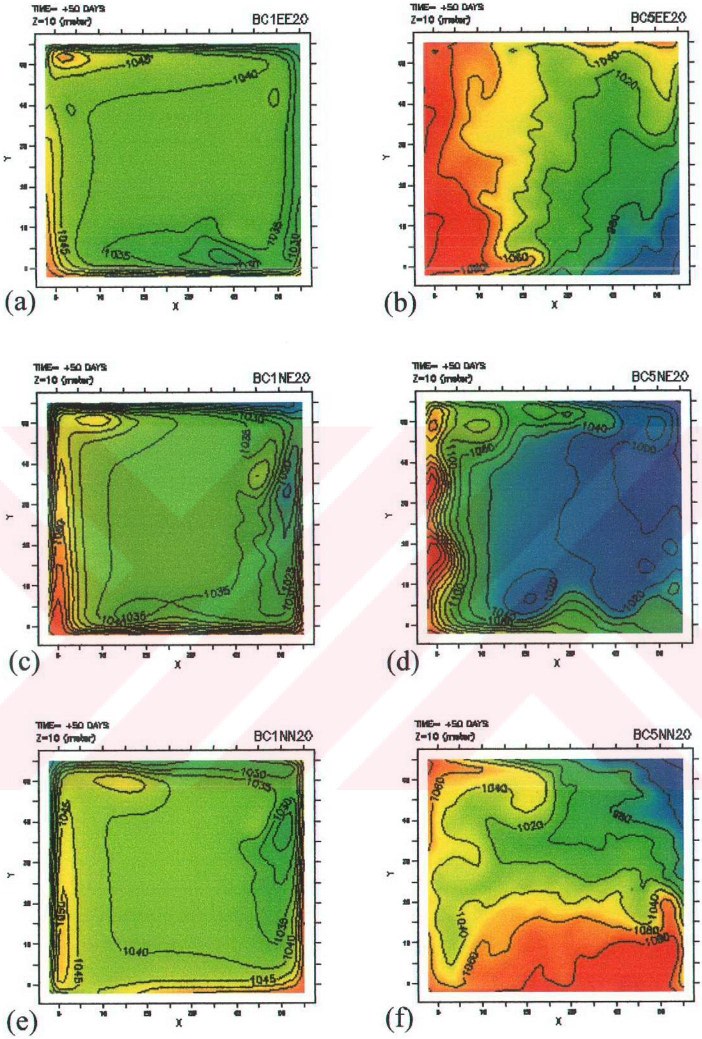

Appendix B.7 Potential temperature at 10 meter depth after 50 days in flat bottom box (BC), Latent + Sensible 20 W/m^2

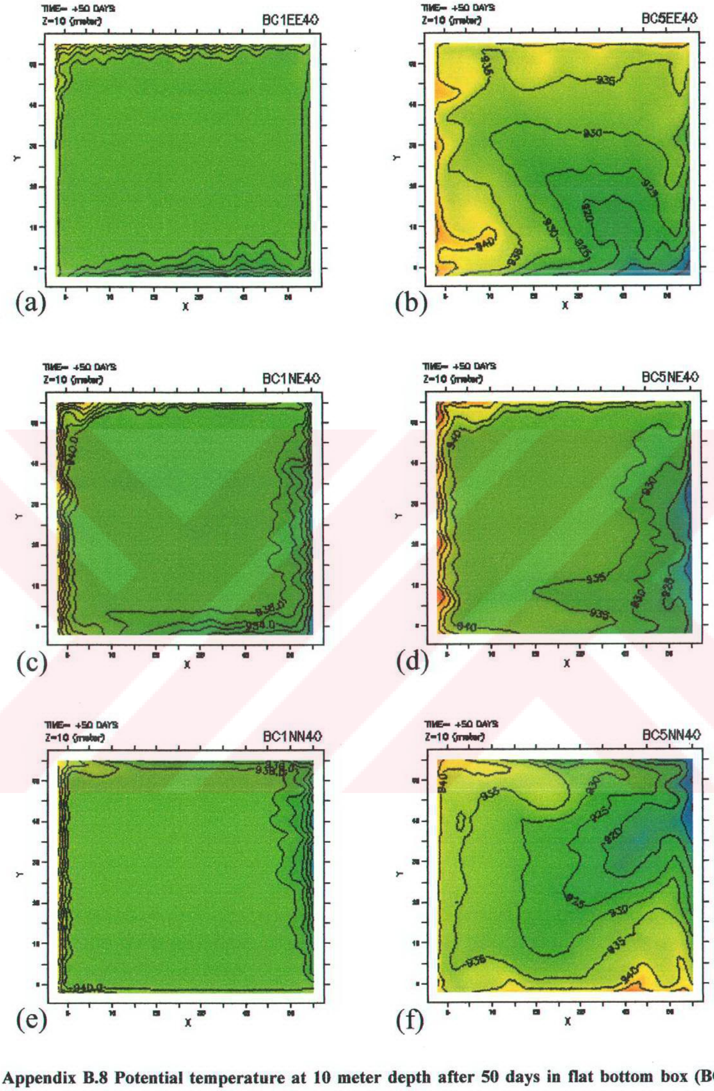

Appendix B.8 Potential temperature at 10 meter depth after 50 days in flat bottom box (BC), Latent + Sensible 40 W/m^2

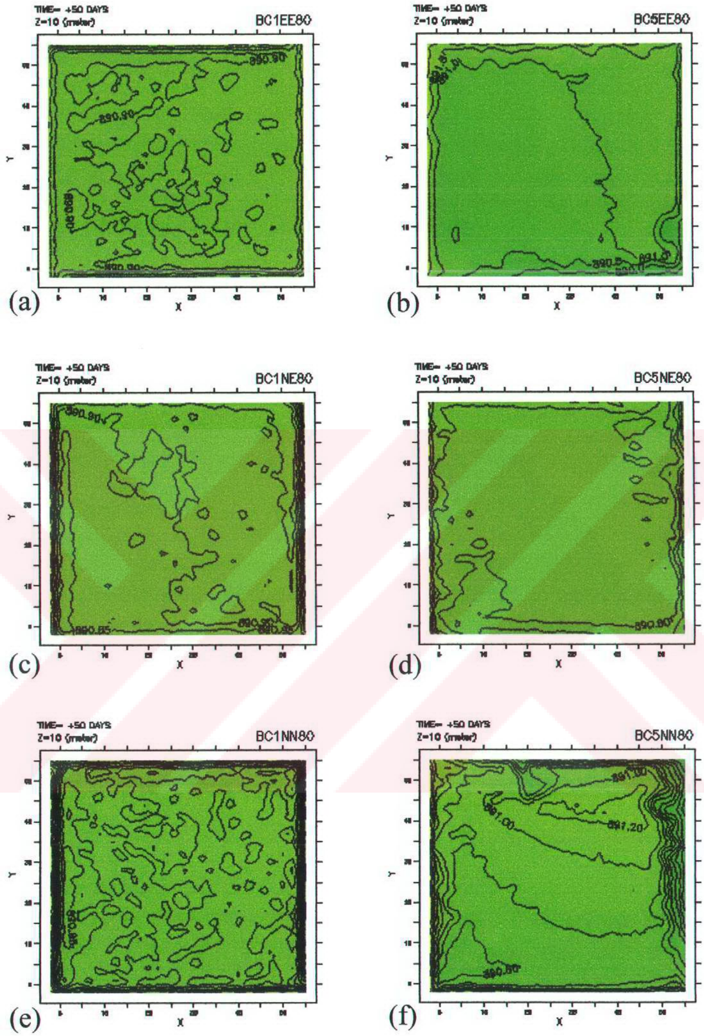

Appendix B.9 Potential temperature at 10 meter depth after 50 days in flat bottom box (BC), Latent + Sensible 80 W/m^2

APPENDIX C

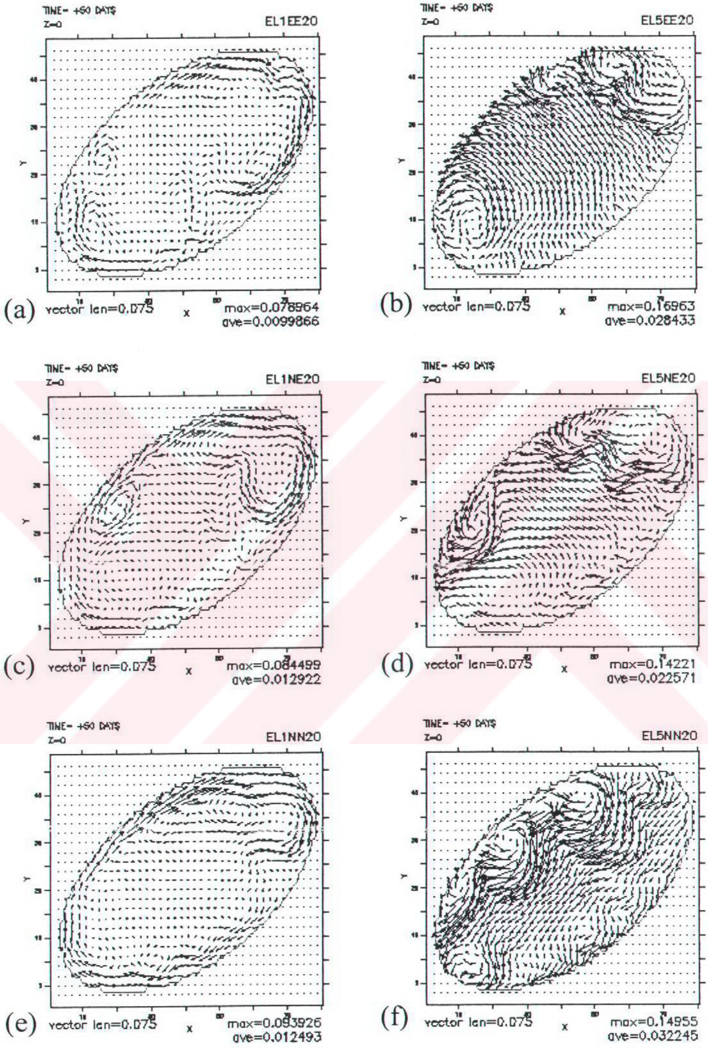

Appendix C.1 Surface currents (m/s) after 50 days in ellipsoid (EL), Latent + Sensible 20 W/m^2

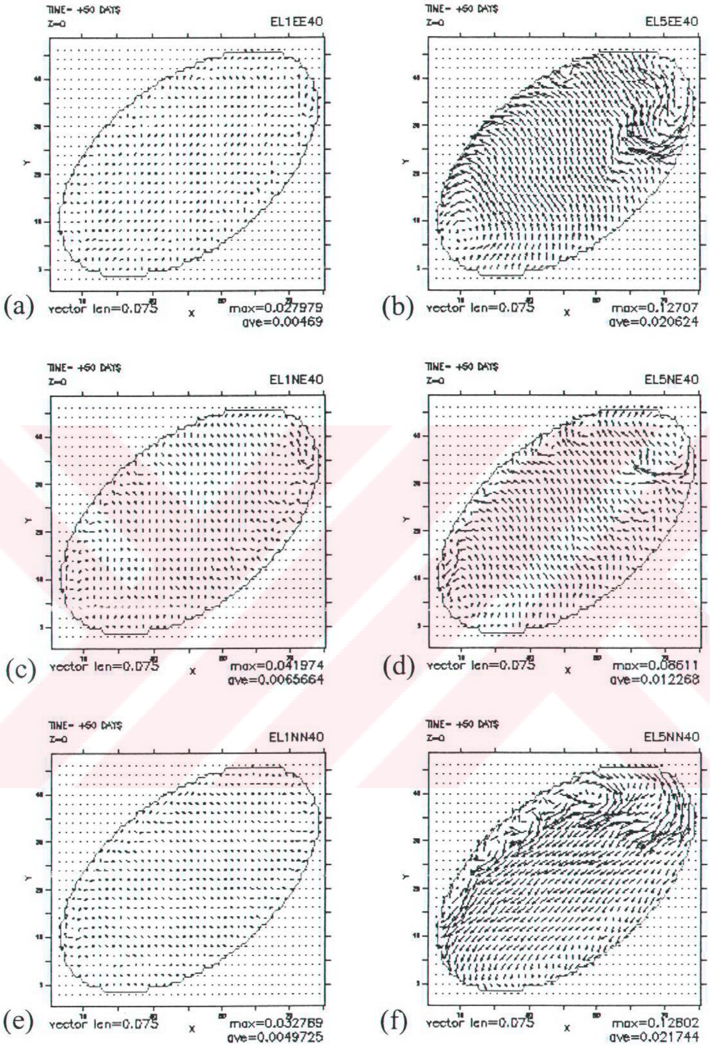

Appendix C.2 Surface currents (m/s) after 50 days in ellipsoid (EL), Latent + Sensible 40 W/m^2

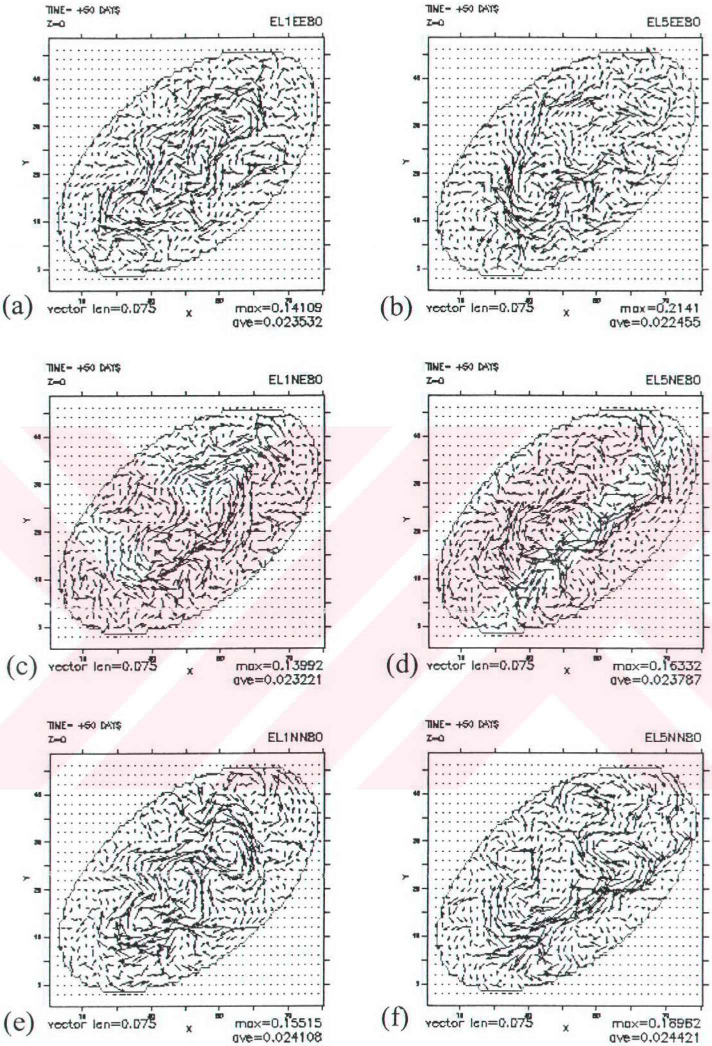

Appendix C.3 Surface currents (m/s) after 50 days in ellipsoid (EL), Latent + Sensible 80 W/m^2

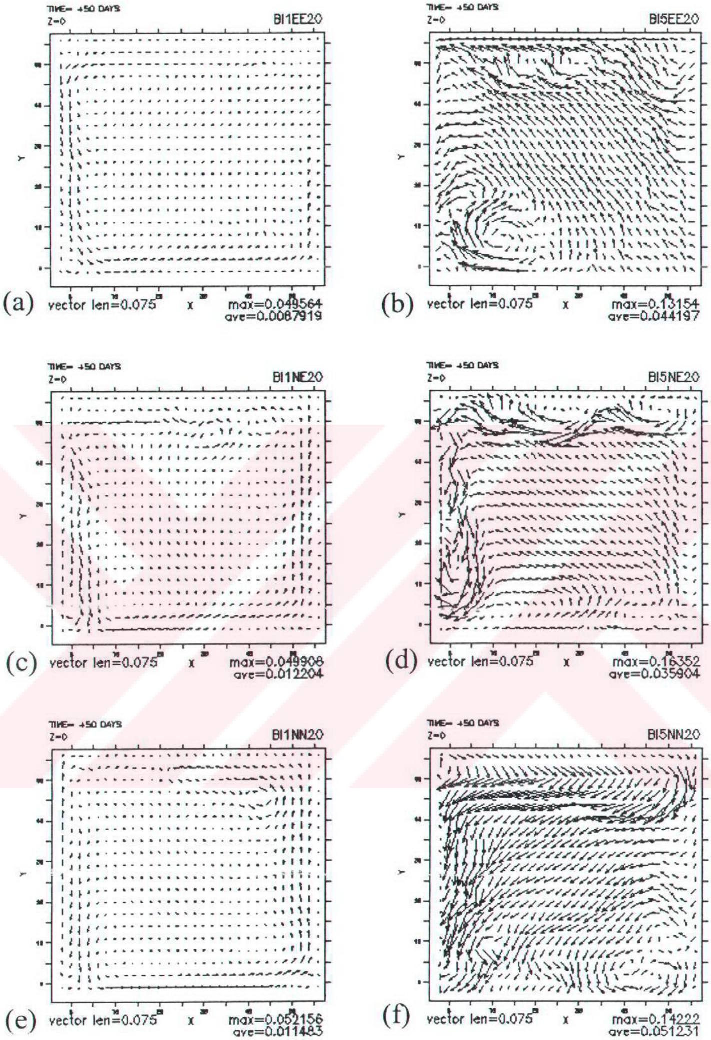

Appendix C.4 Surface currents (m/s) after 50 days in inclined bottom box (BI), Latent + Sensible 20 W/m^2

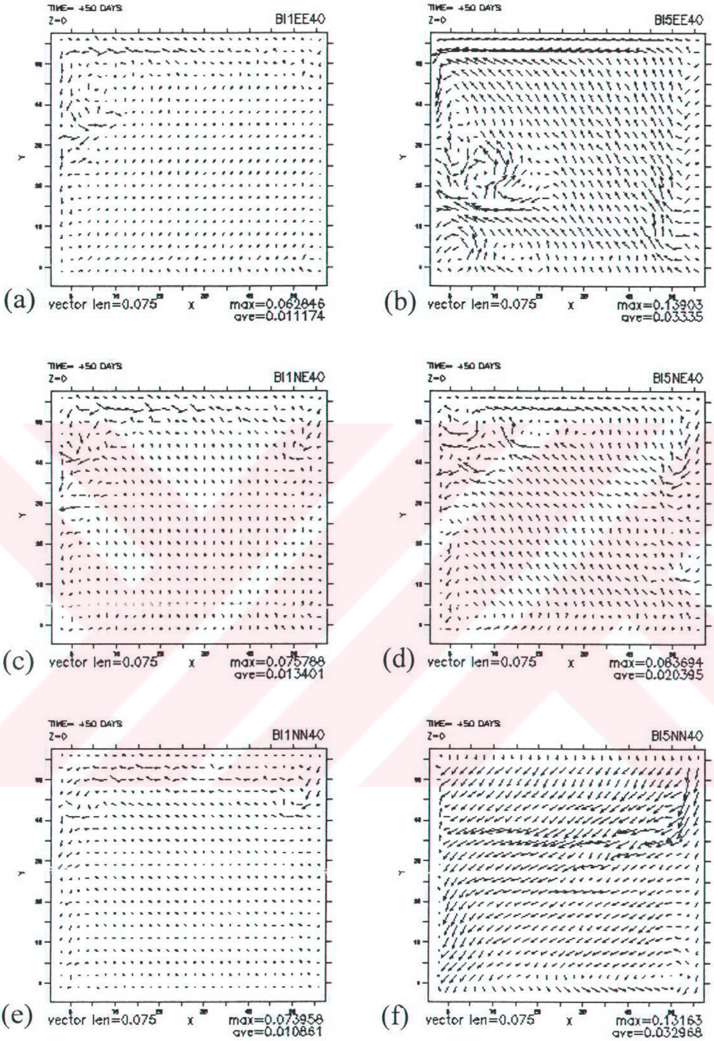

Appendix C.5 Surface currents (m/s) after 50 days in inclined bottom box (BI), Latent + Sensible 40 W/m^2

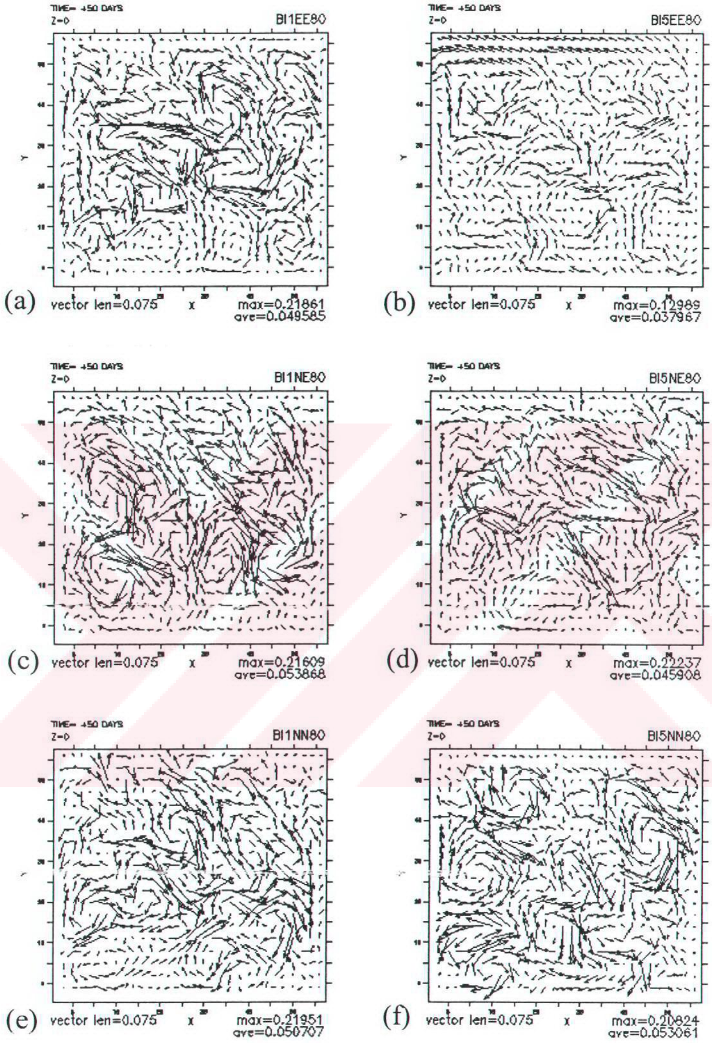

Appendix C.6 Surface currents (m/s) after 50 days in inclined bottom box (BI), Latent + Sensible 80 W/m^2

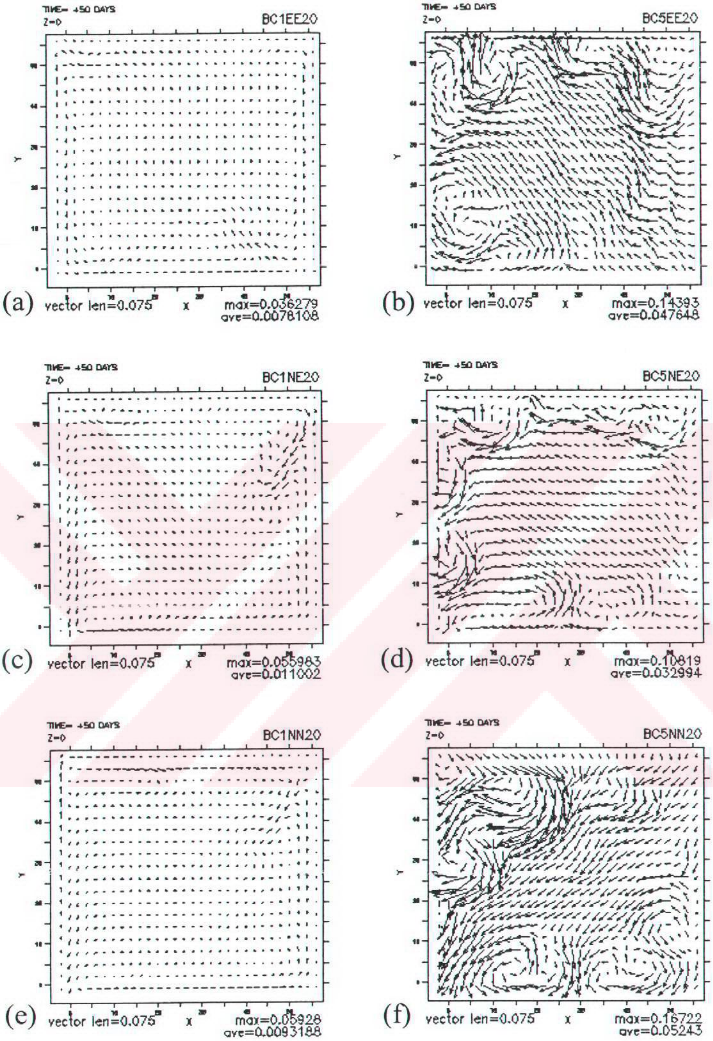

Appendix C.7 Surface currents (m/s) after 50 days in flat bottom box (BC), Latent + Sensible 20 W/m^2

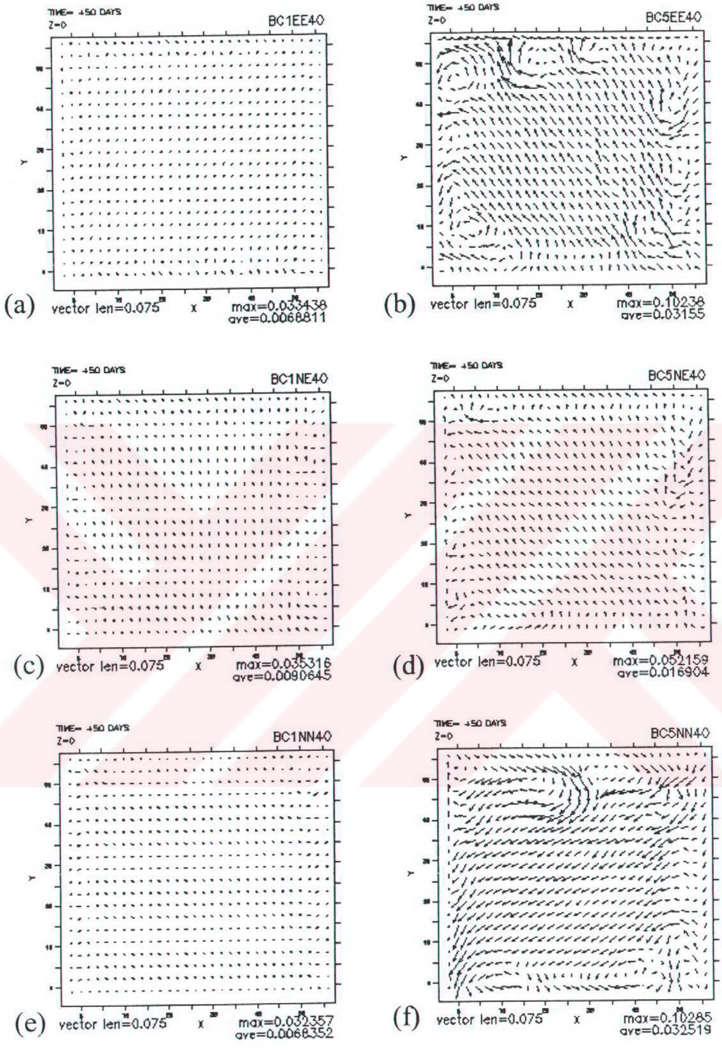

Appendix C.8 Surface currents (m/s) after 50 days in flat bottom box (BC), Latent + Sensible 40 W/m^2

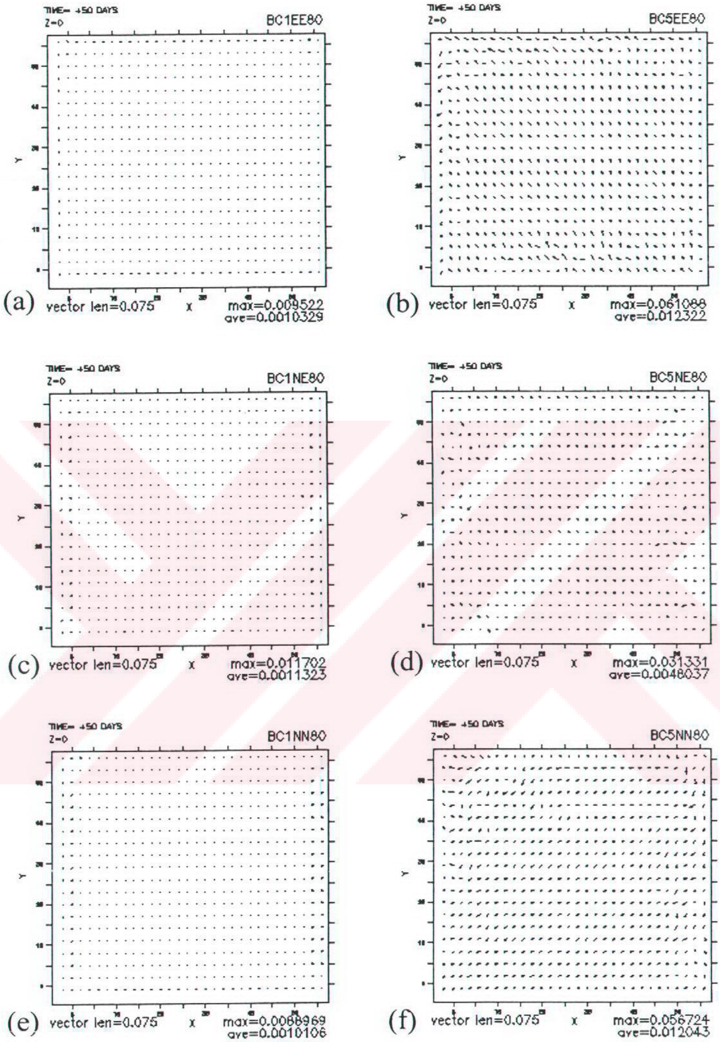

Appendix C.9 Surface currents (m/s) after 50 days in flat bottom box (BC), Latent + Sensible 80 W/m^2

BIOGRAPHY

Ufuk Utku Turunçoglu was born in 09 May 1977, Tokat. He studied his primary, middle and high school in Istanbul and graduated from Istanbul Kurtuluş Lisesi in 1994.

He graduated from Meteorological Engineering, Istanbul Technical University in 2000. While he was working as a software developer, he continued his education during two and half years and then he leaved his job and return back to the graduate education.

He is still studying in Earth Sciences System Program of Department of Climate and Ocean Sciences in Eurasia Institute of Earth Sciences, Istanbul Technical University.